CERN

Advanced Computational Methods for Vacuum Technology with Application to Synchrotron Radiation Light Sources

R. Kersevan, CERN-TE-VSC-VSM

With input from many colleagues, too many to list all of them here… see individual slides…

A few words about me:

- I am a vacuum scientist working on accelerators since the end of the 80s;
- I have graduated from the university of Trieste (Italy) with a thesis on surface science;
- I've worked on the following accelerator projects:
  - 2 GeV ELETTRA light source, Trieste, Italy, (1988-1992);
  - 20+20 TeV SSC pp collider, Dallas TX, USA, (1992-1994);
  - Cornell Electron-Positron Storage Ring (CESR), Cornell University, Ithaca NY, USA, (1994-1997);
  - 6 GeV ESRF light source, Grenoble, France, (1997-2009);
  - Spallation Neutron Source, Oak Ridge TN, USA, (2004-2005, on sabb. leave);
  - International Thermonuclear Experimental Reactor ITER, Cadarache, France, (2009-2011);
  - Vacuum Group, Technology Department, CERN, Geneva, Switerland, (2011-), where I have the position of Applied Physicist, Senior Staff
- I have been a reviewer at various levels of many SR light source projects: NSLS-II, PLS-II, MAX-IV, SIRIUS, APS-U,…
- I have been a member of the Machine Advisory Committee of the DIAMOND and ALBA light source projects, and I am now a member of the MAC for the upgrade of the ESRF, the EBS project.

Outline of tutorial:

1. Basics of gas dynamics: outgassing, conductance, pumping speed;
2. Basics of synchrotron radiation (SR), with examples relevant to vacuum design;
3. SR-induced desorption and materials for vacuum;
4. Computational methods for vacuum: a review;
5. Practical examples of analysis, simulation, and design of key components of light sources;
6. Summary and conclusions.

ANNOUNCEMENT: Do not forget to write down on your agenda this event!... A must for any serious scientist/engineer who wants to become aware of vacuum issues for particle accelerators: http://cas.web.cern.ch/cas/Lund2017/Lund-advert.html

DRAFT PROGRAMME FOR VACUUM FOR PARTICLE ACCELERATORS
6-16 June, 2017, Lund, Sweden

Time	Tuesday 6 June	Wednesday 7 June	Thursday 8 June	Friday 9 June	Saturday 10 June	Sunday 11 June	Monday 12 June	Tuesday 13 June	Wednesday 14 June	Thursday 15 June	Friday 16 June
08:30 09:30	A R R I V A L D A Y	Opening Talks	Materials & Properties IV: Outgassing	Getter Pumps	Vacuum for Thermal Insulation of Cryogenic Equipment	E X C U R S I O N	Surface Characterisation	Transport to Max IV Lab	Controlling Particles/Dust in Vacuum Systems	Vacuum Design Aspects	D E P A R T U R E D A Y
09:30 10:30		Introduction to Machine Parameters	Beam Induced Desorption	Ion Pumps	Vacuum Guages I K. Jousten		Interactions between Beams and Vacuum System Walls	**Seminar** Max IV Laboratory	Beam Induced Radioactivity & Radiation Hardness	Manufacturing & Assembly for Vacuum Technology	
		COFFEE	COFFEE	COFFEE	COFFEE		COFFEE	COFFEE	COFFEE	COFFEE	
11:00 12:00		Fundamentals of Vacuum Technology	Mechanical Vacuum Pumps	Introduction to Cryogenics	Vacuum Gauges II		Surface Finishing	Visit To Max IV	Intercepting Beams & Synchrotron Light	The Real Life of Operation V. Baglin	
12:00 13:00		Impedance & Instabilities	Computation for Vacuum System of Accelerators	Cryo-pumping V. Baglin	Beam-Gas Interaction M. Ferro Luzzi		Thin-Film Coating		Control & Diagnostic	Challenges for Vacuum Technology of Future Accelerators	
		LUNCH	LUNCH	LUNCH	LUNCH		LUNCH	LUNCH	LUNCH	LUNCH	
14:30 15:30		Materials & Properties I: Introduction	Tutorial	Tutorial	Tutorial		Tutorial	**Seminar** ESS	Tutorial	Tutorial Work Closeout	
15:30 16:30		Materials & Properties II: Thermal & Electrical Characteristics	Tutorial	Tutorial	Tutorial		Tutorial		Tutorial		
		TEA	TEA	TEA	TEA		TEA		TEA	TEA	
17:00 18:00		Materials & Properties III: Mechanical Behaviour	Tutorial Work	Tutorial Work	Tutorial Work		Tutorial Work		Tutorial Work	Closing Remarks	
19:30	Buffet Dinner	**Dinner**	**Dinner**	**Dinner**	**Dinner**	**Dinner**	**Dinner**	**Dinner**	**Dinner**	**Special Dinner**	

- Programme (pdf
- Scholarships
- Poster (pdf)
- Indico Link (for

r. Roger Bailey (Head of CAS)
r. Werner Herr (Deputy Head of AS)
r. Bernhard Holzer (CAS Member)
arbara Strasser (CAS Administrator)

Overview:

- Modern particle accelerators, in particular synchrotron radiation light sources need rather **stringent conditions on their vacuum requirements**, namely:
  - Average pressures in the **low 1.0E-9 mbar range**;
  - Average **low-Z residual gas composition**: H_2 must be the main gas component during operation of the machine;
  - **Stable pressure profiles**, with, in in particular, no pressure bumps along the straight sections where insertion devices (ID) are installed, in order to minimize the generation of high-energy bremsstrahlung (BS) photons;
- This translates into flows which are in the **molecular flow regime**, i.e. conditions for which the probability of the residual gas molecules to interact/collide which each other is much lower than the probability of hitting the walls of the vacuum system
- Apart from cases when the different molecular species can promptly react chemically with each other (e.g. chemical reactors, catalysed reactions), the flow regime of a gas can be described by the **mean free path** concept, i.e. the average distance travelled by a molecule between two collisions with another molecule at same density and temperature conditions in a 'infinite' volume;

Why do we need vacuum in accelerators?

Collisions between gas molecules and particles have to be minimized, otherwise:

Particle energy can be reduced and/or trajectories can be modified, so that:

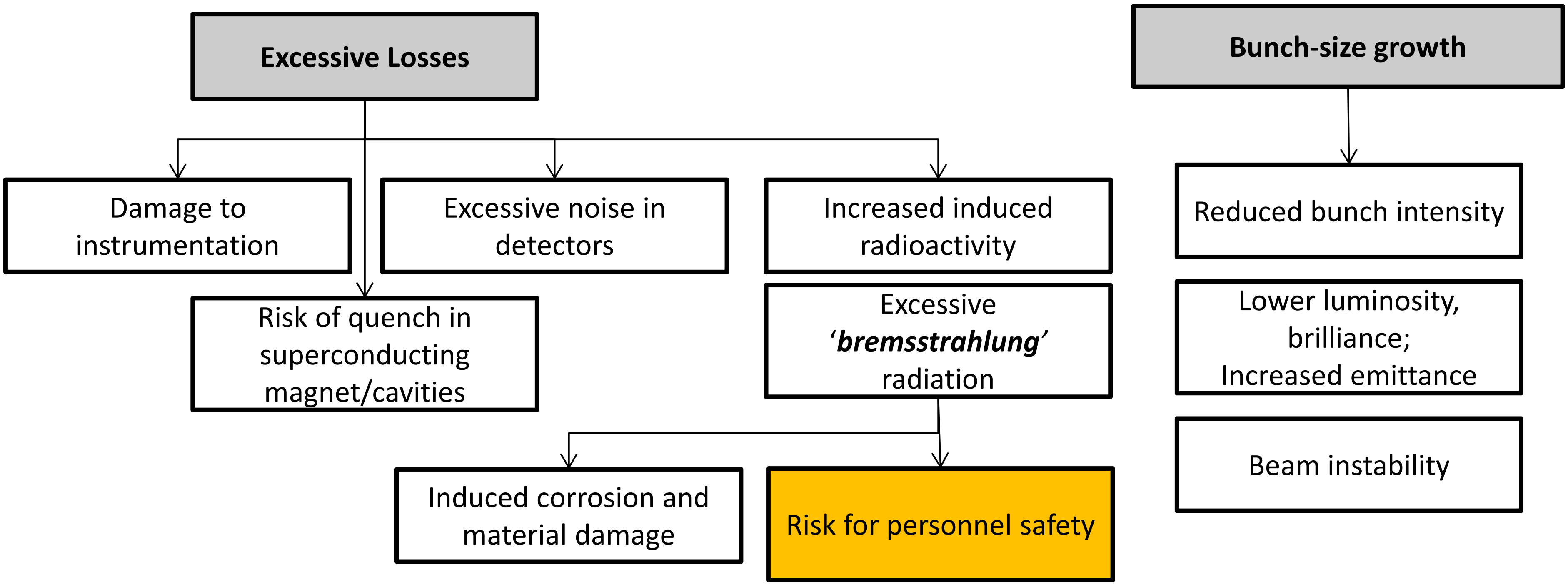

A good vacuum is also necessary:

- To avoid electrical discharge in high-voltage devices (tens of MV/m in RF cavities);
- To reduce the heat transfer to cryogenic devices (e.g. insulating vacuum in cryostats)

Vacuum science concepts:

At equilibrium a rarefied gas is described by the **ideal gas equation of state**:

$$PV = N_{moles}\, RT$$

where P, T and V are the gas pressure, temperature and volume, respectively; R the ideal gas constant (8.314 J K^{-1} mol^{-1} in SI units) .

From statistical physics considerations, this equation may be rewritten in terms of the total number of molecules N in the gas

$$PV = N\, k_B T$$

where k_B is the **Boltzmann constant, k_B=1.38 10^{-23} J K^{-1}** in SI units.

In the International System of Units, the pressure is reported in **Pascal**: 1 Pa is equivalent to the pressure exerted by **one N on a m^2**.
Other units are regularly used in vacuum technology, in particular **bar** and its submultiple the **mbar**. The **Torr** is still used, mostly in the USA; it is equivalent to the **pressure exerted by a one-mm high column of mercury**.

The conversion values between the common pressure units are collected in Tab.1.

Source: "Vacuum technology", P. Chiggiato, R. Kersevan, Joint University Accelerator School (JUAS), 2015; https://indico.cern.ch/event/356897/ ; https://indico.cern.ch/event/356897/contributions/1769003/attachments/709948/974550/JUAS_2015_Vacuum_Technology.pdf

Table 1: conversion values for the most common pressure units of vacuum technology

	Pa	**Bar**	**atm**	**Torr**
1 Pa	1	10^{-5}	$9.87\ 10^{-6}$	$7.5\ 10^{-3}$
1 bar	10^{5}	1	0.987	750.06
1 mbar	10^{2}	10^{-3}	$0.967\ 10^{-3}$	0.75
1 atm	$1.013\ 10^{5}$	1.013	1	760
1 Torr	133.32	$1.33\ 10^{-3}$	$1.32\ 10^{-3}$	1

Table 2 shows the number density n=N/V of molecules/atoms at room temperature and liquid helium boiling point (useful for superconducting devices, e.g. RF cavities, magnets):

Table 2: Typical number density at room temperature and helium boiling point

	Pressure [Pa]	**293 K [molecules cm^{-3}]**	**4.3K [molecules cm^{-3}]**
Atmospheric pressure at sea level	$1.013\ 10^{5}$	$2.5\ 10^{19}$	$1.7\ 10^{21}$
Typical plasma chambers	1	$2.5\ 10^{14}$	$1.7\ 10^{16}$
Linac pressure upper limit	10^{-5}	$2.5\ 10^{9}$	$1.7\ 10^{11}$
Lowest pressure ever measured at room temperature [1]	10^{-12}	250	$1.7\ 10^{4}$

The basis of vacuum technology: pressure

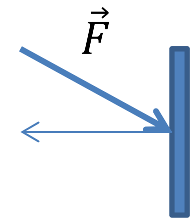

Definition of pressure: $\dfrac{|Force\ component\ in\ \boldsymbol{normal\ direction}|}{Surface\ area}$

Unit of measurement: $\dfrac{[Force]}{[Surface]} \rightarrow \dfrac{N}{m^2} = Pa \rightarrow 10^5 Pa = 1\ bar \rightarrow 1\ atm = 1.013\ bar$

In vacuum technology : $\boldsymbol{mbar}\ or\ \boldsymbol{Pa}$

Still used in vacuum technology:
$1\ Torr = pressure\ exerted\ by\ a\ column\ of\ 1\ mm\ of\ Hg; 1\ atm = 760\ Torr$

- Sometimes it is useful to use **pressure-volume units**, such as **mbar · liters**, i.e. give the number of molecules in a given volume at given temperature and pressure:

1 mbar · liter = $6.022 \cdot 10^{23}$ / 1013.25 / 22.414 = **$2.65 \cdot 10^{19}$ molecules**

where $6.022 \cdot 10^{23}$ is the Avogadro number, 1013.25 is the number of mbar in one standard atmosphere, and 22.414 is the molar volume in liters (**reference T=0 °C**).
(See http://physics.nist.gov/cuu/index.html for a precise list of constants)

- Modern vacuum technology spans ~ 17 orders of magnitude, between atmospheric pressure and the lowest pressure measured so far:

Table 3: Degrees of vacuum and their pressure boundaries

	Pressure boundaries [mbar]	Pressure boundaries [Pa]
Low Vacuum LV	1000-1	10^{5}-10^{2}
Medium Vacuum MV	1-10^{-3}	10^{2}-10^{-1}
High Vacuum HV	10^{-3}-10^{-9}	10^{-1}-10^{-7}
Ultra High vacuum UHV	10^{-9}-10^{-12}	10^{-7}-10^{-10}
Extreme Vacuum XHV	$<10^{-12}$	$<10^{-10}$

The basis of vacuum technology: pressure

Degree of Vacuum

	Pressure boundaries [mbar]	Pressure boundaries [Pa]
Low Vacuum LV	1000-1	10^5-10^2
Medium Vacuum MV	1-10^{-3}	10^2-10^{-1}
High Vacuum HV	10^{-3}-10^{-9}	10^{-1}-10^{-7}
Ultra High vacuum UHV	10^{-9}-10^{-12}	10^{-7}-10^{-10}
Extreme Vacuum XHV	$<10^{-12}$	$<10^{-10}$

As already mentioned, pressures and gas quantities are correlated by the gas equation of state. In vacuum the ideal gas law is **always fulfilled** :

$$P\,V = n\,R\,T \text{ (thermodynamic)}$$

$$P\,V = N\,k_B \mathrm{T} \text{ (statistical mechanics)}$$

P pressure, **V** volume, **T** temperature, **n** molar fraction and **N** number of molecules, **R** gas constant (8.3145 J/mole/K), $\mathbf{k_B}$ Boltzmann constant (1.38110^{-23} J/K)

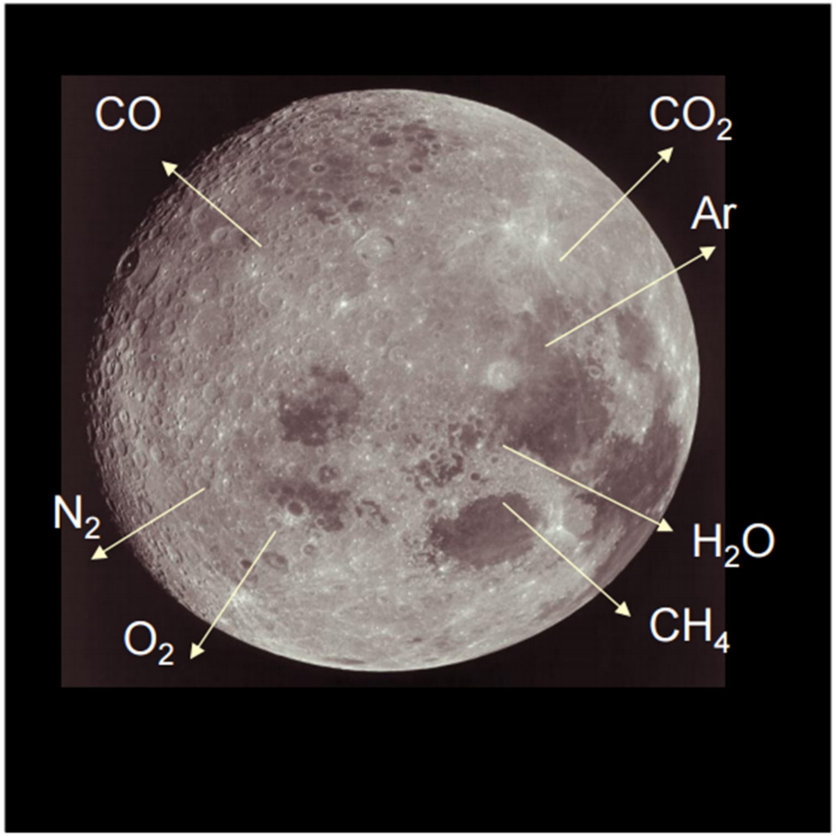

Gas density on the Moon: 10^5 cm^{-3} (10^{-10} Pa) during night and 10^7 cm^{-3} (10^{-8} Pa) during lunar day.

Intergallactical vacuum: 10^{-17} Pa
Vacuum in Via Lattea: 10^{-15} Pa

Lowest pressure ever measured at room temperature: **10^{-12} Pa**

Lowest air pressure variation perceptible by human ears: **2 10^{-5} Pa**
-> about $1/10^{10}$ of the atmospheric pressure

Concepts of gas kinetics:

The kinetics of ideal-gas molecules is described by the **Maxwell-Boltzmann theory**. For an **isotropic gas**, the model provides the probabilistic distribution of the molecular speed magnitudes, see below. The mean speed of molecules $\langle v \rangle$, i.e. the mathematical average of the speed distribution, is given by

$$\langle v \rangle = \sqrt{\frac{8\, k_B T}{\pi\, m}} = \sqrt{\frac{8\, R\, T}{\pi\, M}}$$

where m is the mass of the molecule and M is the molar mass. The unit of both masses is [kg] in SI. Typical mean speed values are shown in Tab. 4.

Table 4: Mean speed of gas molecules of different mass at room temperature and boiling helium point

	H_2	He	CH_4	N_2	Ar
$\langle v \rangle$ at 293 K $\left[\frac{m}{s}\right]$	1761	1244	622	470	394
$\langle v \rangle$ at 4.3 K $\left[\frac{m}{s}\right]$	213	151	75	57	48

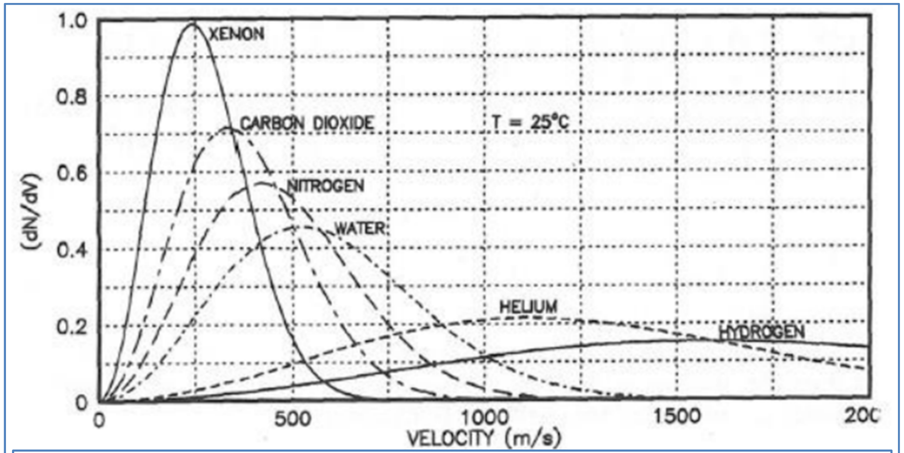

Maxwell-Boltzmann velocity distribution function:

$$f(v) = \sqrt{\left(\frac{m}{2\pi kT}\right)^3}\, 4\pi v^2 e^{-\frac{mv^2}{2kT}}$$

Gas	$\langle v \rangle$ at 293 K $\left[\frac{m}{s}\right]$	$\langle v \rangle$ at 4.3 K $\left[\frac{m}{s}\right]$
H_2	1761	213
He	1244	151
CH_4	622	75
N_2	470	57
Ar	394	48

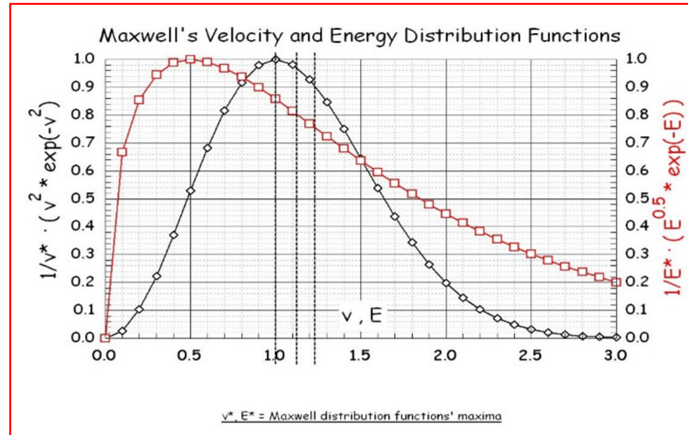

Gas	Pressure [mbar]	Impingement rate 293 K [cm^{-2}s^{-1}]
H_2	10^{-3}	1.1 10^{18}
	10^{-8}	1.1 10^{13}
	10^{-14}	1.1 10^{8}
N_2	10^{-3}	2.9 10^{17}
	10^{-8}	2.9 10^{12}
Ar	10^{-3}	2.4 10^{17}
	10^{-8}	2.4 10^{12}

$$Z_a = \text{impingement rate} = \frac{n \cdot v_a}{4}$$

$$v_a = \text{average speed} = \sqrt{\frac{8 \cdot R \cdot T}{\pi \cdot M}}$$

$$v_{mp} = \text{most probable speed} = \sqrt{\frac{2 \cdot R \cdot T}{M}}$$

$$v_{rms} = \sqrt{< v^2 >} = \sqrt{\frac{3 \cdot R \cdot T}{M}}$$

Concepts of gas kinetics:

Another important result of the Maxwell-Boltzmann theory is the calculation of the **molecular impingement rate** φ on a surface, i.e. the rate at which gas molecules collide with a unit surface area exposed to the gas. Assuming that the density of molecules all over the volume is uniform, it can be shown that

$$\varphi = \frac{1}{4} n \langle v \rangle$$

and using the previous equation for the mean speed as obtained by the Maxwell-Boltzmann theory

$$\varphi = \frac{1}{4} n \sqrt{\frac{8\, k_B T}{\pi\, m}}$$

Numerical values in terms of P, T and molar mass are given by the following equation, and some selected values are reported in Tab. 5.

$$\varphi[cm^{-2}s^{-1}] = 2.635\ 10^{22} \frac{P\,[mbar]}{\sqrt{M[g]T[K]}}$$

Concepts of gas kinetics:

Table 5: Molecular impingement rates at room temperature for H_2, N_2, and Ar at some selected pressures

Gas	Pressure [mbar]	Impingement rate [$cm^{-2}s^{-1}$]
H_2	10^{-3}	$1.1\ 10^{18}$
	10^{-8}	$1.1\ 10^{13}$
	10^{-14}	$1.1\ 10^{7}$
N_2	10^{-3}	$2.9\ 10^{17}$
	10^{-8}	$2.9\ 10^{12}$
Ar	10^{-3}	$2.4\ 10^{17}$
	10^{-8}	$2.4\ 10^{12}$

Concepts of gas kinetics:

Other than in free space, molecules collide between each other and with the walls of the vacuum system. In the first case, the average length of the molecular path between two consecutive collisions, i.e. the **mean free path** $\bar{\lambda}$, is inversely proportional to the number density $n = \frac{P}{k_B T}$ and the collision cross section σ_c , given by

$$\bar{\lambda} = \frac{1}{\sqrt{2}\ n\,\sigma_c}$$

The computation of the cross-section depends on the specific **interaction potential**. For elastic collisions between **hard spheres**, the previous equation can be written in terms of the **molecular diameter** δ:

$$\bar{\lambda} = \frac{1}{\sqrt{2}\ \pi\, n\, \delta^2} = \frac{k_B T}{\sqrt{2}\, \pi\, P\, \delta^2}$$

Typical collision cross sections for common gas species in vacuum systems are listed in Tab. 6.

Table 6: Elastic collision cross sections for five different molecules

Gas	H_2	He	N_2	O_2	CO_2
$\sigma_c\ [nm^2]$	0.27	0.27	0.43	0.40	0.52

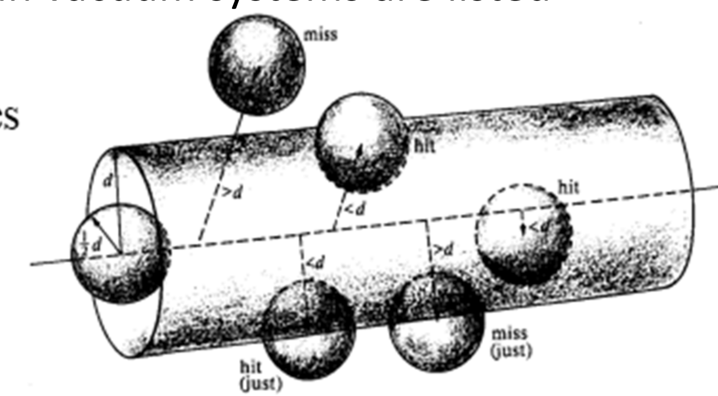

Concepts of gas kinetics:

For numerical purpose, the previous equation can be re-written for a specific gas as a function of temperature and pressure. For H_2

$$\bar{\lambda}_{H_2}[m] = 4.3\ 10^{-5}\,\frac{T[K]}{P[Pa]}$$

The following figure shows the mean free path for H_2 at room temperature as a function of the gas pressure: →

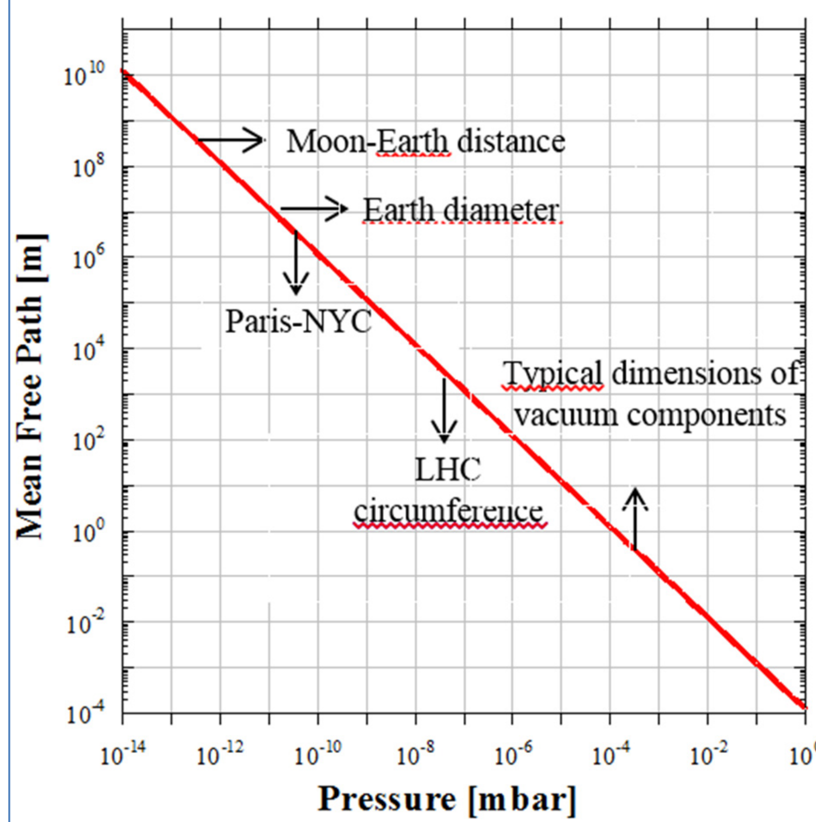

- When the mean free path is of the order of typical dimensions of the vacuum vessel, e.g. the diameter of cylindrical beam pipes, molecular collisions with the wall of the vacuum envelope become preponderant.
- For bigger $\bar{\lambda}$, the dynamics of the gas is dominated by molecule-wall collisions: **Intermolecular interactions cease to have any effect on the gas displacement**.

→"High-vacuum pumps DO NOT suck gases! "←

Concepts of gas kinetics:

(formula as per G. A. Bird, ***Molecular Gas Dynamics and the Direct Simulation of Gas Flows***, Claredon, Oxford, 1994)

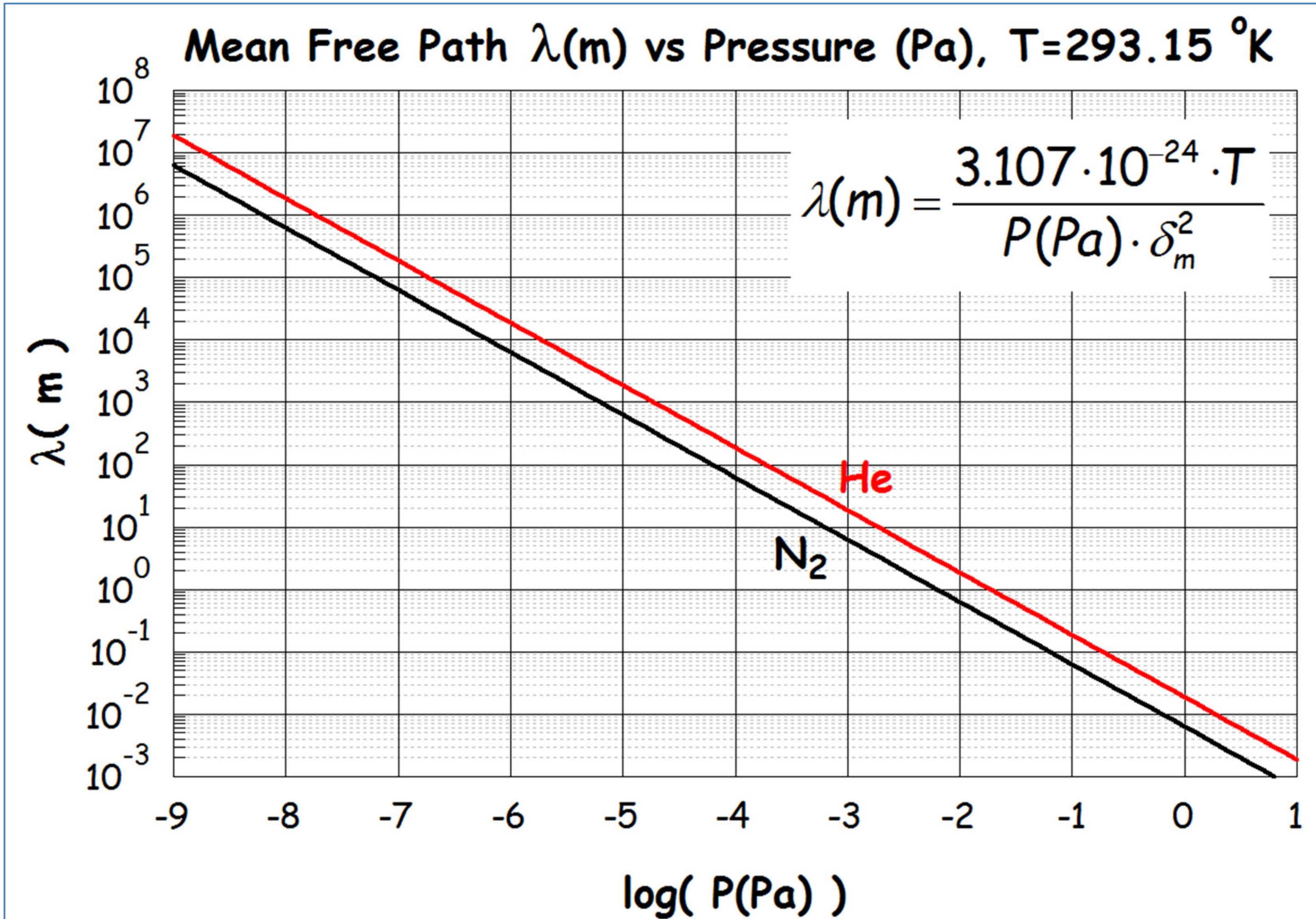

Concepts of gas kinetics:

Gas Collision Rate, Impingement Rate, Number Density and Mean-Free Path all on one plot:

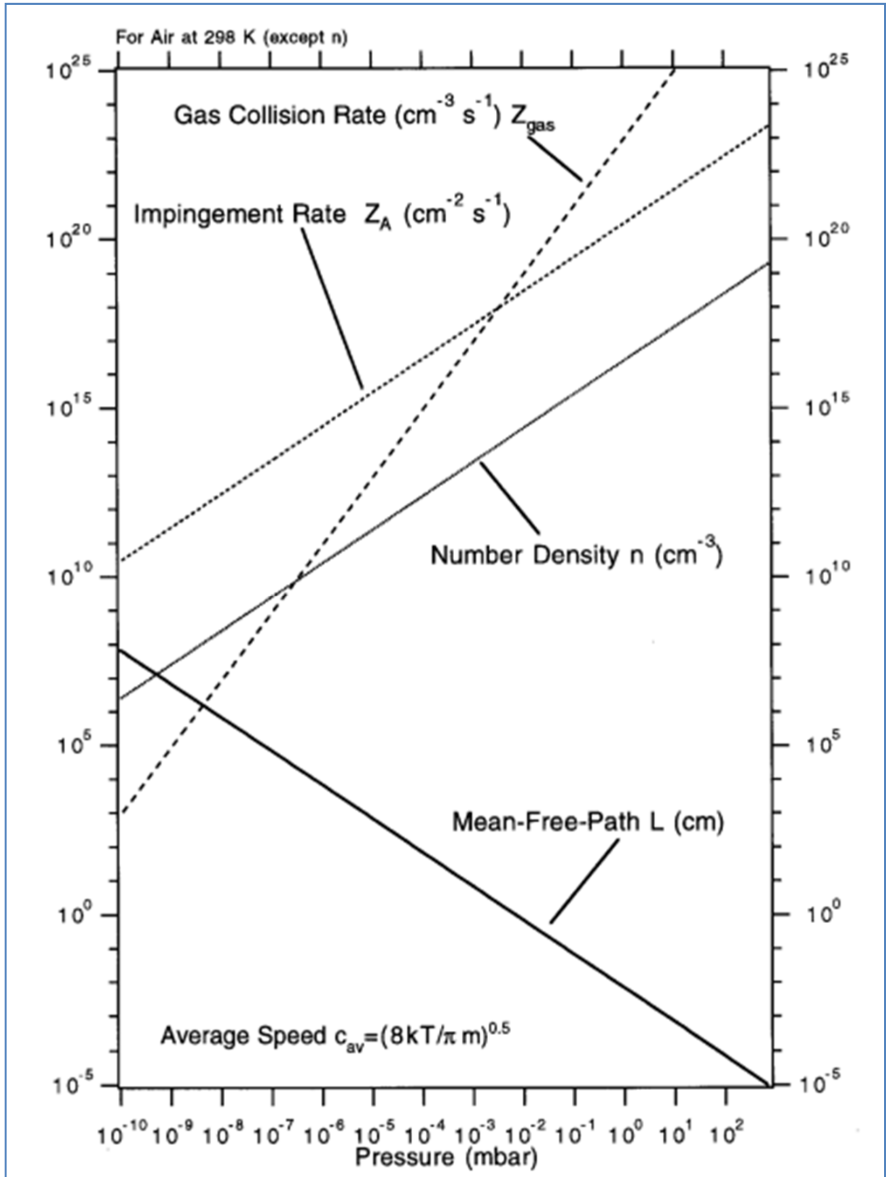

Concepts of gas kinetics:

The a-dimensional **Knudsen number K_n** translates into numerical values the considerations expressed here above. It is defined as the ratio between the mean free path and **a characteristic dimension of a vacuum system** (**D**).

$$K_n = \frac{\bar{\lambda}}{D}$$

The values of K_n delimit **three gas dynamic regimes** as reported in Tab. 7:

Table 7: Gas dynamic regimes defined by the Knudsen number

K_n range	Regime	Description
$K_n >$ 1~10	Free molecular flow	Molecule-wall collisions dominate
$K_n < 0.01$	Continuous (viscous) flow	Gas dynamic dominated by intermolecular collisions
1~10 $< K_n < 0.01$	Transitional flow	Transition between molecular and viscous flow

Concepts of gas kinetics:

- In modern synchrotrons, typical beam pipe diameters are of the order of 1~10 cm. Therefore, free molecular regime is obtained for pressures in the low 10^{-3} mbar range or lower. Except for areas where gas are intentionally injected into the system (e.g. “gas curtain beam detectors”, calibrated-leaks experiments);
- The free molecular flow regime characterizes and determines the pumping and pressure reading mechanisms that can be used in particle accelerators. Pumps and instruments must act on single molecules since there is no interaction between molecules.

→ Collective phenomena like pressure waves and suction do not influence gas dynamics in free molecular flow. ←

Free-molecular flow conductance:

In free molecular regime, the net gas flow Q between two points of a vacuum system is proportional to the pressure difference (P_1-P_2) at the same points:

$$Q = C\,(P_1 - P_2)$$

C is called the gas conductance of the vacuum system between the two points.

- In free molecular regime, the conductance does not depend on pressure. It depends only on the mean molecular speed and vacuum system geometry.
- If the gas flow units are expressed in terms of pressure-volume (for example mbar l s^{-1} or Pa m^3 s^{-1}, the **conductance** is reported as **volume per unit time**, i.e. **l s^{-1}** or **m^3 s^{-1}**).

The conductance is easily calculated for the simplest geometry, i.e. a small wall slot of **surface area A** and infinitesimal thickness dividing two volumes of the same vacuum system:

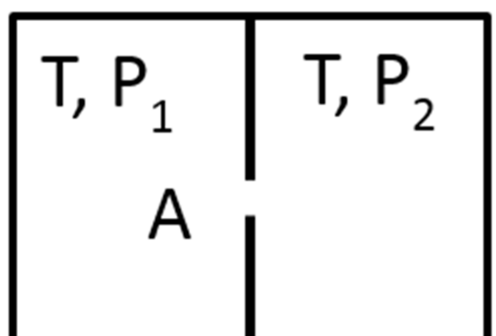

Free-molecular flow conductance:

The net flow of molecules from one volume to the other may be calculated by the **molecular impingement rate** given before. The number of molecules of volume 1 that go into volume 2 ($\varphi_{1\to2}$) is:

$$\varphi_{1\to2} = \frac{1}{4} A\, n_1 \langle v \rangle$$

while that from volume 2 to volume 1 is:

$$\varphi_{2\to1} = \frac{1}{4} A\, n_2 \langle v \rangle$$

The net molecular flow is given by the difference of the two contributions:

$$\varphi_{1\to2} - \varphi_{2\to1} = \frac{1}{4} A\, (n_1 - n_2) \langle v \rangle$$

$$\varphi_{1\to2} - \varphi_{2\to1} = \frac{1}{4} A \frac{\langle v \rangle}{k_B T} (P_1 - P_2)$$

Multiplying both terms of the equality by $k_B T$ and applying the ideal gas equation, the **gas flow in pressure-volume units** is obtained:

$$Q = \frac{1}{4} A \langle v \rangle (P_1 - P_2)$$

Free-molecular flow conductance:

Comparing these equations, it comes out that the conductance of the wall slot is proportional to the surface area of the slot and the mean speed of the molecules:

$$C = \frac{1}{4}A\langle v\rangle \propto \sqrt{\frac{T}{m}}$$

From the previous equations, it comes out that the conductance of the wall slots is **inversely proportional to the square root of the molecular mass**. Therefore, for equal pressure drop the gas flow of H_2 is the highest. Finally, for gas molecules of different masses, the **conductance scales as the square root of the inverse mass ratio**:

$$\frac{C_1}{C_2} = \sqrt{\frac{m_2}{m_1}}$$

As an example, the conductance for N_2 is $\sqrt{\frac{2}{28}} = 0.27$ times that for H_2, namely 3.7 times lower. Table 8 collects conductance values, for an orifice, **per unit surface area** (**C'**) at room temperature for common gas species.

Table 8: Unit surface area conductances for common gas species in two different units

Gas	**H_2**	**He**	**CH_4**	**H_2O**	**N_2**	**Ar**
C' at 293 $K\left[\frac{m^3}{s\,m^2}\right]$	440.25	311	155.5	146.7	117.5	98.5
C' at 293 $K\left[\frac{l}{s\,cm^2}\right]$	44	31.1	15.5	14.7	11.75	9.85

Transmission probability:

For more complex geometries than wall slots, the **transmission probability** τ is introduced. If two vessels, at the same temperature, are connected by a duct (see figure below for symbols), the gas flow from vessel 1 to vessel 2 ($\varphi_{1\to2}$) is calculated by multiplying the number of molecules impinging on the entrance section of the duct by the probability $\tau_{1\to2}$ for a molecule to be transmitted into vessel 2 without coming back to vessel 1:

$$\varphi_{1\to2} = \frac{1}{4} A_1 n_1 \langle v \rangle \, \tau_{1\to2}$$

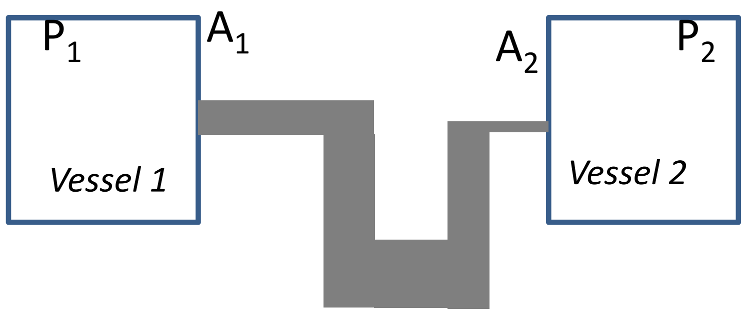

Similarly, the gas flow from vessel 2 to vessel 1 is written as: $\varphi_{2\to1} = \frac{1}{4} A_2 \, n_2 \langle v \rangle \, \tau_{2\to1}$

In absence of net flow, $\varphi_{1\to2} = \varphi_{2\to1}$ and $n_1 = n_2$, then: $A_1 \tau_{1\to2} = A_2 \tau_{2\to1}$

When $n_1 \neq n_2$ a net flow is set up. It can be calculated by combining the previous equations:

$$\varphi_{1\to2} - \varphi_{2\to1} = \frac{1}{4} A_1 \langle v \rangle \, \tau_{1\to2} \, \frac{(P_1 - P_2)}{k_B T}$$

where, as already mentioned, C′ is the **conductance of the unit surface area wall slot**.

Transmission probability:

Comparing the equations, it comes out that the conductance of the connecting duct is equal to the **conductance of the duct entrance in vessel 1**, considered as a wall slot, **multiplied by the molecular transmission probability from vessel 1 to vessel 2**:

$$C = C' A_1 \, \tau_{1\to 2}$$

Evaluation of the transmission probability:

In general, only for simple and constant cross-sections of the tubes can the transmission probability be calculated precisely, via some analytical formulae or tabulated data.

One notable example is **Santeler's equation**, giving t for a tube of circular cross-section of **radius R** and **length L** (accuracy is good, <0.7% error):

$$\tau = \tau_{1\to 2} = \tau_{2\to 1} = \frac{1}{1 + \frac{3L}{8R}\left(1 + \frac{1}{3\left(1 + \frac{L}{7R}\right)}\right)}$$

For long tubes, i. e. $\frac{L}{R} \gg 1$, the equation can be simplified to:

$$\tau \approx \frac{1}{1 + \frac{3L}{8R}} \approx \frac{8}{3}\frac{R}{L}$$

Transmission probability:

Santeler's formula for the transmission probability of a round tube vs Montecarlo calculation:

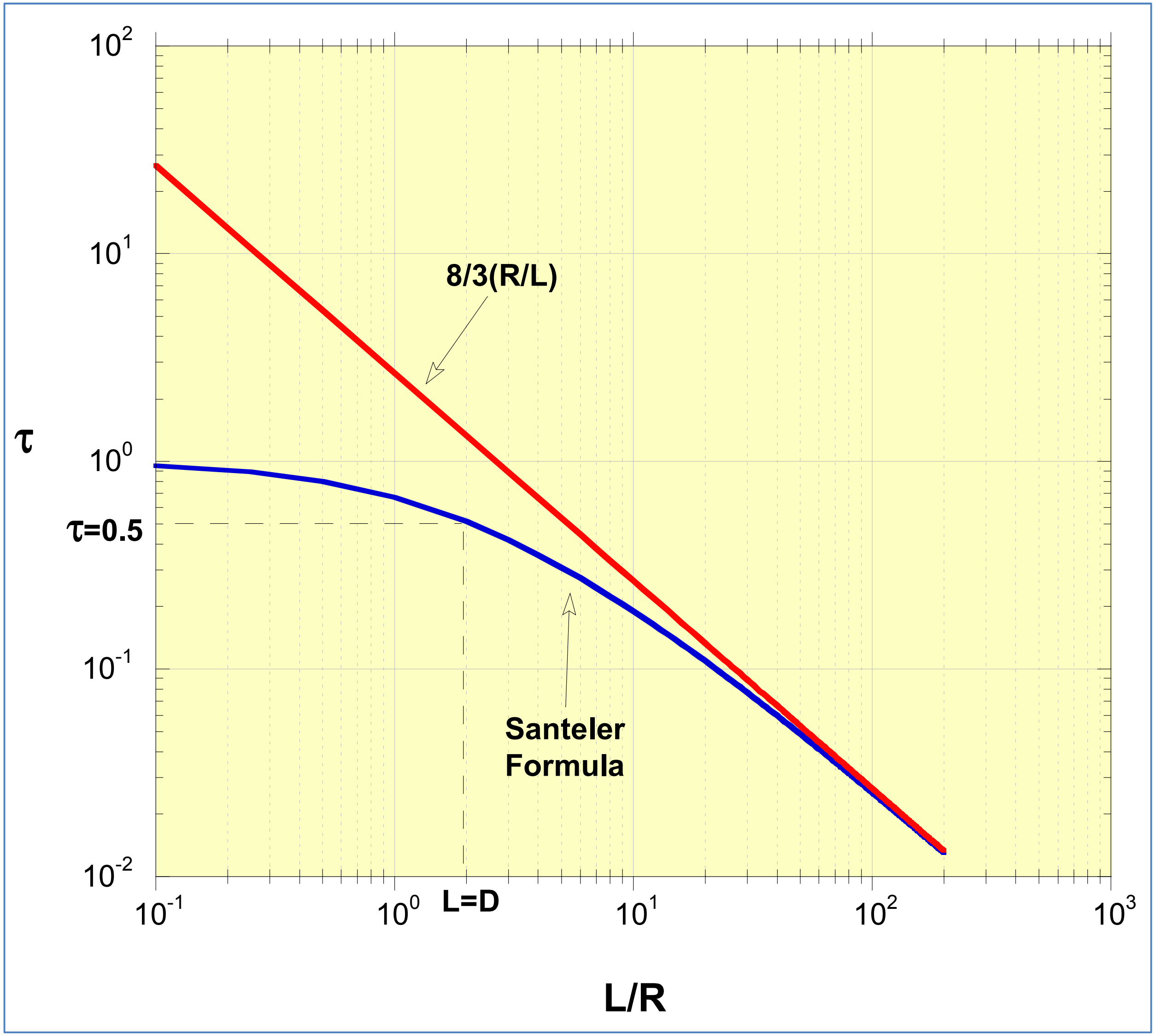

L/R	Cole mean value[e]
0.1	0.952 398 907
0.2	0.909 215 028
0.3	0.869 928 148
0.5	0.801 271 420
0.7	0.743 409 790
0.9	0.694 043 732
1.0	0.671 983 902
1.2	0.632 228 253
1.4	0.597 364 010
1.6	0.566 507 335
1.8	0.538 974 541
2.0	0.514 230 527
3.0	0.420 055 30
4.0	0.356 572 25
5.0	0.310 524 62
6.0	0.275 438 20
7.0	0.247 735 33
8.0	0.225 262 78
9.0	0.206 640 69
10.0	0.190 941 0
20.0	0.109 304
30.0	0.076 912
40.0	0.059 422
50.0	0.048 448
60.0	0.040 913
70.0	0.035 415
80.0	0.031 225
90.0	0.027 925
100.0	0.025 258
200.0	
500.0	
1000.0	0.002 6461

The basis of vacuum technology: conductance

Conductance of components connected in series:

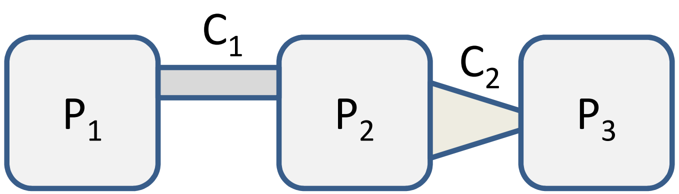

$$Q_1 = C_1(P_1 - P_2)$$
$$Q_2 = C_2(P_2 - P_3)$$
$$Q_{TOT} = C_{TOT}(P_1 - P_3)$$

In stable conditions, there is no gas accumulation in the whole system: $Q_1 = Q_2 = Q_{TOT}$

It can be easily verified that: $C_{TOT} = \frac{C_1 C_2}{C_1 + C_2}$ and $\frac{1}{C_{TOT}} = \frac{1}{C_1} + \frac{1}{C_2}$:

In general for N vacuum components traversed by the same gas flux, i.e. placed **in series** :

$$\frac{1}{C_{TOT}} = \sum_{1}^{N} \frac{1}{C_i}$$

The basis of vacuum technology: conductance

For components connected in **parallel** (same pressures at the extremities):

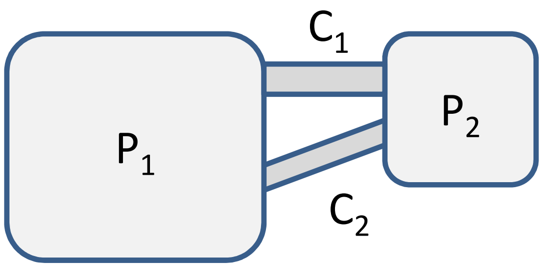

$$Q_1 = C_1(P_1 - P_2)$$
$$Q_2 = C_2(P_1 - P_2)$$
$$Q_{TOT} = C_{TOT}(P_1 - P_2)$$

$$Q_{TOT} = Q_1 + Q_2 \rightarrow C_{TOT} = C_1 + C_2$$

$$C_{TOT} = \sum_{1}^{N} C_i$$

The basis of vacuum technology: pumping speed

In vacuum technology **a pump** is **any 'object' or surface treatment** that remove gas molecules from the gas phase.

The pumping speed **S** of a pump is defined as the **ratio** between the **pump throughput Q_P** (flow of gas definitively removed) and the **pressure P at the entrance** of the pump:

$$S = \frac{Q_P}{P}$$

$$[S] = \frac{[Volume]}{[Time]} = [conductance]$$

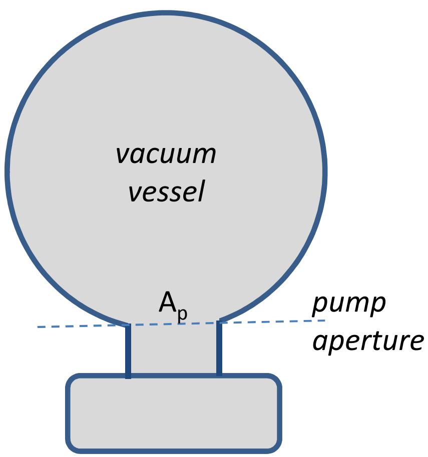

The basis of vacuum technology: pumping speed

The gas removal rate can be written as:

$$Q_P = \frac{1}{4} A_P \, n\langle v\rangle \, \sigma = A_P \, C' n \, \sigma$$

A_P: is the area of the pump aperture
C': is the **conductance of the unit surface area**
n: the gas density
σ : the **capture probability**, i.e. the probability that a molecule entering the pump is ultimately captured; also called **equivalent sticking coefficient**;

As usual, in term of pressure and PV units:

$$Q_P = A_P C' n \, \sigma (k_B T) = A_P C' \sigma \, P$$

From the definition of pumping speed:

$$\boldsymbol{S = A_P C' \sigma}$$

The basis of vacuum technology: pumping speed

S depends on the conductance of the pump aperture $A_P C'$ and the **capture probability σ.**

σ is <u>in general</u> not a constant; it may depend on many parameters including pressure, gas specie, and quantity of gas already pumped ('saturable' pumps, like Ti-sublimation or Non-Evaporable Getter (NEG) pumps):

$$\boldsymbol{S = A_P C' \sigma}$$

→ The **maximum pumping speed** is obtained for $\boldsymbol{\sigma = 1}$ and is **equal to the conductance of the pump aperture** ←

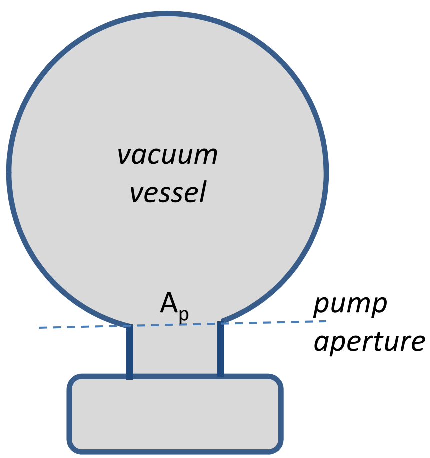

Maximum pumping speed [l s^{-1}]for different **circular** pump apertures (flanged)

ID [mm]	H_2	N_2	Ar
36	448	120	100
63	1371	367	307
100	3456	924	773
150	7775	2079	1739

Example: what is the capture probability for N_2 of a 500 l/s pump having a 150 mm ID flange? $\boldsymbol{\sigma} = \boldsymbol{S}/(\boldsymbol{A_P C'})$ = 500 / 2079 = 0.2405

The basis of vacuum technology: pumping speed

A gas flow restriction interposed between a pump and a vacuum vessel reduces the 'useful' pumping speed.

The **effective pumping speed S_{eff}** 'seen' by the vacuum vessel is easily calculated:

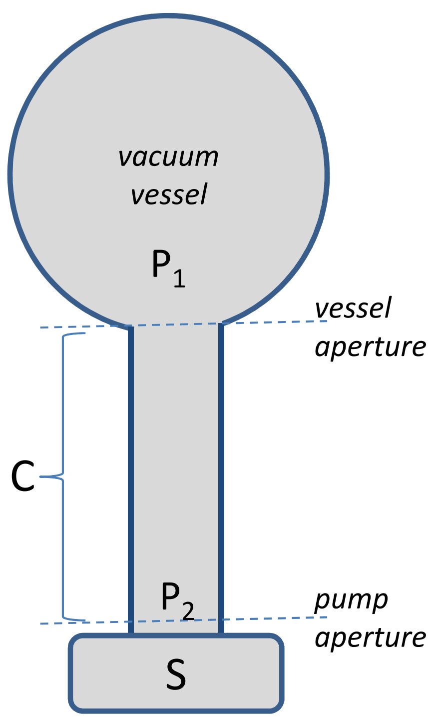

$$Q = C_1(P_1 - P_2) = SP_2 = S_{eff}P_1$$

$$\frac{1}{S_{eff}} = \frac{1}{S} + \frac{1}{C}$$

For C<<S: $S_{eff} \approx C$

The basis of vacuum technology: pumping speed

Example 1:

Vessel and pump connected by a **10 cm diameter** tube; N_2, S=250 l/s and 1000 l/s.

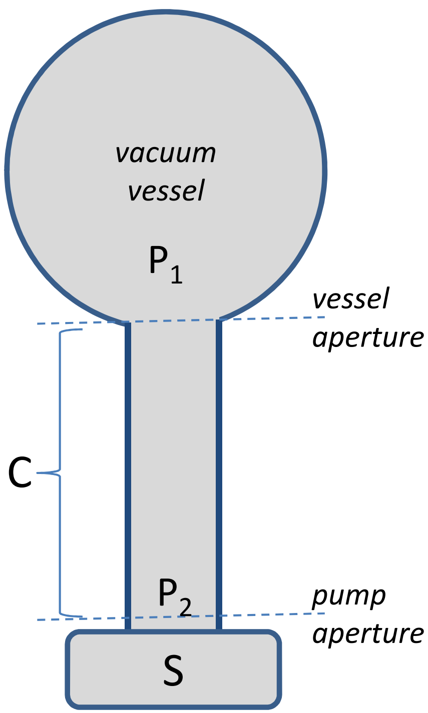

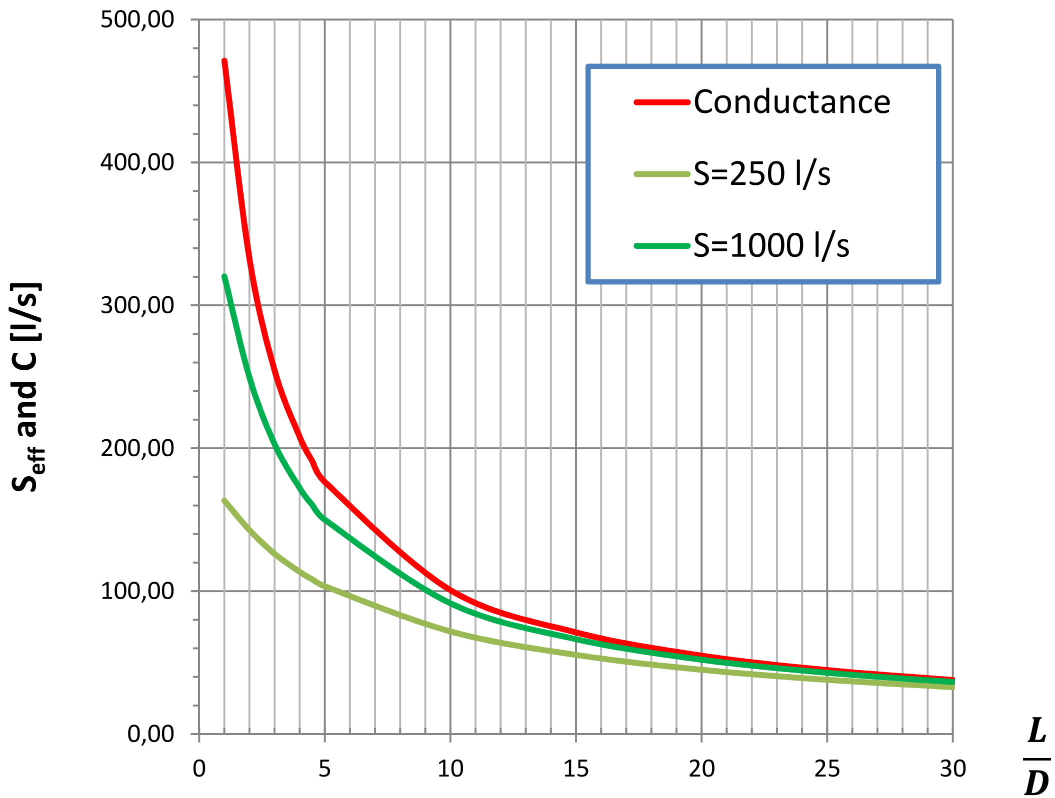

Example 2: Is this pumping arrangement efficient?

Example 3:

- The **specific conductance** of a 22 mm ID m circular cross-section is 1.312 **l·m/s (~MAX-IV and SIRIUS)**
- In a uniform cross-section tube with uniform longitudinal outgassing, a **regular pump spacing** of **L** meters will decrease the installed pumping speed $\mathbf{S_{inst}}$ via the equation seen before:

$$1/S_{eff} = 1/S_{inst} + 1/\mathbf{C_{spec}} \rightarrow S_{eff} = (1/S_{inst} + L/12/\mathbf{C_{spec}})^{-1}$$

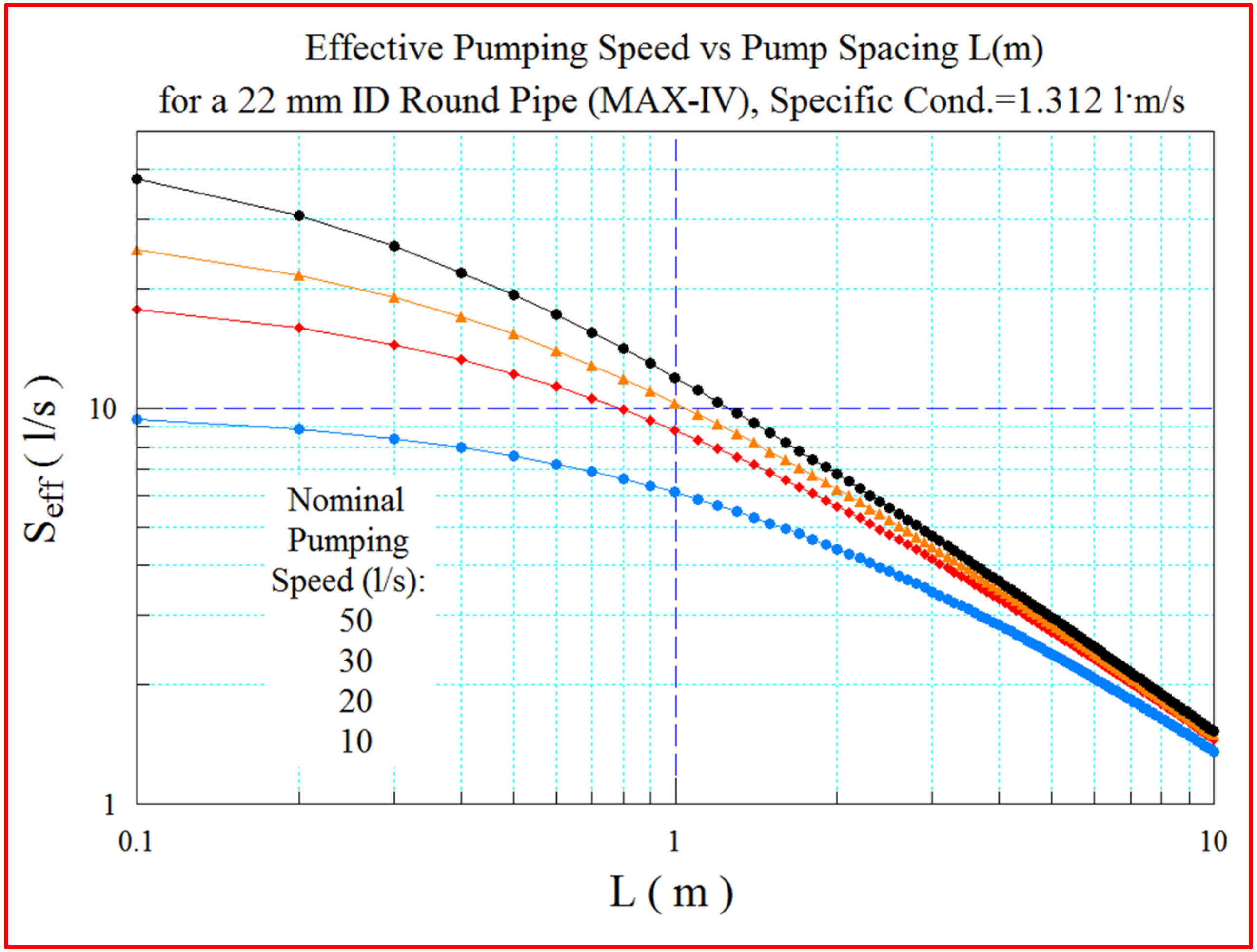

General case; arbitrary shapes:

- For tubes of arbitrary non-uniform cross-section and shape, there is no analytical solution to the **integro-differential equations** (not discussed here for lack of time).
- **Unfortunately this is the case for most synchrotron light sources**, where e.g. the dipole/crotch chambers have a "Y" shape and are connected to straight parts going through the FODO sections (quadrupoles/sextupoles necessary for "beam optics").
- In this case a number of approximate numerical methods have been developed during the years, and among them (*)
  - "Slicing" the system in short segments and applying the **Continuity Principle of Gas Flow** (**Finite-Elements codes**, either proprietary or custom-written);
  - Slicing/subdividing the system in short segments and applying the **Electric-Network Analogy** (**ENA**), and then using codes like **LTSpice**;
  - **Angular coefficients method** (analogy to thermal radiation propagation);
  - Applying the **Test-Particle Monte Carlo method** (**TPMC**). The components are modelled in three dimensions, possibly by means of a CAD program.

In a nutshell:

- The TPMC codes generate molecules at the entrance of the component pointing in 'random' directions according to the **Lambertian cosine distribution**. When the molecules impinge on the internal wall of the component, they are re-emitted again randomly, unless pumped.
- The program follows the molecular traces until they reach the exit of the component.

(*) For a review see for instance: "***Analytical and Numerical Tools for Vacuum Systems***", R. Kersevan, CERN Accelerator School, Platja d'Aro, Spain, 2006,… and references therein.

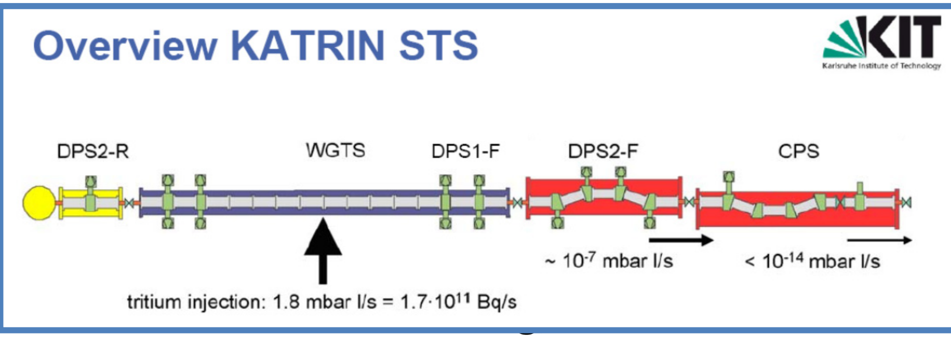

ing, conductance, pumping speed

e of arbitrary shapes:

e ratio between the number of 'escaped'

l molecules are needed to reduce the

(e.g. **KATRIN** neutrino mass experiment case)

- The reference TPMC software at CERN is **MolFlow+**. This powerful tool for high-vacuum applications can import the 3-D drawing of the vacuum components and generate 'random' molecules on any surface of interest.
- The randomness of the generation follows the **physical laws of vacuum technology**: for **thermal desorption** it is assumed to be **spatially uniform** on surfaces and depending only on the wall material properties (temperature, surface finish, chemical cleaning procedure, bake-out,…) while for **synchrotron radiation (SR) induced gas desorption** it is derived from the distribution of photons hitting the walls of the system (e.g. see below, **SYNRAD+** code), which are then converted into molecular fluxes using **empirical/experimental data** (see further below).
- CERN develops, maintains, and uses on a daily basis the TPMC code Molflow+, which has become the *de-facto* standard in the field of particle accelerator design:

https://test-molflow.web.cern.ch/

General case; arbitrary shapes: Molflow+ TPMC code

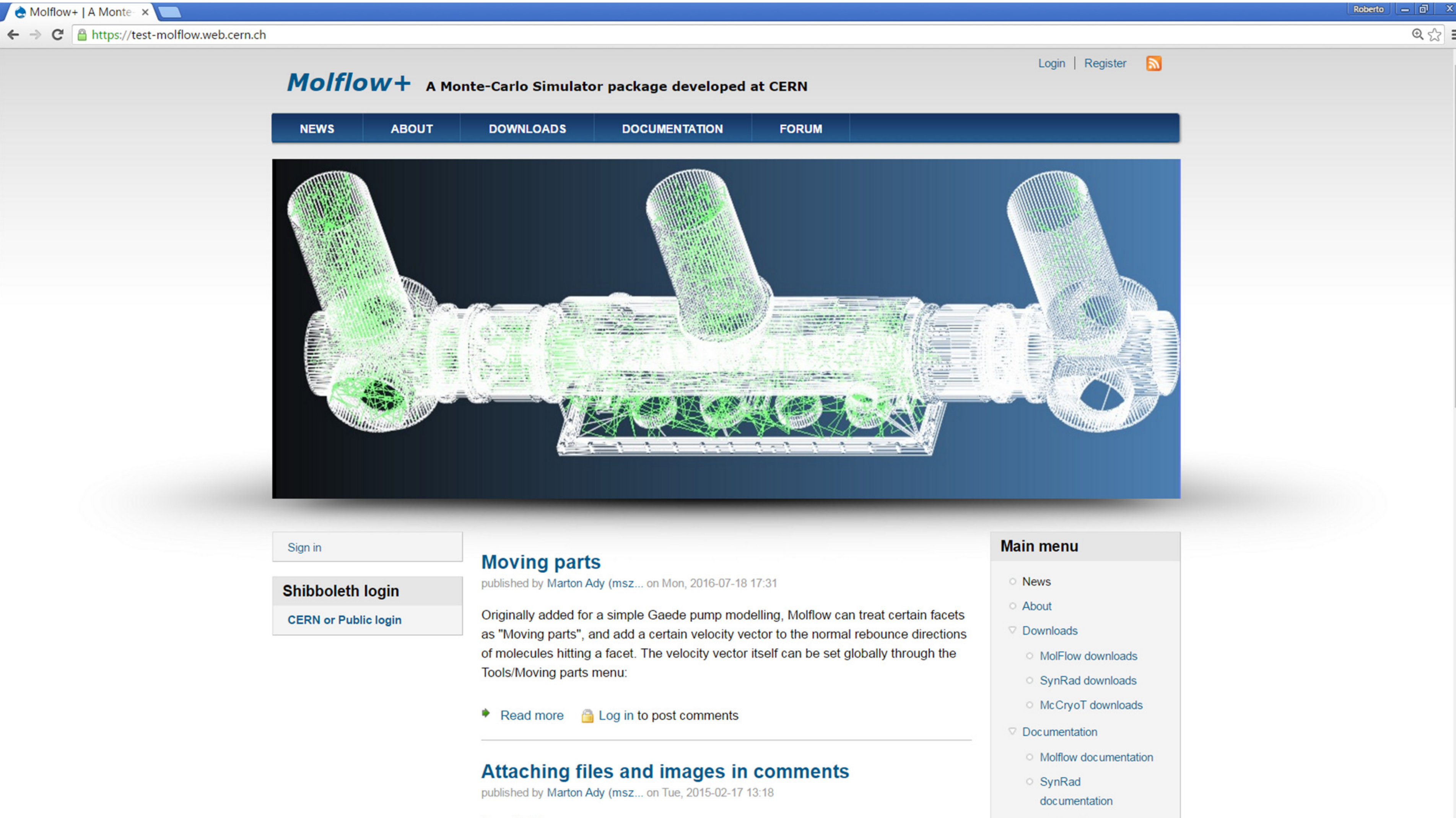

On ***Molflow+*** and the companion code ***SYNRAD+***, please see the excellent reference "***Monte Carlo simulations of Ultra High Vacuum and Synchrotron Radiation for particle accelerators***", M. Ady, CERN, doctoral dissertation at EPFL, Lausanne, CH, May 2016; Dowloadable at https://cds.cern.ch/record/2157666?ln=en

General case; arbitrary shapes: Molflow+ TPMC code

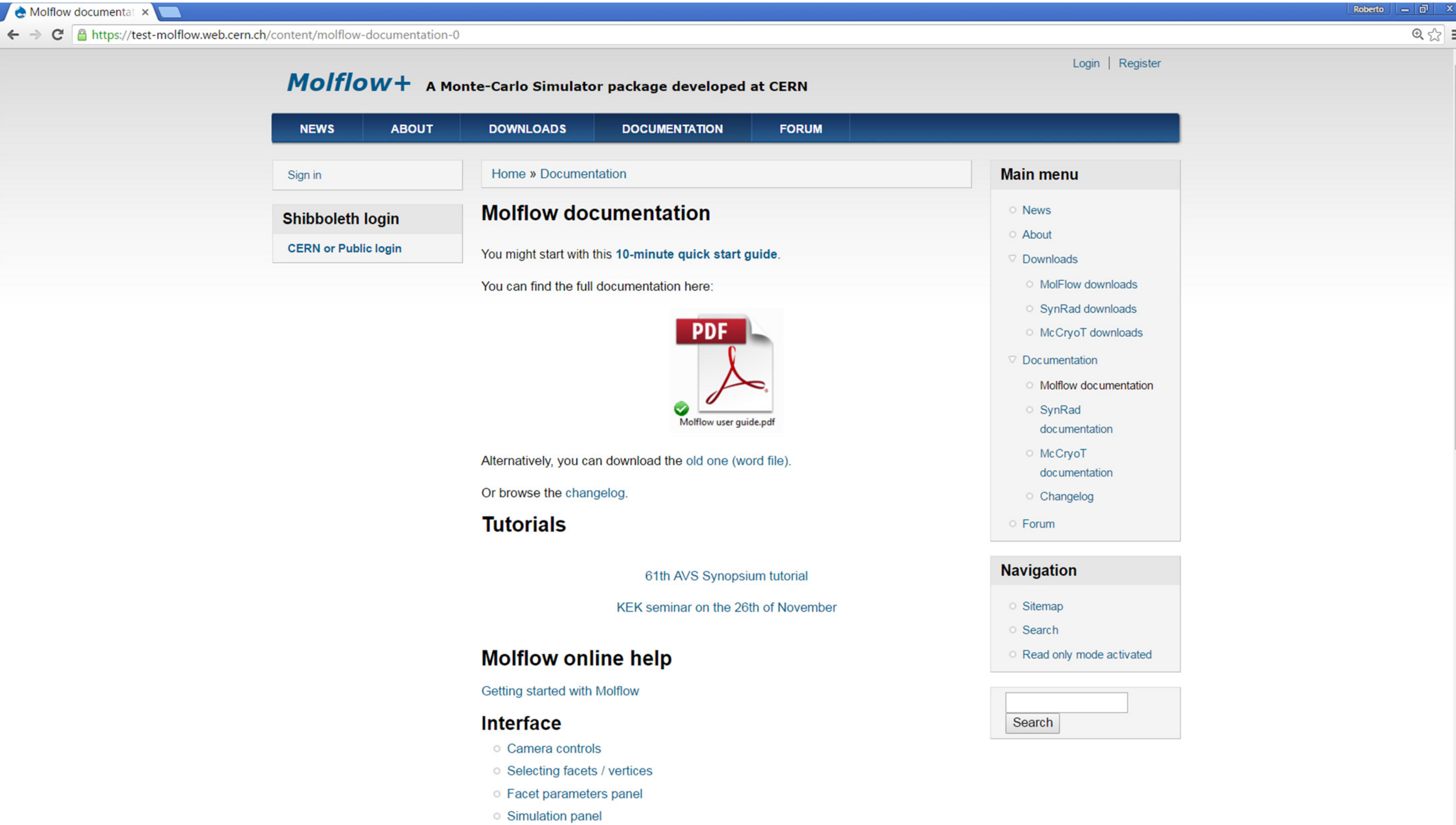

Block diagram of the TPMC algorithm:

Once a geometrical model of the vacuum system is defined, then… →

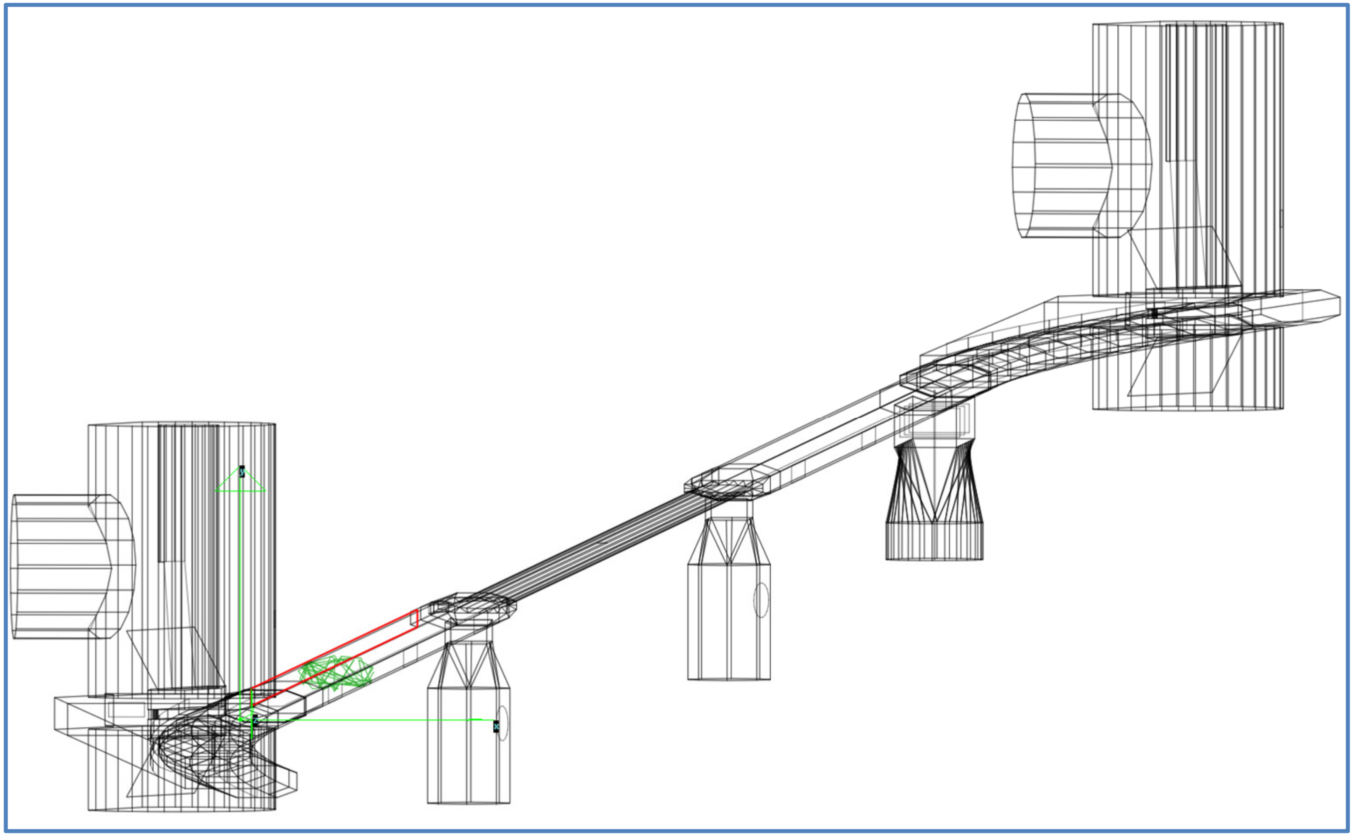

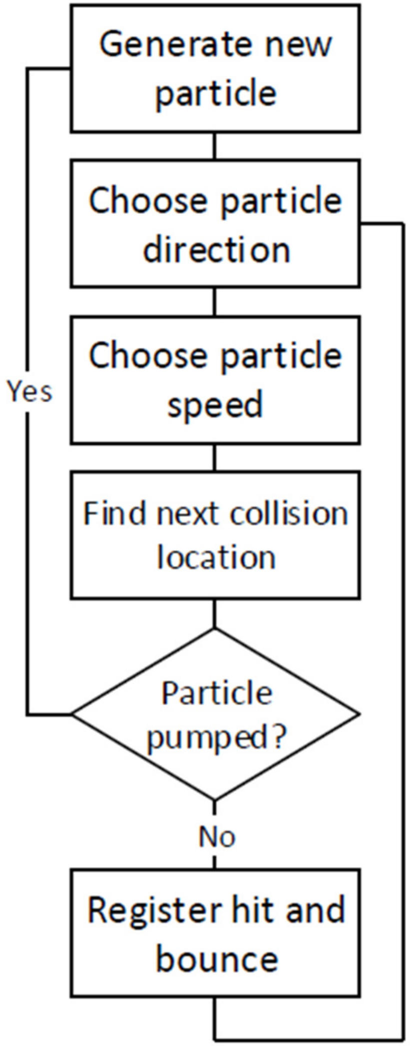

TPMC method

TPMC method and algorithm:

- Let's assume, without loss of generality, that a vacuum system be modeled using polygonal planar facets;
- Let XYZ be an arbitrary cartesian frame of reference;
- Let X"Y"Z" be the frame of reference whose origin corresponds to the location of a molecule located on the facet, with Z" perpendicular to the facet;
- Let X'Y'Z' a frame of reference parallel to X"Y"Z", whose origin is the same as XYZ;
- Let α and β be defined as such: β is the rotation about the Y axis which takes X onto X'; α is the rotation about X (X') which makes Y become Y';
- With such definitions, the following transformations can be written:

$$\begin{pmatrix} X'' \\ Y'' \\ Z'' \end{pmatrix} = \begin{pmatrix} 1 & 0 & 0 \\ 0 & \cos\alpha & \sin\alpha \\ 0 & -\sin\alpha & \cos\alpha \end{pmatrix} \begin{pmatrix} X' \\ Y' \\ Z' \end{pmatrix}$$

$$\begin{pmatrix} X \\ Y \\ Z \end{pmatrix} = \begin{pmatrix} \cos\beta & 0 & \sin\beta \\ 0 & 1 & 0 \\ -\sin\beta & 0 & \cos\beta \end{pmatrix} \begin{pmatrix} X'' \\ Y'' \\ Z'' \end{pmatrix}$$

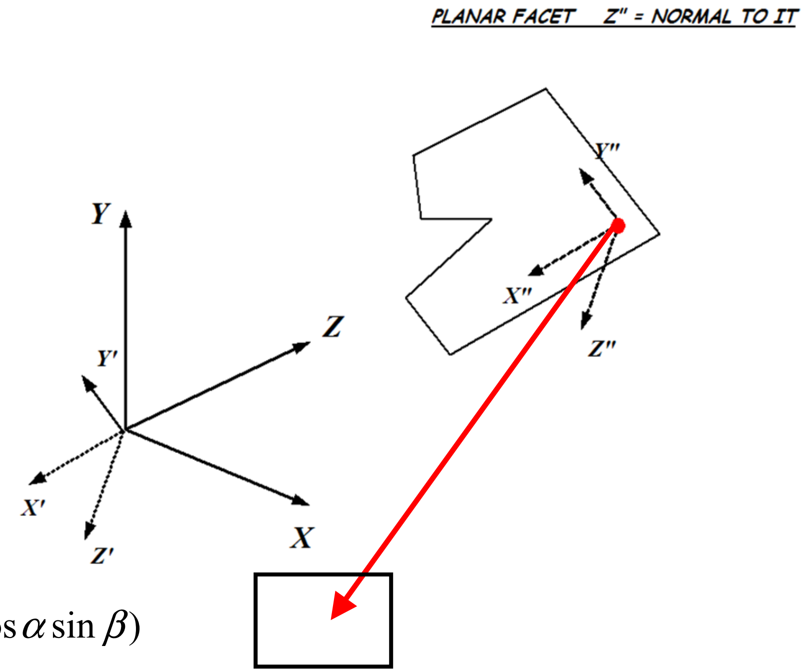

- Upon desorption of the molecule from the source facet s, let L be the generic length of the trajectory to the next target facet t;

$$X'' = L\sin\theta\cos\varphi$$
$$Y'' = L\sin\theta\sin\varphi$$
$$Z'' = L\cos\theta$$

- Combining the two relations, one gets

$$X_t = X_s + L_t(\sin\theta\cos\varphi\cos\beta - \sin\theta\sin\varphi\sin\alpha\sin\beta - \cos\theta\cos\alpha\sin\beta)$$
$$Y_t = Y_s + L_t(\sin\theta\sin\varphi\cos\alpha - \cos\theta\sin\alpha)$$
$$Z_t = Z_s + L_t(\sin\theta\cos\varphi\sin\beta + \sin\theta\sin\varphi\sin\alpha\cos\beta + \cos\theta\cos\alpha\cos\beta)$$

where the value for L, L_t, i.e. the length of the trajectory to the next facet encountered, is a function of the geometric description of facet t, and it is not given here (see (*) and references therein)

(*) "Molflow User´s Guide, R. Kersevan, Note ST/M-91/17, Sincrotrone Trieste

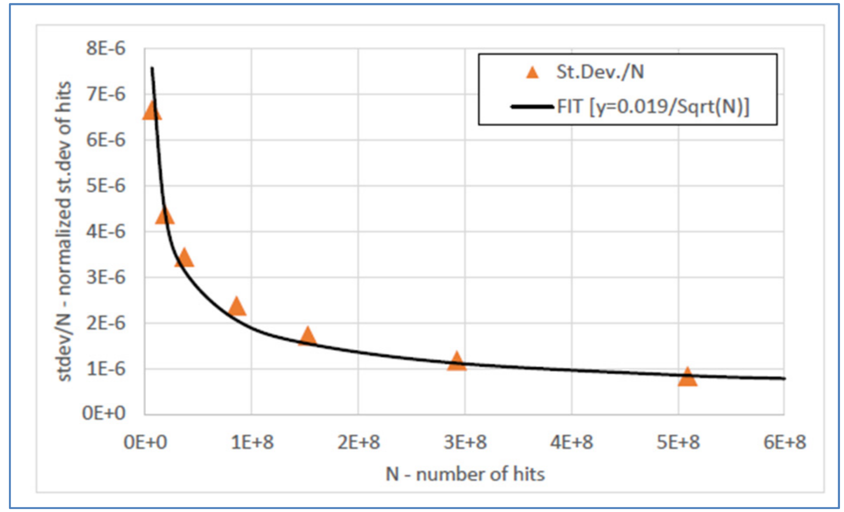

<u>TPMC method #2:</u>

- **Averaging over a large number of molecular traces yields estimates of the pressure, inpingement rate, conductance, pumping speed, etc…:**

- Let N be the number of molecules entering, for instance, a tube from one end;

- Let m be the number of molecules leaving the tube at the other end:

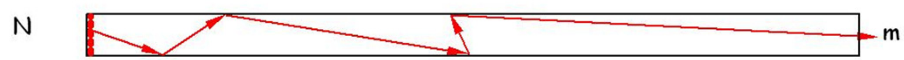

w = m/N   is the **<u>transmission probability</u>**;

- The values for w follow a **<u>binomial distribution</u>**, which has a standard deviation

$$\sigma = \sqrt{\frac{w \cdot (1-w)}{N}}$$

- If n_i is the number of molecular hits in the i-th segment of the tube, and P_i the associated pressure, then the normalized standard deviation for the pressure P_i is:

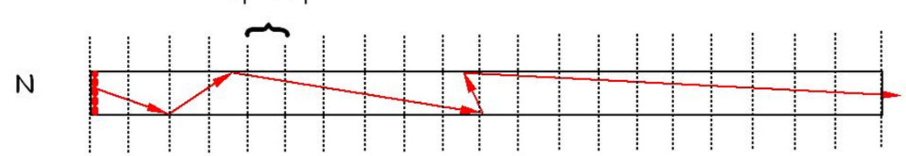

$$\sigma_{n_i}(\%) = \sqrt{\frac{1}{n_i}\left(1-\frac{n_i}{N}\right)} \cdot 100$$

From Y. Suetsugu, JVST A14(1), 1996 p.245-250; M. Ady, op. cit.

TPMC method #3: how to convert from molecular hits to pressures:

- If n_i is the number of collisions on one segment of the vacuum chamber (A cm^2), and Q is the outgassing (in mbar·l/s), then Q/kT is the number of molecules/s. If N is the number of molecules traced, then, the mean number of collisions/cm^2 in that segment is

$$Z_i = {}^{n_i}\!/_{AN}$$

- The estimate of the impingement rate is

$$Z_i = \frac{n_i Q}{ANkT}$$

- At equilibrium, the relation between the pressure P_i (on segment i) and the corresponding impingement rate Z_i is

$$P_i = {}^{4kTZ_i}\!/_{v_a} = \frac{4Qn_i}{v_a AN}$$

$$P_{avg} = \frac{4Q}{v_a AN}\sum n_i$$

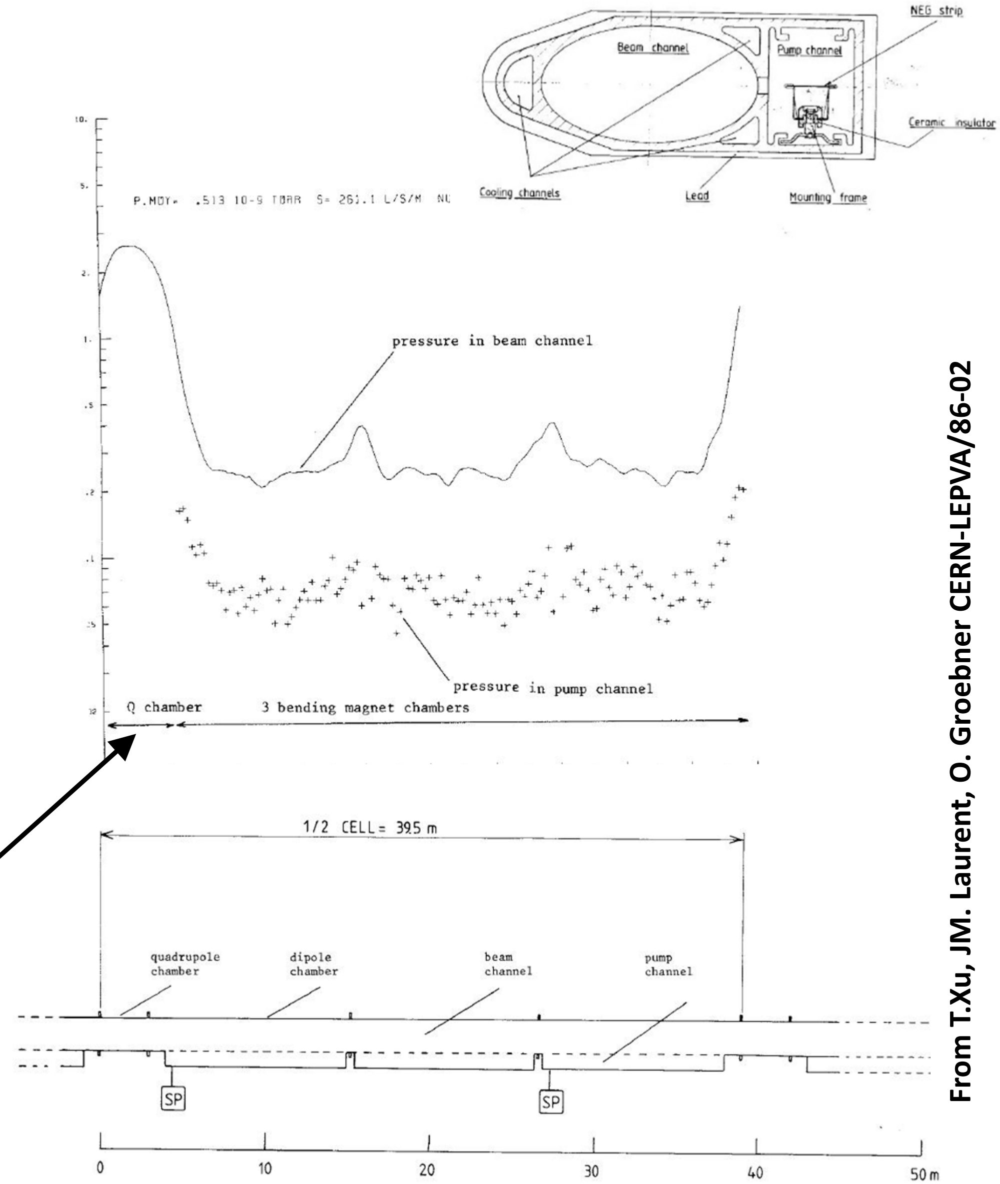

From T.Xu, JM. Laurent, O. Groebner CERN-LEPVA/86-02

TPMC method #4: non-stationary, time-dependent case

- **Time-dependent case**: **acoustic delay line** at Tristan synchrotron

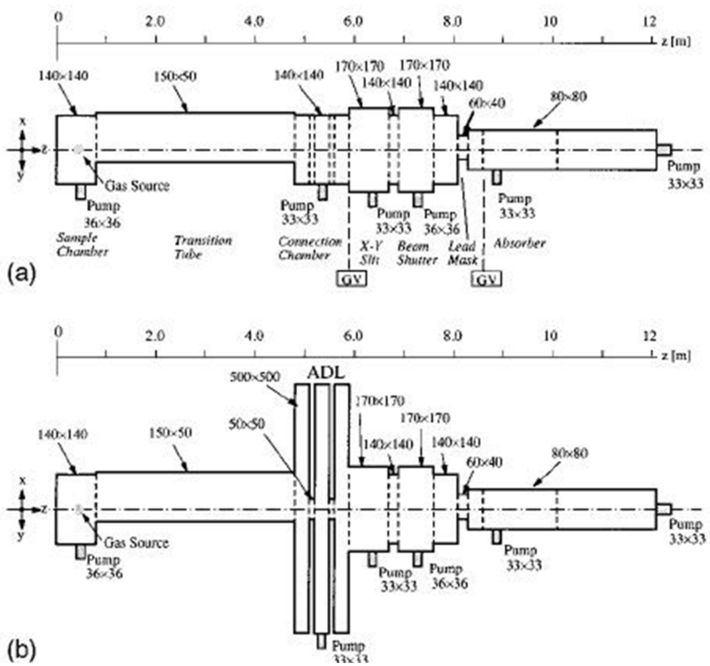

- **The length of all trajectories is translated into time intervals by means of the average molecular speed**

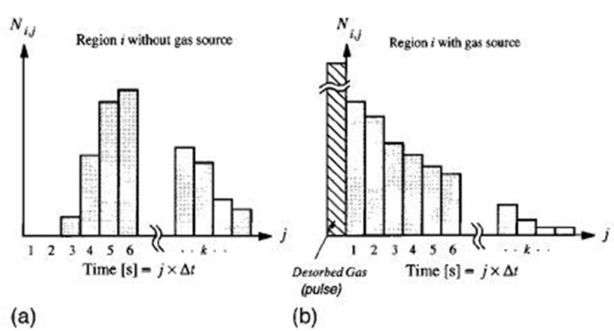

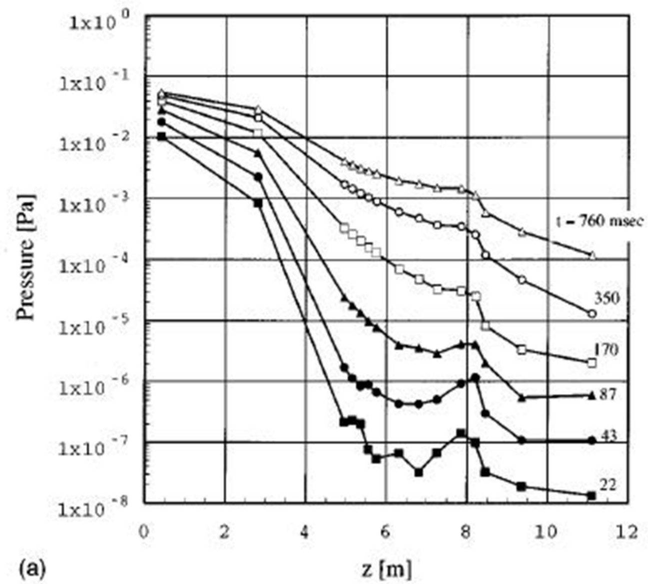

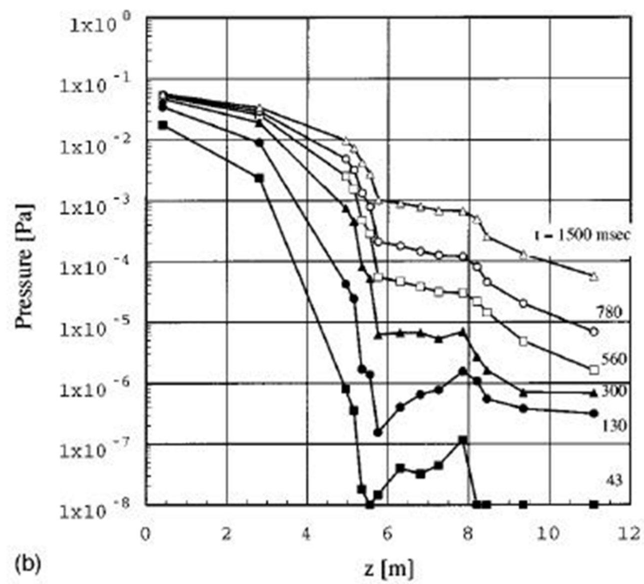

From Y. Suetsugu, JVST A14(1), 1996 p.245-250

TPMC method #5: non-stationary, time-dependent case via Molflow+

When there is a need to simulate transient vacuum effect one can instruct Molflow+ to use "**moments**", i.e. short intervals in time during which the collisions with the surfaces of the model are taken into consideration, and then translated into pressures or densities as in the steady-state, stationary case:

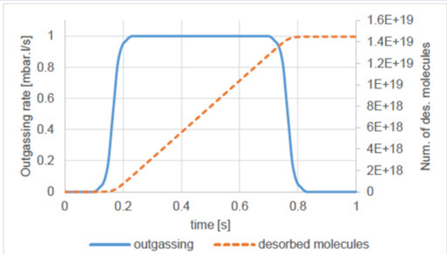

Desorption rate and number of desorbed molecules during injection

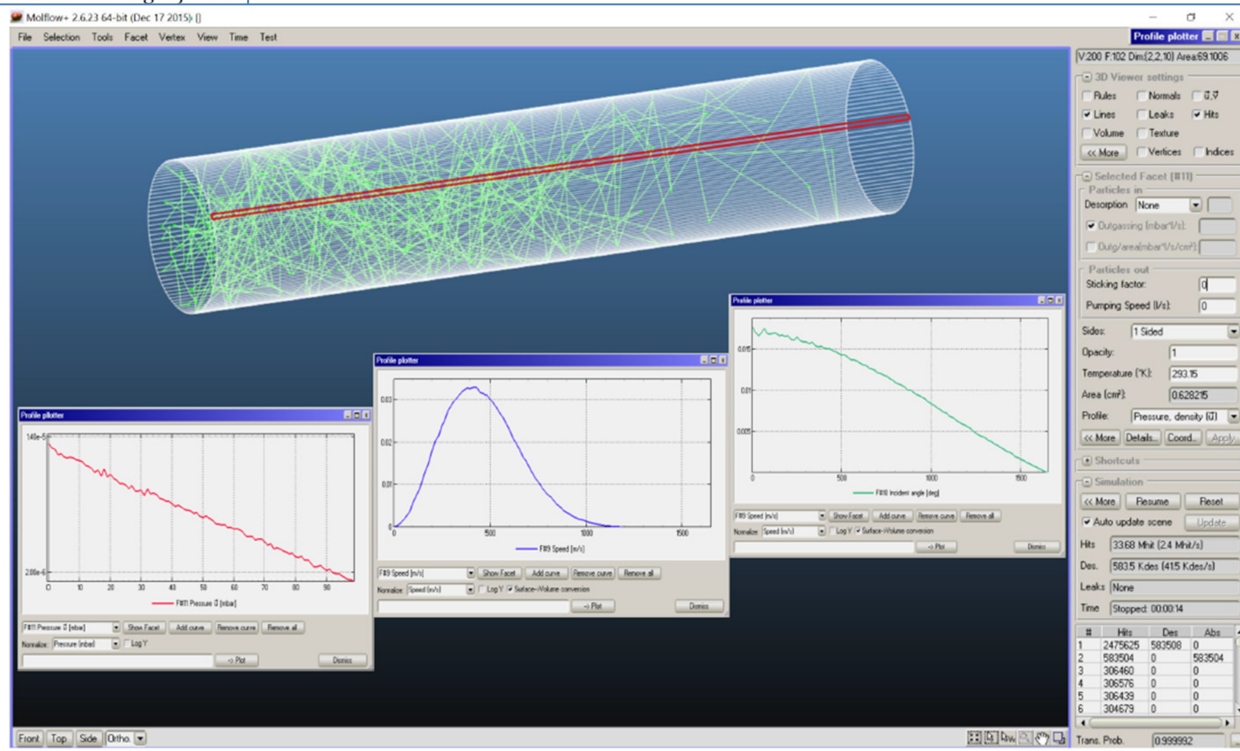

Figure 1.23: Pressure, speed and angular profiles for a simple tube within Molflow's interface

Ref: "Monte Carlo simulations of Ultra High Vacuum and Synchrotron Radiation for particle accelerators", M. Ady, CERN, doctoral dissertation at EPFL, Lausanne, CH, May 2016

TPMC method #6: convergence of the calculation

Ref: “Monte Carlo simulations of Ultra High Vacuum and Synchrotron Radiation for particle accelerators”, M. Ady, CERN, doctoral dissertation at EPFL, Lausanne, CH, May 2016

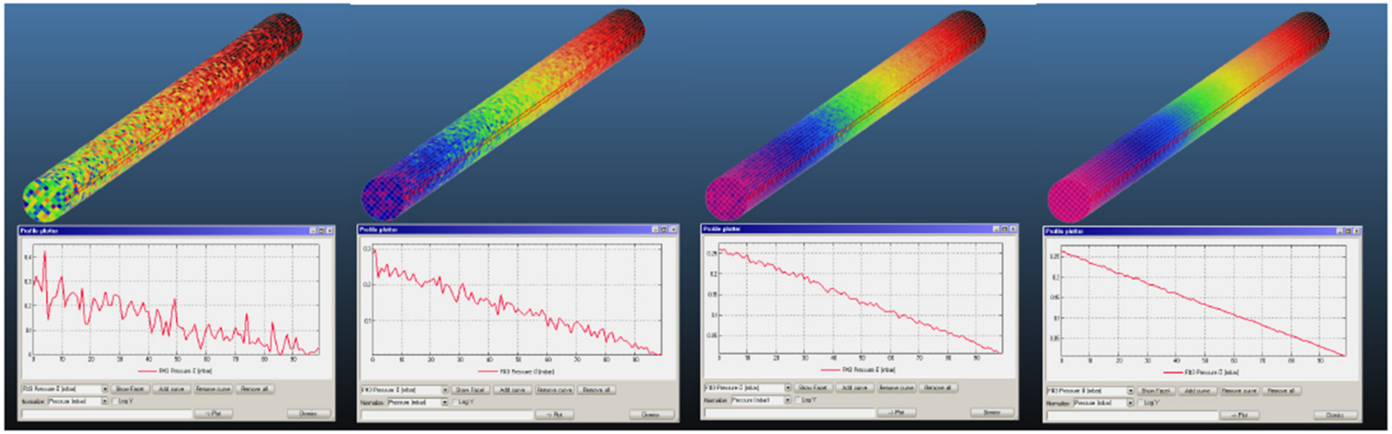

N=1.000 N=10.000 N=100.000 N=1.000.000

Figure 1.18: Texture and profile results for a vacuum tube with desorption at the left and pumping at both sides, as a function of the number of traced particles.

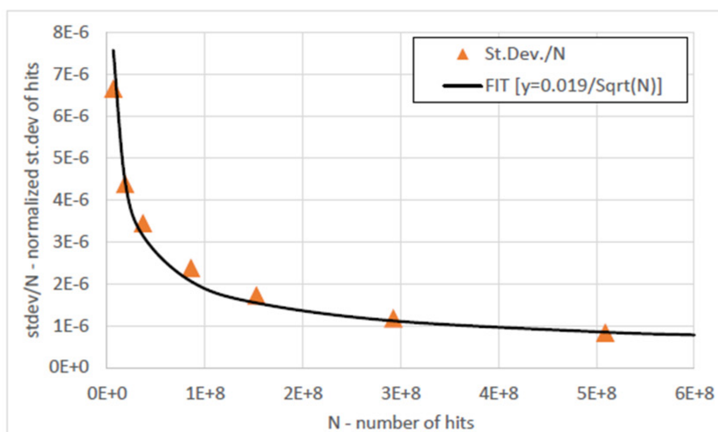

Figure 1.19: Normalized standard deviation of Molflow+ results as a function of the simulated

Sources: Schwinger; Sokolov-Ternov;

PHYSICAL REVIEW VOLUME 75, NUMBER 12 JUNE 15, 1949

On the Classical Radiation of Accelerated Electrons

JULIAN SCHWINGER
Harvard University, Cambridge, Massachusetts
(Received March 8, 1949)

This paper is concerned with the properties of the radiation from a high energy accelerated electron, as recently observed in the General Electric synchrotron. An elementary derivation of the total rate of radiation is first presented, based on Larmor's formula for a slowly moving electron, and arguments of relativistic invariance. We then construct an expression for the instantaneous power radiated by an electron moving along an arbitrary, prescribed path. By casting this result into various forms, one obtains the angular distribution, the spectral distribution, or the combined angular and spectral distributions of the radiation. The method is based on an examination of the rate at which the electron irreversibly transfers energy to the electromagnetic field, as determined by half the difference of retarded and advanced electric field intensities. Formulas are obtained for an arbitrary charge-current distribution and then specialized to a point charge. The total radiated power and its angular distribution are obtained for an arbitrary trajectory. It is found that the direction of motion is a strongly preferred direction of emission at high energies. The spectral distribution of the radiation depends upon the detailed motion over a time interval large compared to the period of the radiation. However, the narrow cone of radiation generated by an energetic electron indicates that only a small part of the trajectory is effective in producing radiation observed in a given direction, which also implies that very high frequencies are emitted. Accordingly, we evaluate the spectral and angular distributions of the high frequency radiation by an energetic electron, in their dependence upon the parameters characterizing the instantaneous orbit. The average spectral distribution, as observed in the synchrotron measurements, is obtained by averaging the electron energy over an acceleration cycle. The entire spectrum emitted by an electron moving with constant speed in a circular path is also discussed. Finally, it is observed that quantum effects will modify the classical results here obtained only at extraordinarily large energies.

EARLY in 1945, much attention was focused on the design of accelerators for the production of very high energy electrons and other charged particles.[1] In connection with this activity, the author investigated in some detail the limitations to the attainment of high energy electrons imposed by the radiative energy loss[2] of the accelerated electrons. Although the results of this work were communicated to various interested persons,[1,3,4] no serious attempt at publication[5] was made. However, recent experiments on the radiation from the General Electric synchrotron[6] have made it desirable to publish the portion of the investigation that is concerned with the properties of the radiation from individual electrons, apart from the considerations on the practical attainment of very high energies. Accordingly, we derive various properties of the radiation from a high energy accelerated electron; the comparison with experiment has been given in the paper by Elder, Langmuir, and Pollock.

I. GENERAL FORMULAS

Before launching into the general discussion, it is well to notice an elementary derivation of the total rate of radiation, based on Larmor's classical formula for a slowly moving electron, and arguments of relativistic invariance. The Larmor formula for the power radiated by an electron that is instantaneously at rest is

$$P=\frac{2}{3}\frac{e^2}{c^3}\left(\frac{d\mathbf{v}}{dt}\right)^2=\frac{2}{3}\frac{e^2}{m^2c^3}\left(\frac{d\mathbf{p}}{dt}\right)^2. \qquad \text{(I.1)}$$

Now, radiated energy and elapsed time transform in the same manner under Lorentz transformations, whence the radiated power must be an invariant. We shall have succeeded in deriving a formula for the power radiated by an electron of arbitrary velocity if we can exhibit an invariant that reduces to (I.1) in the rest system of the electron. To accomplish this, we first replace the time derivative by the derivative with respect to the invariant proper time. The differential of proper time is defined by

$$ds^2=dt^2-1/c^2(dx^2+dy^2+dz^2),$$

or

$$ds=(1-v^2/c^2)^{\frac{1}{2}}dt. \qquad \text{(I.2)}$$

Secondly, we replace the square of the proper time derivative of the momentum by the invariant combination

$$(d\mathbf{p}/ds)^2-1/c^2(dE/ds)^2.$$

Hence, as the desired invariant generalization of (I.1), we have

$$P=\frac{2}{3}\frac{e^2}{m^2c^3}\left[\left(\frac{d\mathbf{p}}{ds}\right)^2-\frac{1}{c^2}\left(\frac{dE}{ds}\right)^2\right]$$

$$=\frac{2}{3}\frac{e^2}{m^2c^3}\left(\frac{E}{mc^2}\right)^2\left[\left(\frac{d\mathbf{p}}{dt}\right)^2-\frac{1}{c^2}\left(\frac{dE}{dt}\right)^2\right]. \qquad \text{(I.3)}$$

The conventional form of this result is obtained on

[1] See L. I. Schiff, Rev. Sci. Inst. **17**, 6 (1946).
[2] D. Iwanenko and I. Pomeranchuk, Phys. Rev. **65**, 343 (1944).
[3] Edwin M. McMillan, Phys. Rev. **68**, 144 (1945).
[4] John P. Blewett, Phys. Rev. **69**, 87 (1946).
[5] Julian Schwinger, Phys. Rev. **70**, 798 (1946).
[6] Elder, Langmuir, and Pollock, Phys. Rev. **74**, 52 (1948).

1912

Fundamental paper by J Schwinger:

it gave for the first time quantitative and qualitative insights into the properties of radiation emitted by relativistic charged particles moving in a magnetic field.

Followed by second paper…

PHYSICAL REVIEW D VOLUME 7, NUMBER 6 15 MARCH 1973

Classical Radiation of Accelerated Electrons. II. A Quantum Viewpoint*

Julian Schwinger
University of California, Los Angeles, California 90024
(Received 27 November 1972)

The known classical radiation spectrum of a high-energy charged particle in a homogeneous magnetic field is rederived. The method applies, and illuminates, an exact (to order α) expression for the inverse propagation function of a spinless particle in a homogeneous field. An erratum list for paper I is appended.

… while in the meantime <u>Sokolov and Ternov</u> in the USSR had come to similar results expanding the breadth of knowledge (radiative polarization of electrons and positrons in a magnetic field).

As the velocity v increases, <u>the emission of photons</u> from an electron subjected to an acceleration perpendicular to its velocity vector changes and goes from being “isotropic” to being highly skewed and collimated in the forward direction

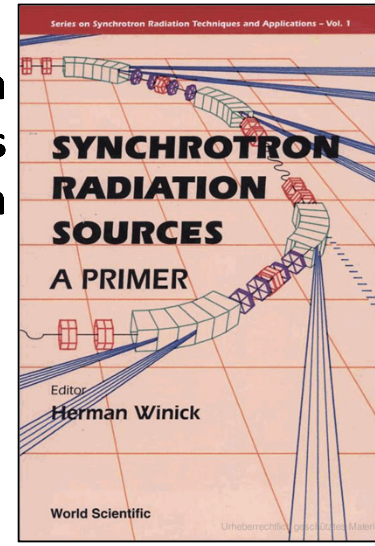

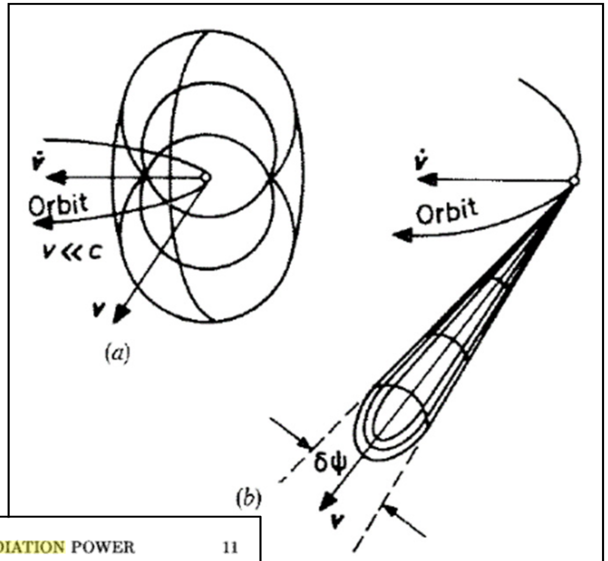

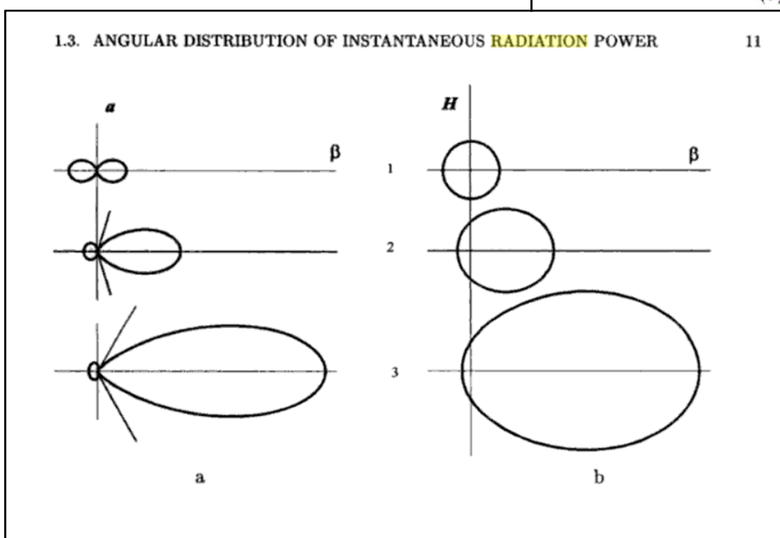

Fig. 1.4. βa (a) and $H\beta$ (b) plane sections of the indicatrix of SR at $\beta = 0.01$ (1), $\beta = 0.3$ (2), and $\beta = 0.5$ (3).

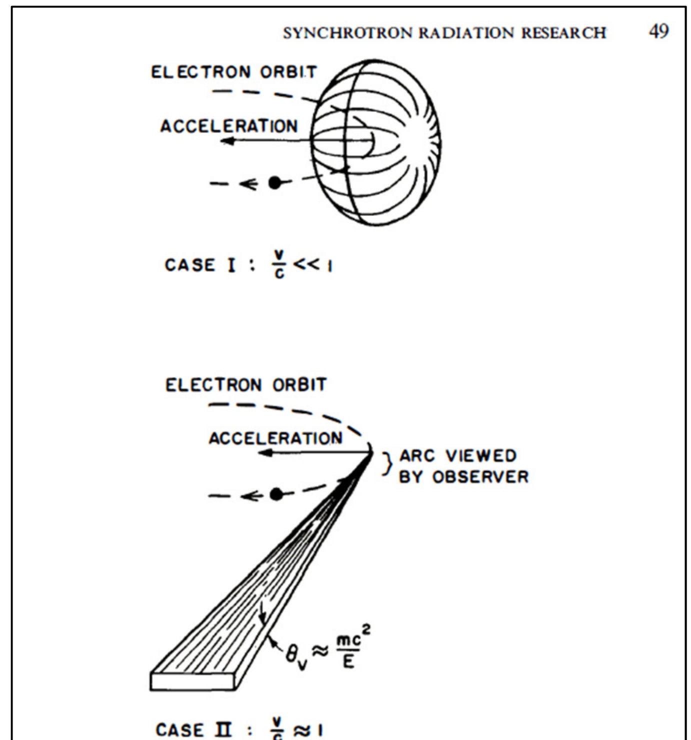

Figure 3 Pattern of radiation emitted by electrons in circular motion. *Case I*: non-relativistic electrons, $v/c \ll 1$. *Case II*: relativistic electrons, $v/c \approx 1$.

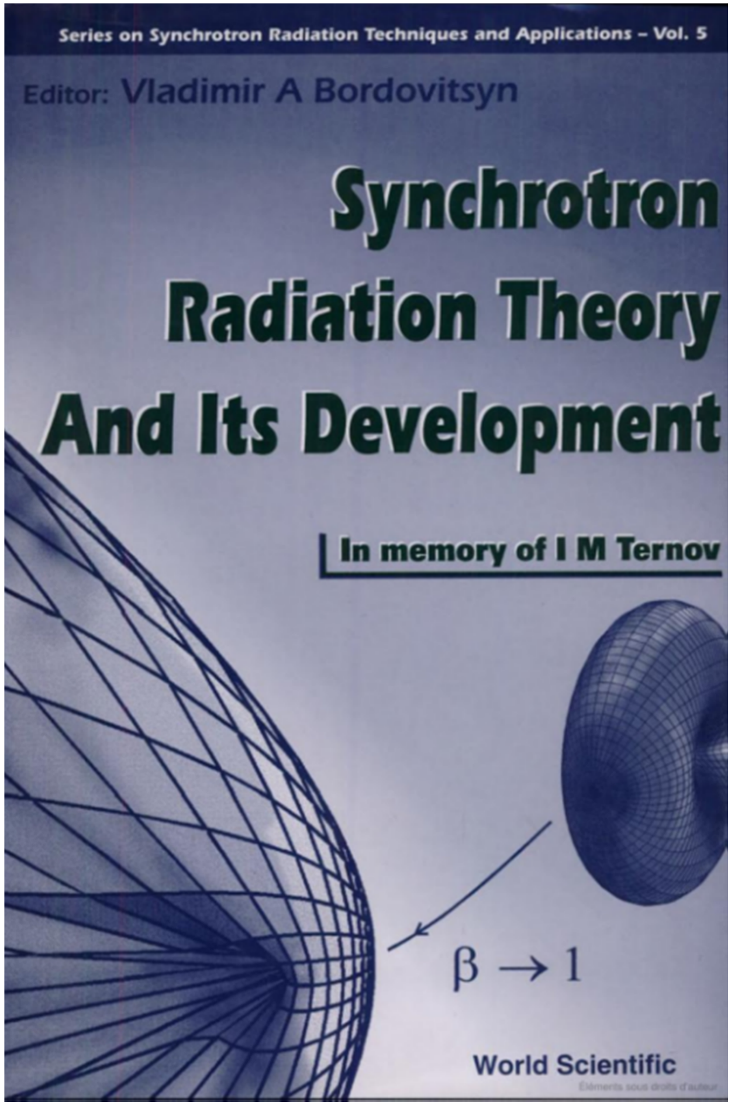

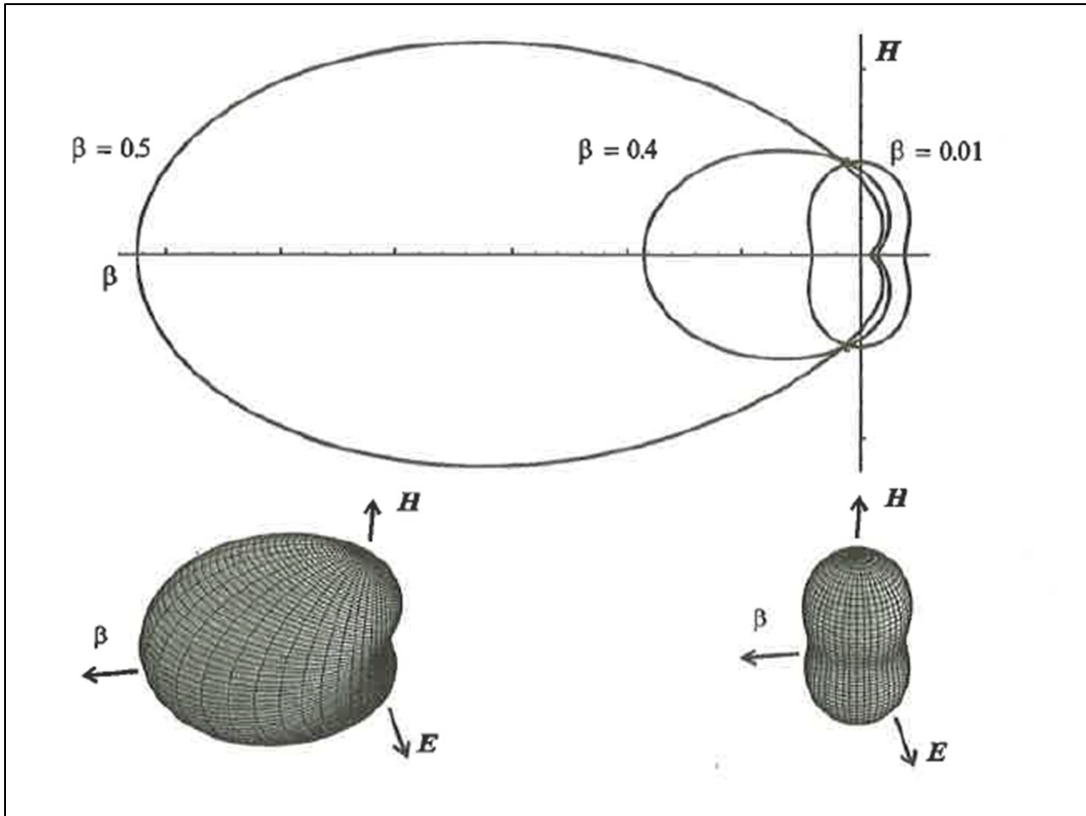

Fig. 4.2. Space indicatrix of radiation and its XZ plane section in the case of magneton motion perpendicular to the plane of the mutually orthogonal fields.

Relativistic factor: $\gamma = \dfrac{1}{\sqrt{1-\dfrac{v^2}{c^2}}}$

Practical Formulae, as a function of relativistic factor γ:

Integrated Photon Flux, F : $F = 4.1289 \cdot 10^{14} \cdot \gamma \cdot I(mA) \cdot k_F$ (ph/s/mA)

Integrated Photon Power, P: $P = 6.0344 \cdot 10^{-12} \cdot \dfrac{\gamma^4}{\rho(m)} \cdot I(mA) \cdot k_P$ (W/mA)

Critical Energy, e_{crit} : $e_{crit} = 2.9596 \cdot 10^{-7} \cdot \dfrac{\gamma^3}{\rho(m)}$ (eV)

As a function of beam energy (GeV), for e-/e+ machines:

$$F = 8.08 \cdot 10^{17} \cdot E(GeV) \cdot I(mA) \cdot k_F \qquad P = 88.46 \cdot \frac{E(GeV)^4}{\rho(m)} \cdot I(mA) \cdot k_P \qquad e_{crit} = 2218 \cdot \frac{E(GeV)^3}{\rho(m)}$$

k_f, k_p = fraction of photons with energies above given energy threshold (see next slide);

Photon distributions: power- and flux-wise

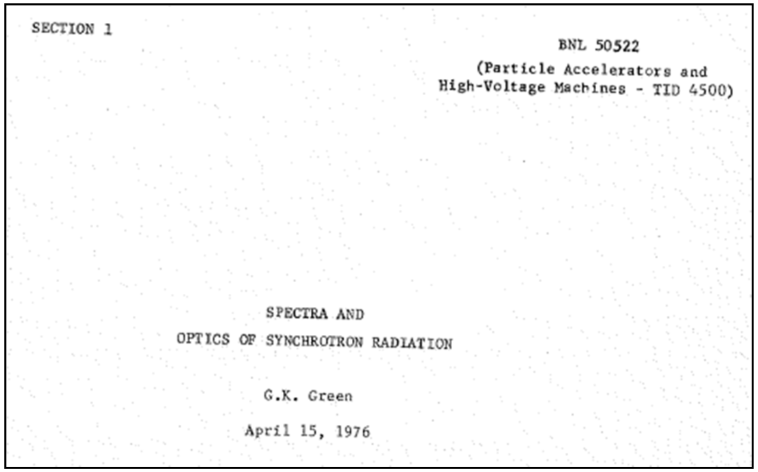

SECTION 1

BNL 50522
(Particle Accelerators and
High-Voltage Machines - TID 4500)

SPECTRA AND
OPTICS OF SYNCHROTRON RADIATION

G.K. Green

April 15, 1976

- **POWER: critical energy is the median of the SR power distribution: ½ of the power at photon energies ABOVE e_c, ½ BELOW**
- **FLUX: only 9% of the SR photons are generated above e_c.**

→ Most photons have low energy! ←

Average photon energy: 0.30792 · e_c

Percent of POWER at all wavelengths greater than λ vs λ/λ_C.

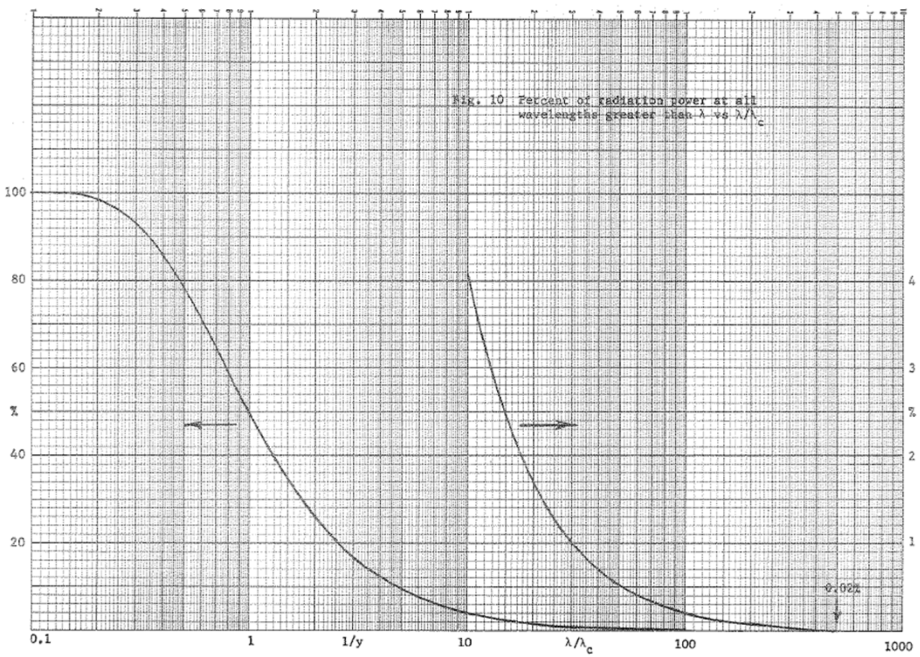

Percent of FLUX at all wavelengths greater than λ vs λ/λ_C.

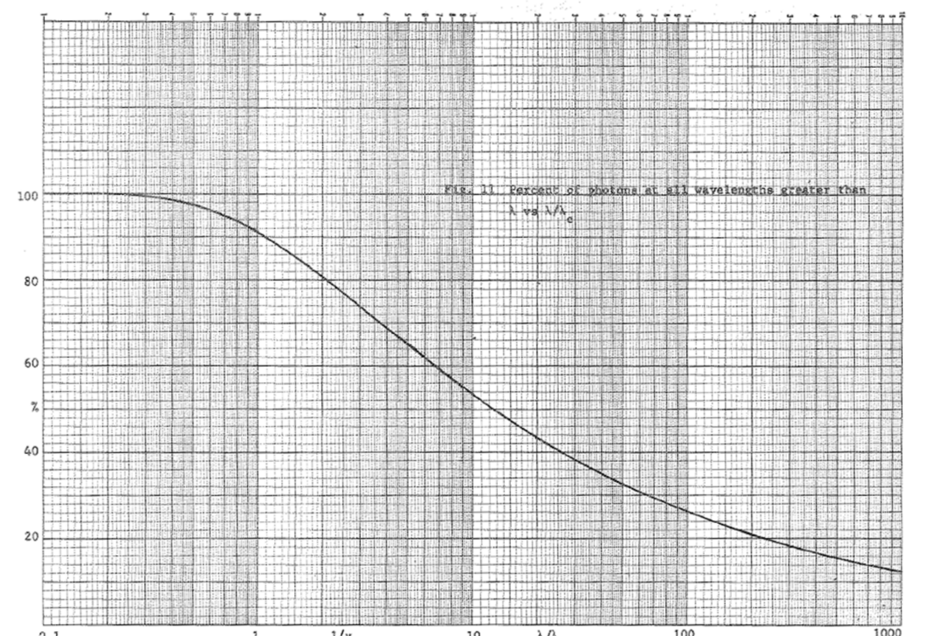

Photon distributions: Sources: X-Ray Data Booklet, LBNL; "Spectra and Optics of SR", BNL

LBNL/PUB-490 Rev. 3

Center for X-Ray Optics
and
Advanced Light Source

X-RAY DATA BOOKLET

Albert Thompson
David Attwood
Eric Gullikson
Malcolm Howells
Kwang-Je Kim
Janos Kirz
Jeffrey Kortright
Ingolf Lindau
Yanwei Liu
Piero Pianetta
Arthur Robinson
James Scofield
James Underwood
Gwyn Williams
Herman Winick

October 2009

Lawrence Berkeley National Laboratory
University of California
Berkeley, CA 94720

This work was supported in part by the U.S. Department of Energy under Contract No. DE-AC02-05CH11231

SECTION 1

BNL 50522
(Particle Accelerators and
High-Voltage Machines - TID 4500)

SPECTRA AND
OPTICS OF SYNCHROTRON RADIATION

G.K. Green

April 15, 1976

ACCELERATOR DEPARTMENT
B R O O K H A V E N   N A T I O N A L   L A B O R A T O R Y
A S S O C I A T E D   U N I V E R S I T I E S,   I N C.
U P T O N,   N E W   Y O R K   11973

under contract No. E(30-1)-16 with the
UNITED STATES ENERGY RESEARCH AND DEVELOPMENT ADMINISTRATION

Photon distributions: Sources: X-Ray Data Booklet, LBNL; “Spectra and Optics of SR”, BNL

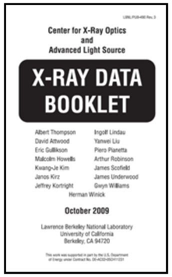

SECTION 2

SYNCHROTRON RADIATION

2.1A CHARACTERISTICS OF SYNCHROTRON RADIATION

Kwang-Je Kim

Synchrotron radiation occurs when a charge moving at relativistic speeds follows a curved trajectory. In this section, formulas and supporting graphs are used to quantitatively describe characteristics of this radiation for the cases of circular motion (bending magnets) and sinusoidal motion (periodic magnetic structures).

We will first discuss the ideal case, where the effects due to the angular divergence and the finite size of the electron beam—the emittance effects—can be neglected.

A. BENDING MAGNETS

The angular distribution of radiation emitted by electrons moving through a bending magnet with a circular trajectory in the horizontal plane is given by

$$\frac{d^2\mathcal{F}_B(\omega)}{d\theta d\psi} = \frac{3\alpha}{4\pi^2}\gamma^2\frac{\Delta\omega}{\omega}\frac{I}{e}y^2(1+X^2)^2 \times\left[K_{2/3}^2(\xi)+\frac{X^2}{1+X^2}K_{1/3}^2(\xi)\right] \qquad (1)$$

2-2

where

$\mathcal{F}_B$ = photon flux (number of photons per second)
θ = observation angle in the horizontal plane
ψ = observation angle in the vertical plane
α = fine-structure constant
γ = electron energy/$m_e c^2$ (m_e = electron mass, c = velocity of light)
ω = angular frequency of photon ($\varepsilon = \hbar\omega$ = energy of photon)
I = beam current
e = electron charge = 1.602×10^{-19} coulomb
y = $\omega/\omega_c = \varepsilon/\varepsilon_c$
ω_c = critical frequency, defined as the frequency that divides the emitted power into equal halves,
= $3\gamma^3 c/2\rho$
ρ = radius of instantaneous curvature of the electron trajectory (in practical units,
$\rho[\text{m}] = 3.3\, E[\text{GeV}]/B[\text{T}]$)
E = electron beam energy
B = magnetic field strength
ε_c = $\hbar\omega_c$ (in practical units,
$\varepsilon_c\,[\text{keV}] = 0.665\, E^2\,[\text{GeV}]\, B[\text{T}]$)
X = $\gamma\psi$
ξ = $y(1+X^2)^{3/2}/2$

The subscripted K’s are modified Bessel functions of the second kind. In the horizontal direction ($\psi = 0$), Eq. (1) becomes

$$\left.\frac{d^2\mathcal{F}_B}{d\theta d\psi}\right|_{\psi=0} = \frac{3\alpha}{4\pi^2}\gamma^2\frac{\Delta\omega}{\omega}\frac{I}{e}H_2(y), \qquad (2)$$

where

$$H_2(y) = y^2 K_{2/3}^2(y/2) \quad . \qquad (3)$$

In practical units [photons·s^{-1}·mr^{-2}·(0.1% bandwidth)$^{-1}$],

$$\left.\frac{d^2\mathcal{F}_B}{d\theta d\psi}\right|_{\psi=0} = 1.327\times10^{13}\, E^2\,[\text{GeV}]\, I[\text{A}]\, H_2(y).$$

The function $H_2(y)$ is shown in Fig. 2-1.

From now on, θ is the horizontal observation angle, and Ψ the vertical one, with respect to the plane of the orbit

Sources: X-Ray Data Booklet, LBNL; "Spectra and Optics of SR", BNL

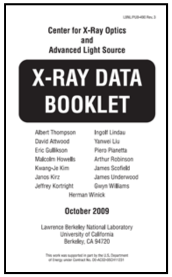

2-3

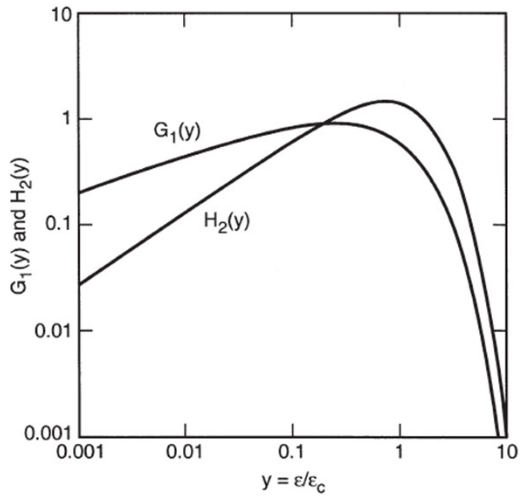

Fig. 2-1. The functions $G_1(y)$ and $H_2(y)$, where y is the ratio of photon energy to critical photon energy.

The distribution integrated over ψ is given by

$$\frac{d\mathcal{F}_B}{d\theta} = \frac{\sqrt{3}}{2\pi}\alpha\gamma\frac{\Delta\omega}{\omega}\frac{I}{e}G_1(y), \qquad (4)$$

where

$$G_1(y) = y\int_y^\infty K_{5/3}(y')dy' \quad . \qquad (5)$$

In practical units [photons·s^{-1}·mr^{-1}·(0.1% bandwidth)$^{-1}$],

$$\frac{d\mathcal{F}_B}{d\theta} = 2.457\times10^{13}\,E[\mathrm{GeV}]\,I[\mathrm{A}]\,G_1(y).$$

The function $G_1(y)$ is also plotted in Fig. 2-1.

Radiation from a bending magnet is linearly polarized when observed in the bending plane. Out of this plane, the polarization is elliptical and can be decomposed into its horizontal and vertical components. The first

2-4

and second terms in the last bracket of Eq. (1) correspond, respectively, to the intensity of the horizontally and vertically polarized radiation. Figure 2-2 gives the normalized intensities of these two components, as functions of emission angle, for different energies. The square root of the ratio of these intensities is the ratio of the major and minor axes of the polarization ellipse. The sense of the electric field rotation reverses as the vertical observation angle changes from positive to negative.

Synchrotron radiation occurs in a narrow cone of nominal angular width ~$1/\gamma$. To provide a more specific measure of this angular width, in terms of electron and photon energies, it is convenient to introduce the effective rms half-angle σ_ψ as follows:

$$\frac{d\mathcal{F}_B}{d\theta} \frac{d^2\mathcal{F}_B}{d\theta d\psi}\bigg|_{\psi=0} = \sqrt{2\pi}\,\sigma_\psi, \qquad (6)$$

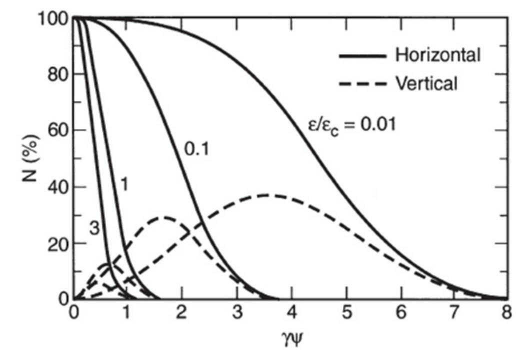

Fig. 2-2. Normalized intensities of horizontal and vertical polarization components, as functions of the vertical observation angle ψ, for different photon energies. (Adapted from Ref. 1.)

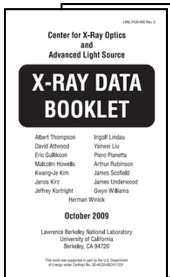

2-5

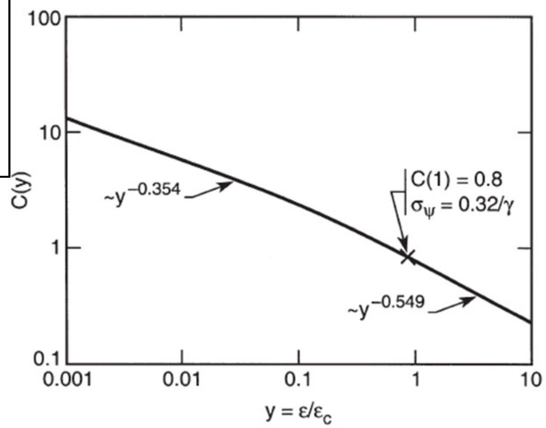

Fig. 2-3. *The function C(y). The limiting slopes, for $\varepsilon/\varepsilon_c << 1$ and $\varepsilon/\varepsilon_c >> 1$, are indicated.*

where σ_ψ is given by

$$\sigma_\psi = \frac{2}{\gamma\sqrt{2\pi}}\, C(y) = 0.408\, \frac{C(y)[\text{mr}]}{E[\text{GeV}]} \quad . \qquad (7)$$

The function $C(y)$ is plotted in Fig. 2-3. In terms of σ_ψ, Eq. (2) may now be rewritten as

$$\left.\frac{d^2\mathcal{F}_B}{d\theta d\psi}\right|_{\psi=0} = \frac{d\mathcal{F}_B}{d\theta}\,\frac{1}{\sigma_\psi\sqrt{2\pi}} \qquad (2a)$$

B. PERIODIC MAGNETIC STRUCTURES

In a wiggler or an undulator, electrons travel through a periodic magnetic structure. We consider the case where the magnetic field B varies sinusoidally and is in the vertical direction:

$$B(z) = B_0 \cos(2\pi z/\lambda_u) \quad , \qquad (8)$$

where z is the distance along the wiggler axis, B_0 the peak magnetic field, and λ_u the magnetic period. Electron motion is also sinusoidal and lies in

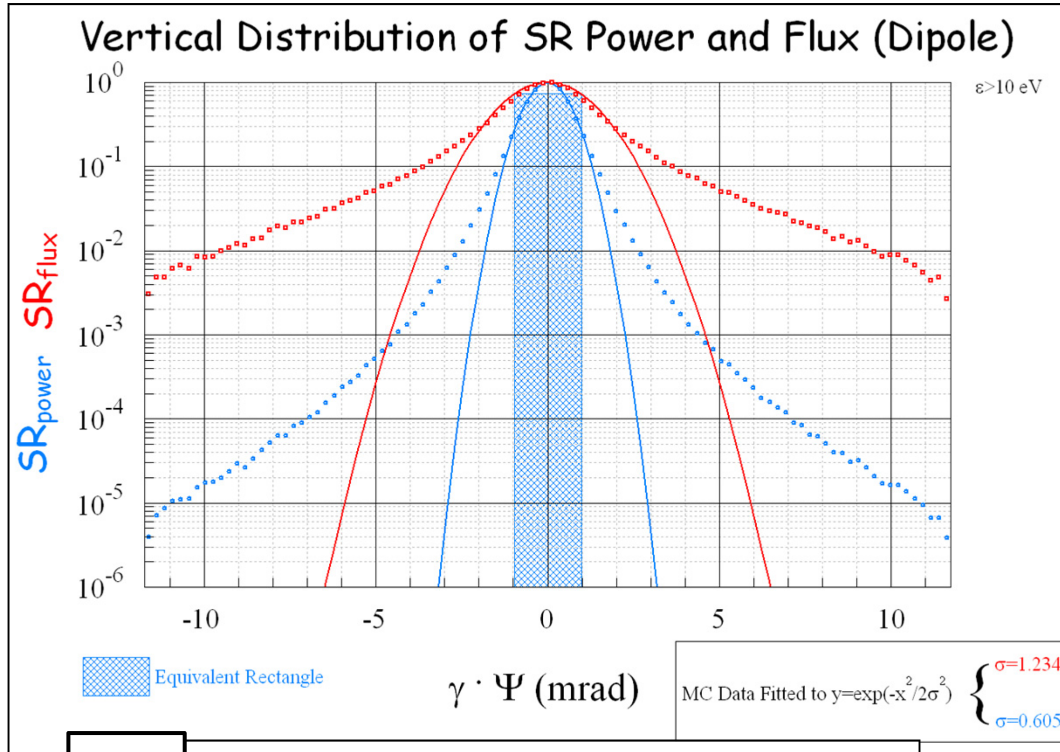

MC simulation, SYNRAD --> author;

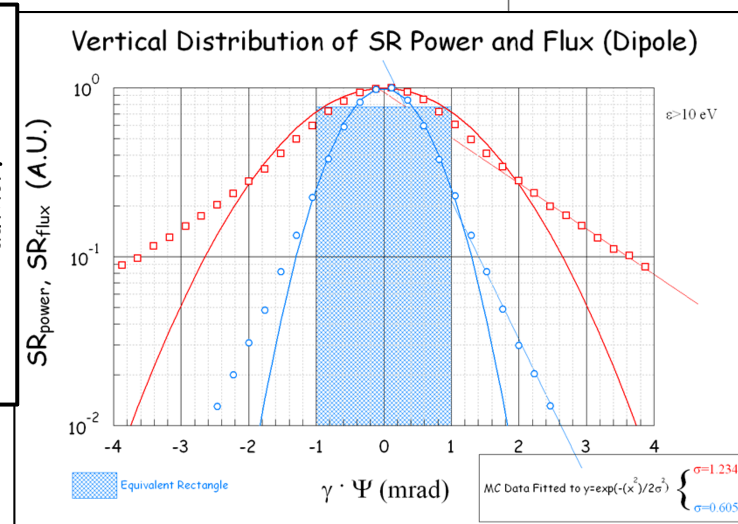

Source: “Monte Carlo simulations of Ultra High Vacuum and Synchrotron Radiation for particle accelerators”, M. Ady, CERN

At $\psi = 0$

$$F\left(\frac{\lambda_c}{2\lambda}, 0\right) = F_{\parallel}(0) = K_{2/3}^2\left(\frac{\lambda_c}{2\lambda}\right)$$

And generally at angle ψ

$$F_{\parallel}(\psi) = (1+\gamma^2\psi^2)\, K_{2/3}^2\left[\frac{\lambda_c}{2\lambda}(1+\gamma^2\psi^2)^{3/2}\right]$$

$$F_{\perp}(\psi) = \gamma^2\psi^2(1+\gamma^2\psi^2)\, K_{1/3}^2\left[\frac{\lambda_c}{2\lambda}(1+\gamma^2\psi^2)^{3/2}\right]$$

where $K_{1/3}$ and $K_{2/3}$ are modified Bessel functions. We often use the expression *degree of polarization* which is defined as $P_{lin} = (F_{\parallel} - F_{\perp})/(F_{\parallel} + F_{\perp})$. The solution of this analytic expression can be visualized (see Fig.2.6) on a relative scale where the vertical angle is expressed in units of γ, and with a different X axis range for each energy.

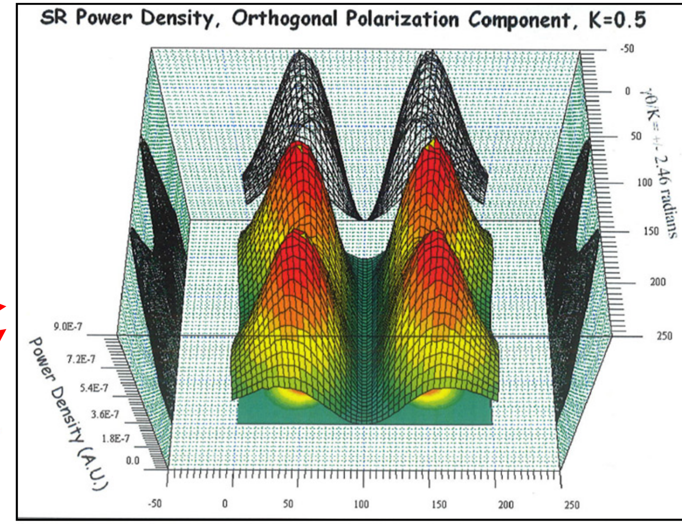

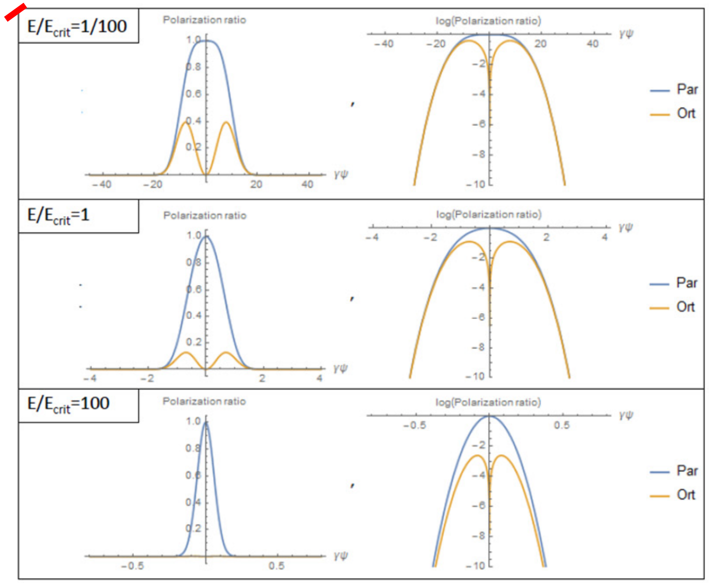

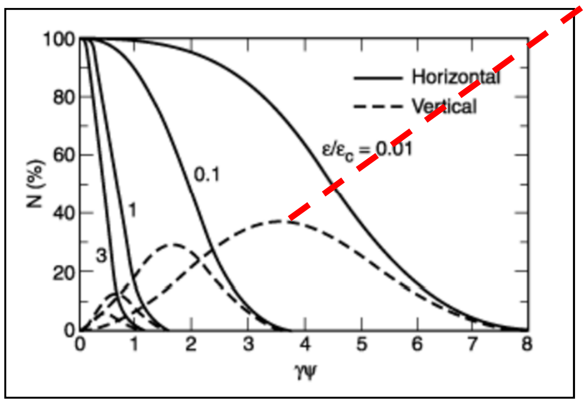

Figure 2.6: Polarization components for different lambda ratios. Each plot has an X scale that depends on the relative photon energy:
$\gamma\psi = [-4/(E/E_c)^{0.35} .. +4/(E/E_c)^{0.35}]$
Left: linear scale, Right: logarithmic scale

7/8 of the total power is generated as parallel polarization photons, 1/8 only in the perpendicular case;

Photon distributions: SYNRAD+, 3-d ray-tracing code

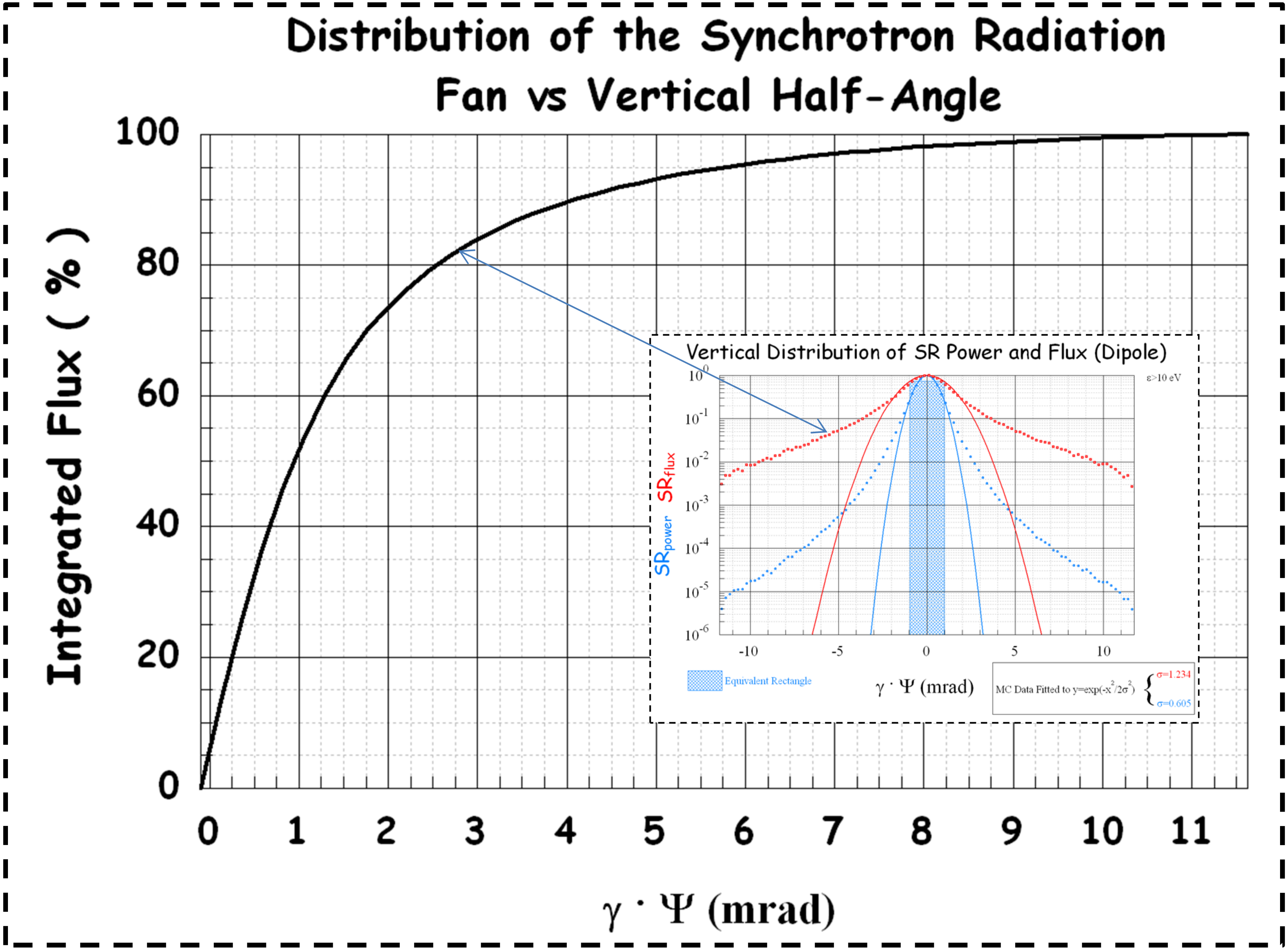

Source: "Efficient computation of synchrotron radiation spectrum", H.H. Umstatter, CERN/PS/SM/81-13, 1981

How can spectra and fluxes be calculated efficiently and fast?

- **Several numerical algorithms have been developed during the years:**
- **This one, is particularly fast:**

f) The highest speed is obtained if one computes directly $\int K_{5/3}$ by a Chebyshev series instead of separate computation of $K_{2/3}$ and $\int K_{1/3}$. Since it is not known whether Chebyshev expansion coefficients of $\int K_{5/3}$ exist in the literature they are given in the following listing of subroutine SYNRAD, rounded to 10 digits after the decimal point. Coefficients of 19 – 20 digit precision are given in the following table. They have been computed by linear combination of Luke's coefficients for $K_{2/3}$ and $\int K_{1/3}$. SYNRAD calls no external subroutine and uses no array in order to gain more speed. It is about 400 times faster than method a. On the IBM it evaluates $\int K_{5/3}$ in $7.6 \cdot 10^{-6}$ sec. on the CDC 7600 in $2.6 \cdot 10^{-5}$ sec. (i.e. 38600 values in 1 sec. computing time).

EUROPEAN ORGANISATION FOR NUCLEAR RESEARCH

/lmg

CERN/PS/SM/81-13
10.3.1981.

EFFICIENT COMPUTATION OF SYNCHROTRON RADIATION SPECTRUM

H.H. Umstätter

- **Note: compared to the CDC 7600 supercomputer of the 70's, the same code running on just *one* core of a modern multi-core CPU looks like a rocket: 1.6M values/sec *vs* 38600 values/sec, an improvement of > 40x:**

This means that today Montecarlo simulations of SR are affordable even on laptops and desktops.

3. SR-induced desorption

Since SR has been observed for the first time in an accelerator (1949), scientists have immediately realized that X-ray photons of energies higher than few eV were capable of causing desorption of molecules from the walls of the vacuum system, via a number of different phenomena, namely:

- Generation of photo-electrons;
- Direct desorption via X-ray excitation;
- Thermal desorption caused by heating deposited by SR;

- In order to design the vacuum system of e-/e+ storage rings-- **in particular light sources where the e- beam <u>needs to be stored</u> sometimes for tens of hours without interruptions**--, scientist had to develop an experimental program in order to measure carefully the **photon-induced desorption** (**PID**) yield, usually indicated by the letter η.
- η gives the average number of molecules of a given gas species per incident photon, and allows the designer of the vacuum system to size and space properly the pumping system, a **major input to the budget of a light source**;

Some examples of PID yield measurements: design of 2.75 GeV SOLEIL light source

JVSTA Journal of Vacuum Science & Technology A

Photon stimulated desorption of an unbaked stainless steel chamber by 3.75 keV critical energy photons

C. Herbeaux, P. Marin, V. Baglin, and O. Gröbner

Citation: Journal of Vacuum Science & Technology A **17**, 635 (1999); doi: 10.1116/1.581630
View online: http://dx.doi.org/10.1116/1.581630
View Table of Contents: http://scitation.aip.org/content/avs/journal/jvsta/17/2?ver=pdfcov
Published by the AVS: Science & Technology of Materials, Interfaces, and Processing

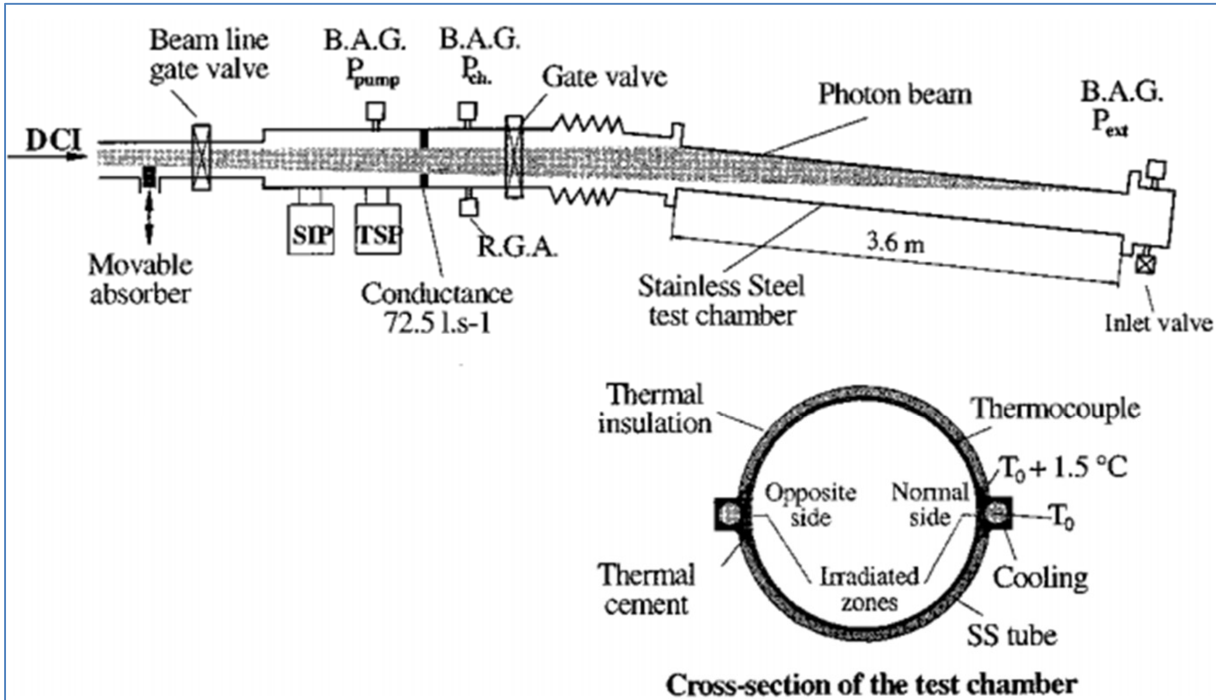

FIG. 1. Synopsis of the beamline for PSD studies at DCI.

Some examples of PID yield measurements: design of 2.75 GeV SOLEIL light source

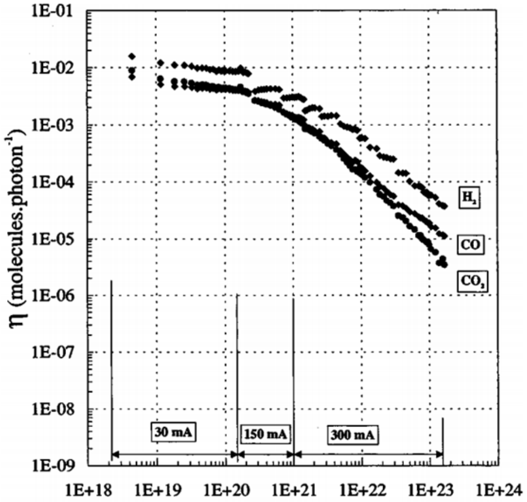

(a)

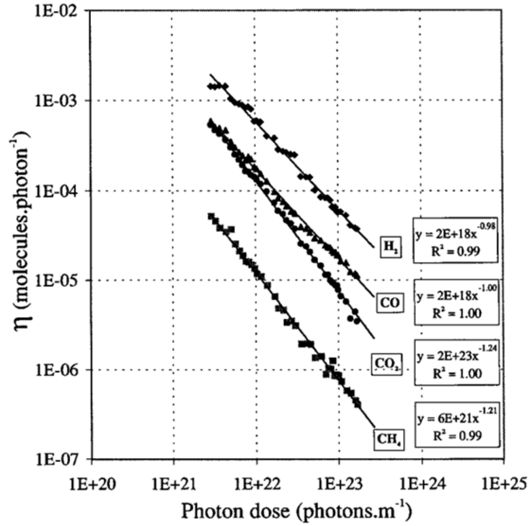

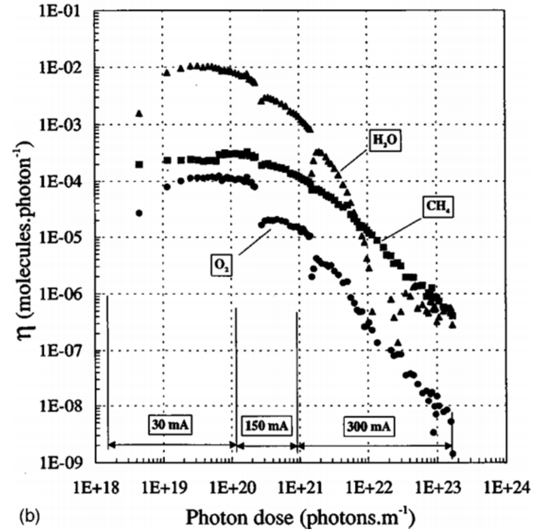

(b)

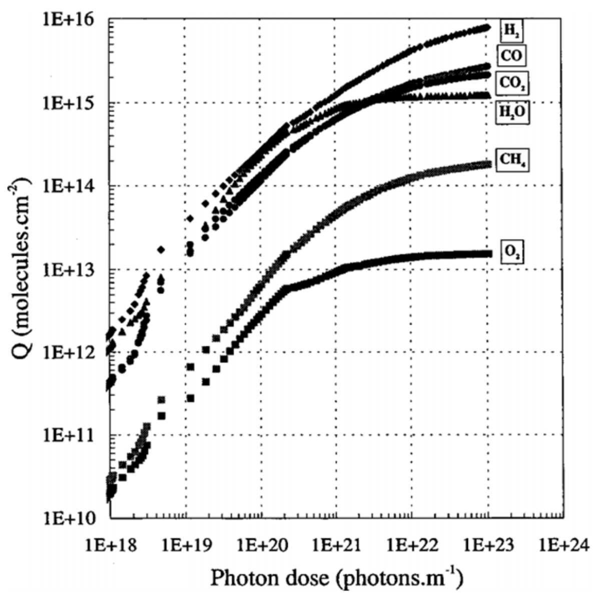

FIG. 5. Number of molecules desorbed per square centimeter of surface area as a function of the photon beam dose.

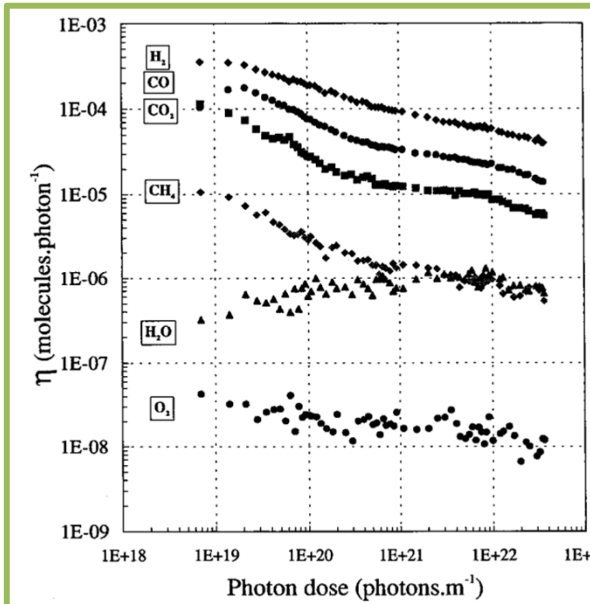

FIG. 7. Molecular yields vs photon beam dose for the irradiation of the opposite side.

Some examples of PID yield measurements: design of 6 GeV ESRF light source

(NEG-coating developments, 1999 onwards)

TUPS002 Proceedings of IPAC2011, San Sebastián, Spain

PHOTODESORPTION MEASUREMENTS AT ESRF D31

H.P. Marques*, G. Debut, M. Hahn, ESRF, Grenoble, France

Abstract

Since 1998 exists at ESRF a dedicated beamline for photodesorption measurement from vacuum chambers - D31. The original goal of this installation was to study the wall pumping effect. When exposed to synchrotron radiation surfaces exhibit strong outgassing of the adsorbed gas layer despite UHV conditions. Long term outgassing leads to the depletion of the adsorbed layer and produces a very clean surface which turns the walls of the vacuum chamber into an active pumping surface.

At D31 have been tested chambers of stainless steel, aluminium and copper, with or without coatings (e.g. NEG, copper), designed by ESRF and other institutes like ALBA, CERN, ELETTRA and Soleil. Here we review some of the results obtained and outline the future plans of D31.

leading to the requirement of additional shielding and thus reducing the availability of the beamline to the users.

PHOTODESORPTION

The first successful models to describe electron stimulated desorption (ESD) or photon stimulated desorption (PSD) where the MGR model, independently proposed by Menzer and Gomer [6] and Redhead[7], and later the Knotek-Feibelman [8] (KF) model. Briefly, in the MGR model an atom is excited to an anti-bonding state and it may gain sufficient kinetic energy so that it overcomes the lower potential barrier of one of the bonding states in the de-excitation pathway. The KF model is based in an interatomic Auger decay. The original excitation leaves a hole in the core level to be filled by an electron from a neighbour atom and, due to

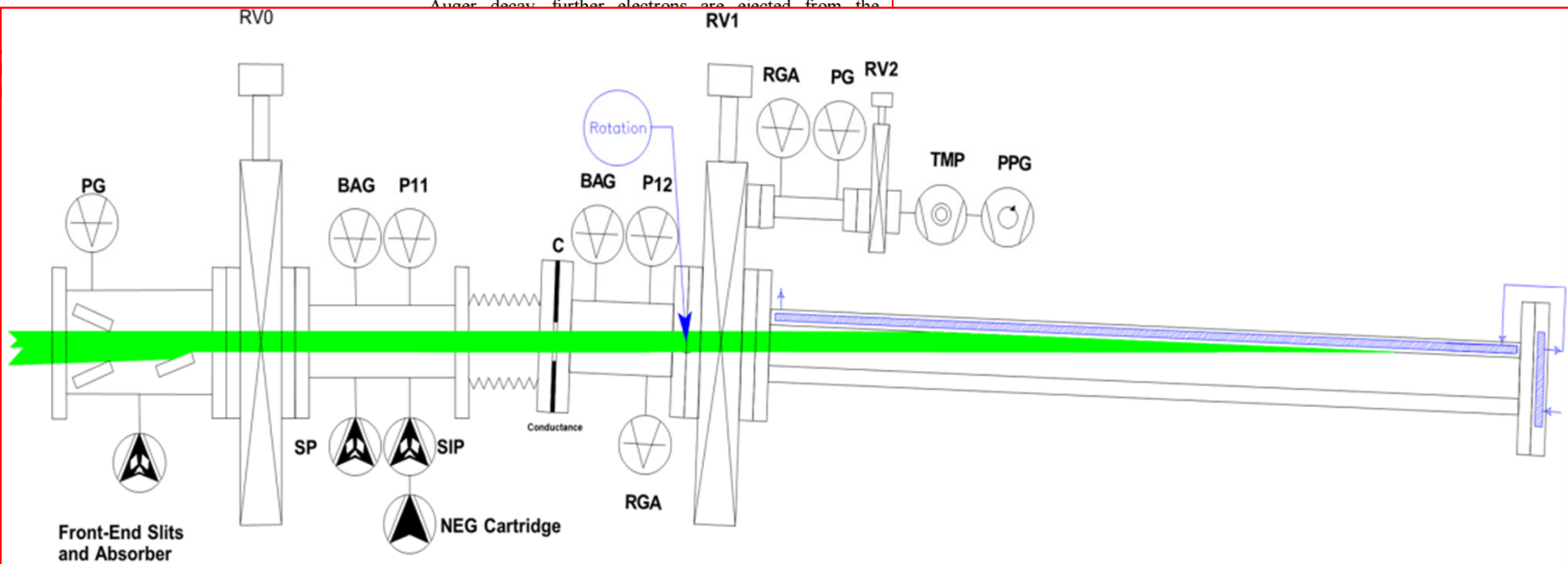

Figure 1: D31 schematics. PG – Pirani gauge; RV – Remote Valve ; SIP – Sputter Ion Pump; BAG – Bayard-Alpert Gauge ; P – Penning Gauge; TMP – Turbo Molecular Pump; PPG – Primary Pumping Group

Some examples of PID yield measurements: design of 6 GeV ESRF light source

(NEG-coating developments, 1999 onwards)

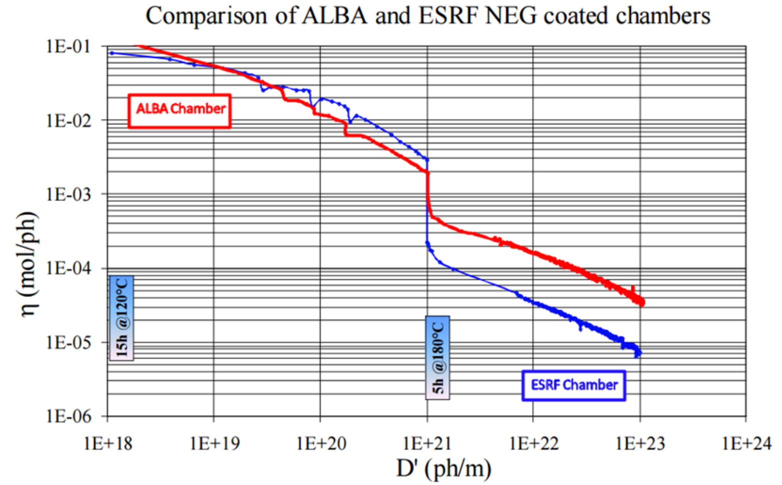

Figure 2: Activation of an ALBA chamber coated by SAES Getters and an ESRF chamber coated at ESRF

Memory Effect

When continually exposed to synchrotron radiation the yield of a surface decreases with accumulated dose. This decrease is in part due to the progressive cleaning of the adsorbed surface layers. In Figure 5 it can be observed that after exposure of a thoroughly irradiated chamber to air its yield, although increasing, remains at a lower than the initial value. Even at the second consecutive venting it can still be observed a small improvement. As such the chamber retains some "memory" of the previous condition.

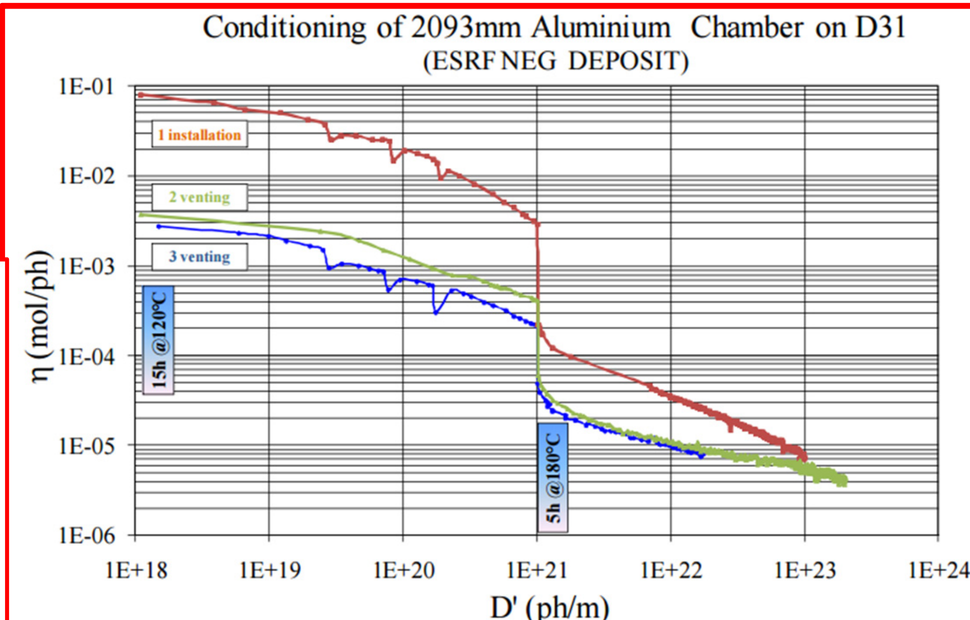

Figure 5: Repeated activation test. After each test the chamber was vented. The initial yield was progressively lower. The step behaviour is due to NEG activation.

Question: What happens if the PID yield is not sufficiently low and/or the corresponding pressure profile is too high-- for instance because of lack of pumping speed?

→ Beam-gas scattering ←

Effect on the beam lifetime!

Proceedings of the 1999 Particle Accelerator Conference, New York, 1999

STUDY OF THE BESSY II BEAM LIFETIME *

S. Khan †, BESSY, Berlin, Germany

2 THEORY

In this section, the relations used in the analysis are reviewed. A list of symbols is given in table 1.

The beam lifetime τ is defined by the current decay rate $1/\tau = -\dot{I}/I$, which is the sum of the Touschek (T) rate and the gas scattering (G) rate

$$\frac{1}{\tau} = \frac{1}{\tau_\mathrm{T}} + \frac{1}{\tau_\mathrm{G}} = \frac{1}{\tau_\mathrm{T}} + c\,n\left(\sigma^\mathrm{N}_\mathrm{elast} + \sigma^\mathrm{N}_\mathrm{inel} + \sigma^\mathrm{e}_\mathrm{elast} + \sigma^\mathrm{e}_\mathrm{inel}\right). \quad (1)$$

The Touschek decay rate can be written as (e.g. [4])

$$\frac{1}{\tau_T} = \frac{N r_e^2 c}{8\pi\sigma_x\sigma_y\sigma_z\,\gamma^2\,(\Delta p/p)^3}\cdot D\left(\frac{(\Delta p/p)^2\sigma_{x'}^2}{\gamma^2}\right), \quad (2)$$

where $D \approx 0.3$ is a slowly varying function that is evaluated numerically. Relativistic effects and beam polarization modify the Touschek rate on the level of 10-20% [5].

The total cross sections for elastic and inelastic scattering on residual gas nuclei (N) and electrons (e) are [4]

$$\sigma^\mathrm{N}_\mathrm{elast} = \frac{2\pi r_e^2 Z^2}{\gamma^2}\frac{\bar{\beta}\beta_a}{a^2} \quad (3)$$

$$\sigma^\mathrm{N}_\mathrm{inel} = \frac{4 r_e^2 Z^2}{137}\frac{4}{3}\left(\ln\frac{183}{Z^{1/3}}\right)\left(\ln\frac{1}{\Delta p/p} - \frac{5}{8}\right) \quad (4)$$

$$\sigma^\mathrm{e}_\mathrm{elast} = \frac{2\pi r_e^2 Z}{\gamma}\frac{1}{\Delta p/p}$$

$$\sigma^\mathrm{e}_\mathrm{inel} = \frac{4 r_e^2 Z}{137}\frac{4}{3}\left(\ln\frac{2.5\gamma}{\Delta p/p} - 1.4\right)\left(\ln\frac{1}{\Delta p/p} - \frac{5}{8}\right),$$

The distinctly different dependence of Touschek scattering and inelastic gas scattering on the momentum acceptance $\Delta p/p$ (equations 2 and 4) can be used to distinguish the two effects by changing the rf voltage (which also changes the bunch length). Coulomb scattering is identified by variation of the physical aperture using scrapers.

Question: What happens if the PID yield is not sufficiently low and/or the corresponding pressure profile is too high-- for instance because of lack of pumping speed?

→ Beam-gas scattering → **Generation of bremsstrahlung (BS) radiation:**

Bremsstrahlung (BS) radiation:

It is a "braking "radiation generated by the e- in the beam interacting with the strong electric field of a proton in the field of a nucleus of a residual gas molecule/atom.

- **Depends strongly on the atomic number Z of the gas species: generation of extremely high-energy gamma rays, with upper energy range close to the e- beam energy: ~ Z(Z+1) …. see further below…**
- **Consequences: → the vacuum designer must do his/her best to keep the residual gas composition as close as possible to "pure H2", with as low as possible components made up by CH4, CO, CO2, Ar, etc… ←**
- **For light sources it is particularly important to keep BS low along the straight sections where experimental beamlines are installed: radiation protection dose limits are more and more stringent!... This has an impact on the availability of a given beamline.**
- **We'll come back to this issue a bit later…**

How to calculate the SR photon distribution and related gas loads?

(valid, of course, also for assuring proper cooling of surfaces)

1) Do like the ESRF "*Blue Book*", CAD ray-tracing (in the plane of the orbit only):

ESRF

SYNCHROTRON RADIATION POWER DISTRIBUTION IN THE ESRF STORAGE RING VACUUM CHAMBERS

* FAN DRAWINGS

* POWER DISTRIBUTION ON THE ABSORBERS

Update March 2004

B. OGIER - B. PLAN - L. ZHANG

-CONTENTS-

ESRF: STANDARD CELL IP/NEG DISTRIBUTION AND LOCATION OF VACUUM GAUGES:

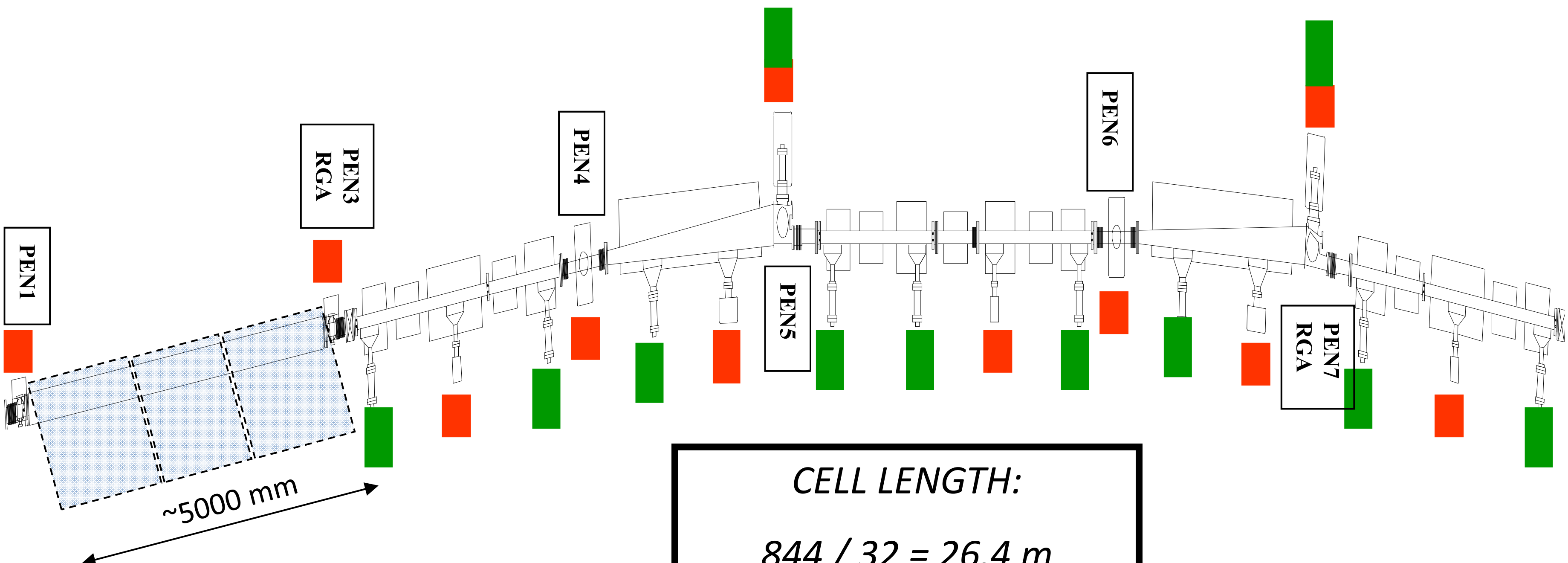

CELL LENGTH:

844 / 32 = 26.4 m

Ion pumps (Varian): ID:120 l/s ; CV4/CV11: 120 l/s; CV3/CV10/CV15: 45 l/s; dipoles: 60 l/s ; crotches: 400 l/s

NEG pumps (SAES): crotches: GP500 ; elsewhere: GP200

3. SR-induced desorption

ESRF "Blue Book" CAD ray-tracing (in the plane of the orbit only):

Introduction

The basic synchrotron radiation sources are the bending magnets, which cover 2π radian angle. At the ESRF a major part of this synchrotron radiation is removed by water cooled heater absorbers installed inside the vacuum chambers of the Storage Ring. The power distribution on the absorbers is a basic data for the design of the vacuum chambers as well as the absorbers.

Additional sources of synchrotron radiation are Insertion Devices (ID's) placed in the straight section, between two successive bending magnets. At the ESRF the synchrotron radiation from the insertion devices has, in most cases, a very small horizontal opening angle so that it does not touch any components of the Storage Ring.

This document is intended to give out the power density and the spot size of the synchrotron radiation on all the absorbers of the ESRF Storage Ring vacuum chambers. Only the synchrotron radiation from bending magnets has been considered.

Basic Formula

The synchrotron radiation from a bending magnet in the ESRF has a much smaller vertical size and divergent angle than the horizontal ones. This synchrotron radiation can be considered as a horizontal divergent blade. The power distribution is then described by the angular power density which is defined by the power per unit angle in the horizontal plane, and a vertical Gaussian height.

The angular power density P_θ is given by

$$P_\theta = 4.224\, B\, E^3\, I \qquad (1)$$

where E : electron beam energy, in GeV
I : electron beam current intensity, in A
B : magnet field intensity of the bending magnet, in T
P_θ : angular power density in horizontal plane, in W/mrad

In the case of the ESRF, E = 6 GeV, I = 200 mA = 0.2 A, (nominal values)

- for the standard bending magnet B = 0.857 T,
  P_θ = 156.38 W/mrad
- for the soft end magnet B = 0.40 T,
  P_θ = 72.99 W/mrad

The linear power density P_l on the absorber is then

$$P_l = P_\theta \sin(\beta)/d \qquad (2)$$

where d is the distance between the source point and the absorber, in meter, β the incident angle of photon beam on the absorber (see Figure 1), P_l in W/mm.

The photon beam size on an absorber is characterised by the vertical Gaussian height σ (mm) which is calculated by

$$\sigma = \sqrt{\sigma_0^2 + (\sigma' d)^2 + \left(\frac{d}{\gamma}\right)^2} = \sqrt{\sigma_0^2 + (\sigma'' d)^2} \qquad (3)$$

where σ_0 : vertical standard deviation of the e-beam at source point (mm)
σ' : vertical angular standard deviation of the e-beam at source point (mrad)
σ'' : total effective vertical angular standard deviation at source point (mrad)
d : distance between source point and the absorber (m)
γ : = 1957 E (GeV)

For a coupling factor of 1% and a vertical emittance $\varepsilon_z = 4\ 10^{-11}$ m.rad in the case of the ESRF,

σ_0 = 37 µm
σ' = 1.07 µrad
γ =1.174 10^4
$\sigma'' = \sqrt{\sigma'^2 + \frac{1}{\gamma^2}}$ =85.2 µrad

ESRF "Blue Book" CAD ray-tracing (in the plane of the orbit only):

The surface power density on the absorber P_a is given by

$$P_a(z) = P_a \exp(-\frac{z^2}{2\sigma^2}) \qquad (4)$$

with peak power density per unit surface area :

$$P_a = \frac{P_l}{\sqrt{2\pi}\sigma} \qquad (5)$$

Once the distance d between the source point and the absorber is defined as well as the incidence angle β of the synchrotron radiation on the absorber, the power densities P_l, P_a and spot size on the absorber can be calculated by equations (2)-(5).

Geometrical calculation

There are two types of dipole bending magnets per cell in the ESRF storage ring :

1) with downstream soft end B1
2) with upstream soft end B2

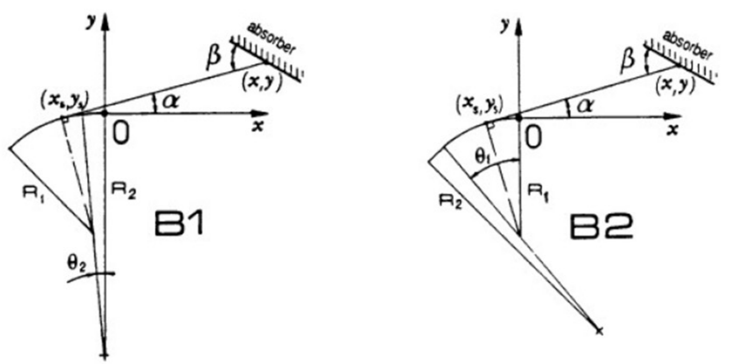

case 1 : dipole magnet B1 — case 2 : dipole magnet B2

Figure 1 : Co-ordinate systems

The co-ordinate systems concerning the two types of dipole magnets are shown in Figure 1. The origin of the co-ordinate system is always at the exit of the magnets, the axis-x is parallel to the electron beam in the straight section. The absorber is defined by a certain number of key points and inclined angles $\gamma = \alpha + \beta$ of surface to the axis-x (or to the electron beam trajectory in the straight section).

It is easy to give out the co-ordinates of a point on the absorber (x, y) and the angle γ. The associated source point (x_s, y_s) and the angle α between the photon beam and the electron beam (see Figure 1) can be calculated from the co-ordinates (x, y) and the geometrical parameters of the bending magnets.

Case 1 : dipole magnet B1 :

1) $\alpha > \theta_2$: source point on the main bending magnet (B1)

$$x_s = - R_1 \sin(\alpha) - (R_2 - R_1) \sin(\theta_2) \qquad (6a)$$
$$y_s = - R_2 + R_1 \cos(\alpha) + (R_2 - R_1) \cos(\theta_2) \qquad (6b)$$

2) $\alpha < \theta_2$: source point on the soft end magnet

$$x_s = - R_2 \sin(\alpha) \qquad (7a)$$
$$y_s = - R_2 (1 - \cos(\alpha)) \qquad (7b)$$

Case 2 : dipole magnet B2 :

3) $\alpha < \theta_1$: source point on the main bending magnet (B2)

$$x_s = - R_1 \sin(\alpha) \qquad (8a)$$
$$y_s = - R_1 (1 - \cos(\alpha)) \qquad (8b)$$

4) $\alpha > \theta_1$: source point on the soft end magnet

$$x_s = - R_2 \sin(\alpha) + (R_2 - R_1) \sin(\theta_1) \qquad (9a)$$
$$y_s = - R_1 - (R_2 - R_1) \cos(\theta_1) + R_2 \cos(\alpha) \qquad (9b)$$

where R and θ are respectively the radius and the curvature angle of the magnet, index 1 for standard magnet and 2 for soft end magnet. At the ESRF,

ESRF "Blue Book" CAD ray-tracing (in the plane of the orbit only):

Notation

The power distribution on the absorbers installed inside the vacuum chambers of the Storage Ring is presented as following.

(sample)

Pt n°	Src	Src n°	X *mm*	Y *mm*	α *°*	β *°*	σ *mm*	Pl *W/mm*	Pa *W/mm2*	Ptot *W*	CV n° / drawing n°
1		2	10 614	37.00	0.199	0.199	0.518	**0.05**	**0.04**		
2		2	12 728	37.00	0.166	0.166	0.620	**0.04**	**0.02**		
3	2H	2	12 846	37.34	0.166	9.628	0.625	**2.03**	**1.29**	**130**	CV 03 / 85.41.0073
4		2	12 848	37.00	0.165	9.627	0.626	**2.02**	**1.29**		
5		2	13 965	37.00	0.151	0.151	0.679	**0.03**	**0.02**		

Some symbols in the notation have been used in the previous sections. Here below is a summary of the notation.

Pt n° number of points, marked in the drawings
Src synchrotron radiation source type
Src n° synchrotron radiation source number
1H : dipole type 1, **n° =1**
2H : dipole type 2, **n° =2**
1S : soft end dipole type 1, **n° =0**
2S : soft end dipole type 2, **n° =3**
X *(mm)* co-ordinate X, axis X parallel to the e-beam orbit
Y *(mm)* co-ordinate Y, axis Y parallel to radial direction of the ring
the origin of the co-ordinate system X-Y is at the intersection of e-beam orbit and the exit of upstream dipole magnet (B1)
α *(degree °)* angle between X-ray and e-beam orbit
β *(degree °)* X-ray incidence angle on the absorbers
σ *(mm)* Gaussian vertical height of X-ray
Pl *(W/mm)* linear power density on the absorber in the horizontal plan
Pa *(W/mm2)* surface power density on the absorber
Ptot *(W)* total power on the absorber
CV n° / drawing n° name of vacuum chamber / number of corresponding drawing

-COMMON PART CELLS-
from CV03 to CV15
(except CELL 03-04-07-15)

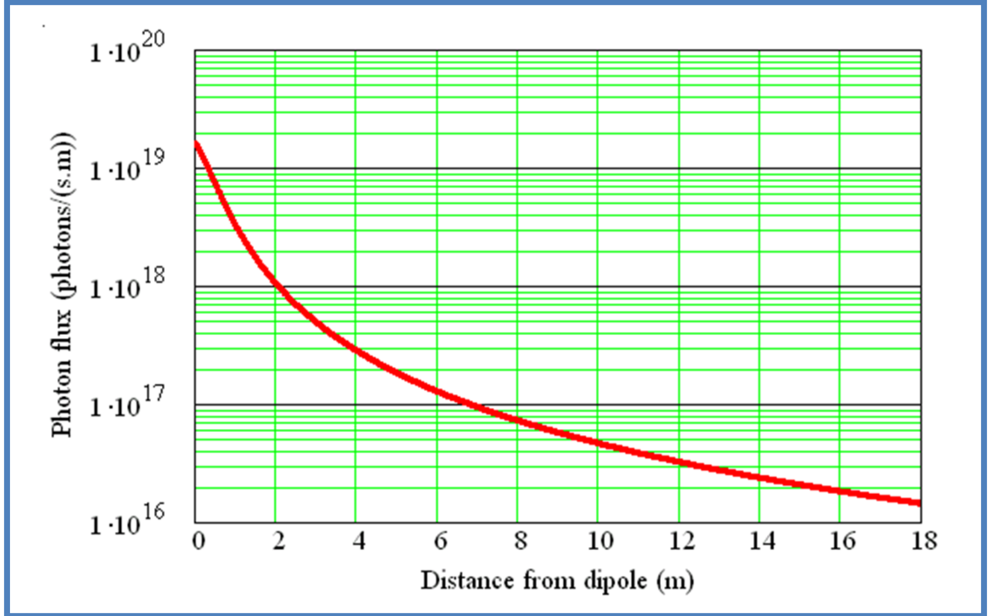

Source: O.B. Malyshev, pers. comm., for the DIAMOND Light Source

ESRF "Blue Book" CAD ray-tracing (in the plane of the orbit only):

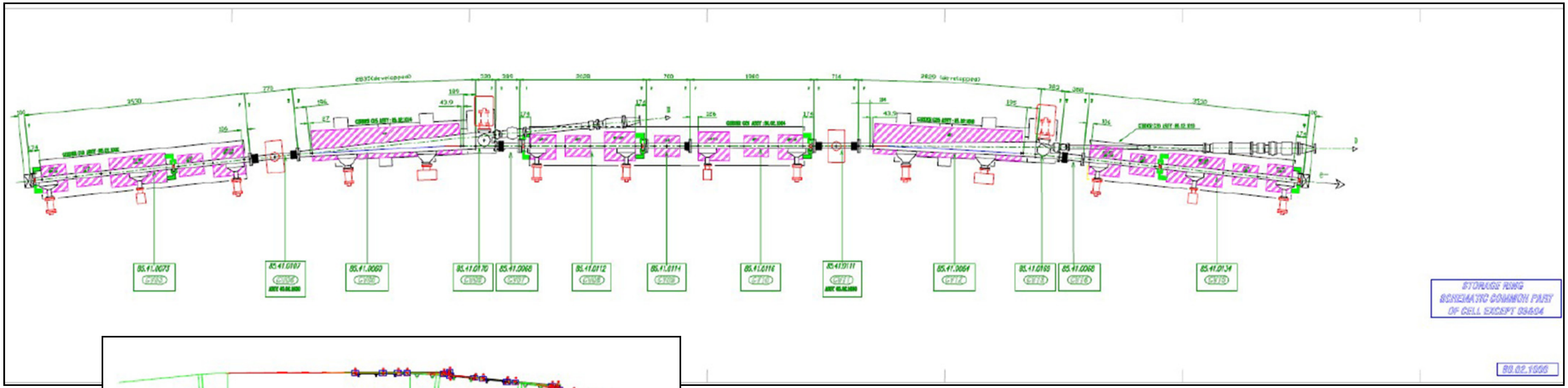

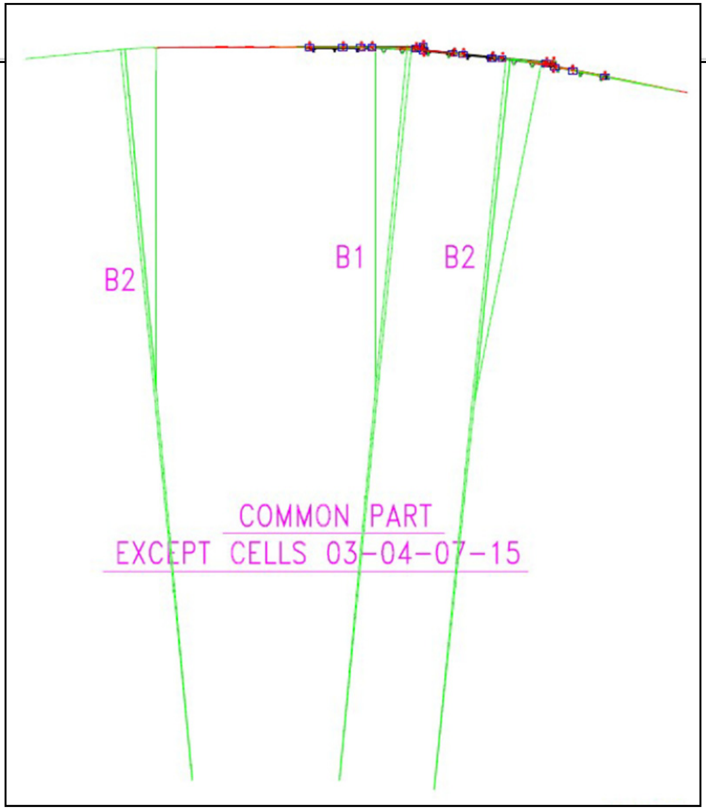

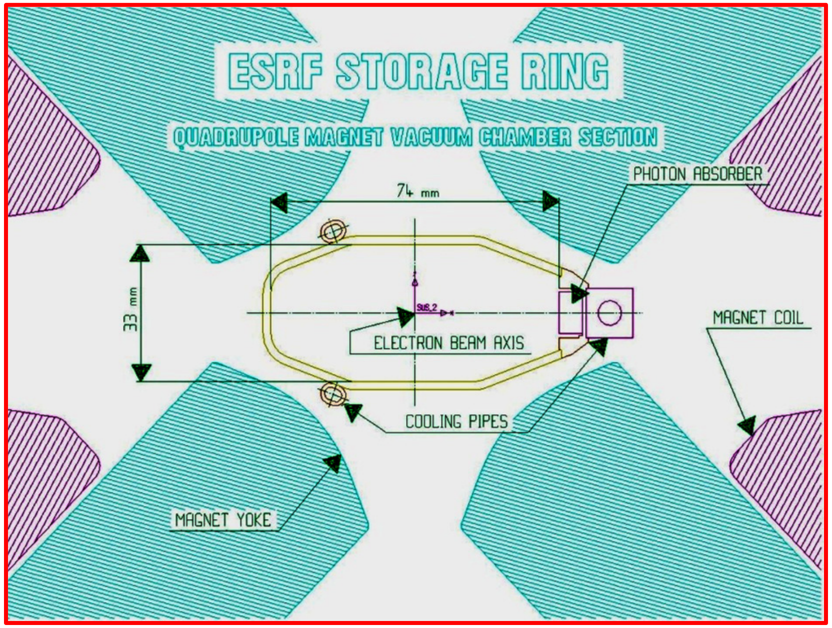

ESRF "Blue Book" CAD ray-tracing (in the plane of the orbit only):

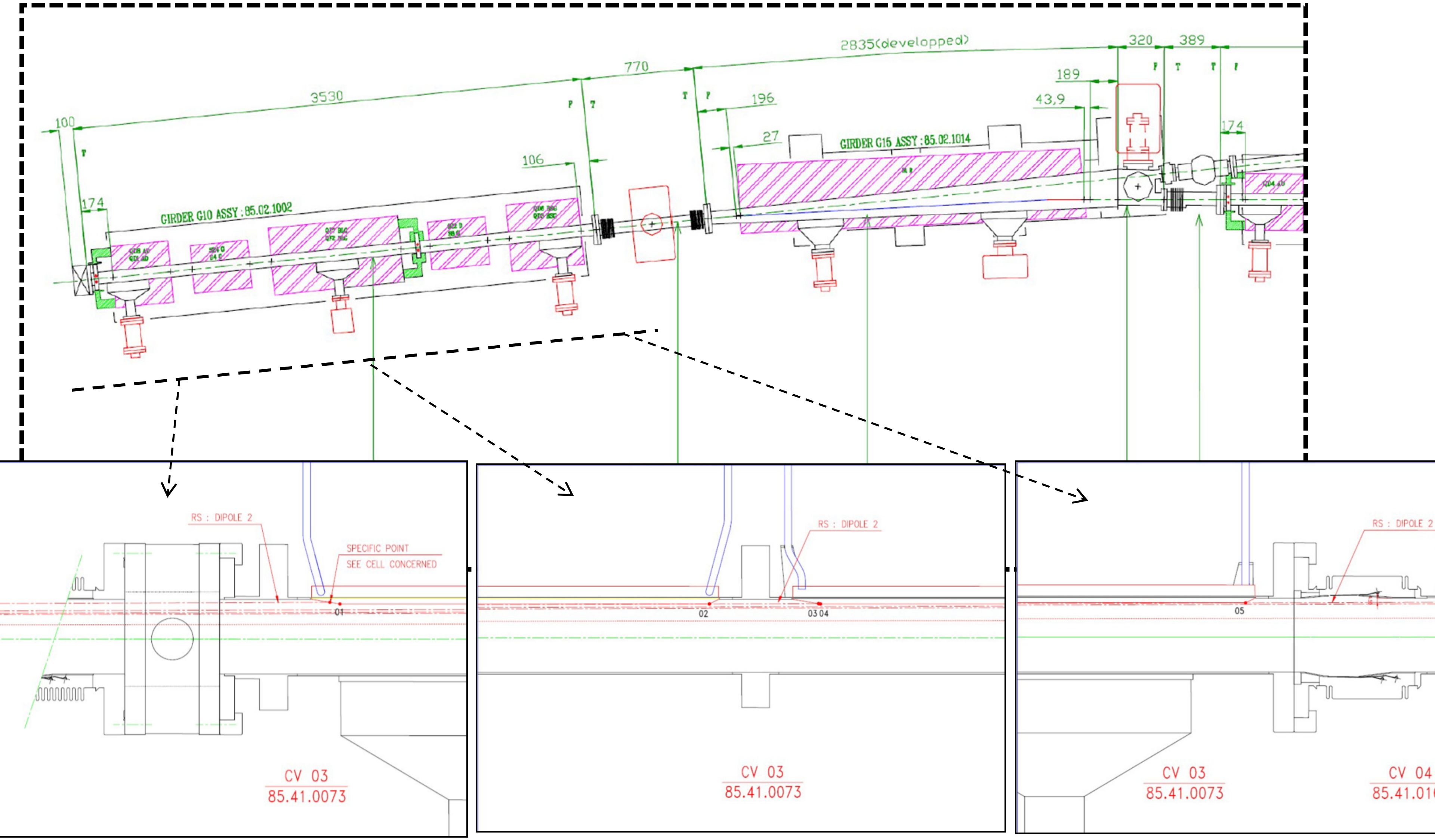

75

ESRF "Blue Book" CAD ray-tracing (in the plane of the orbit only):

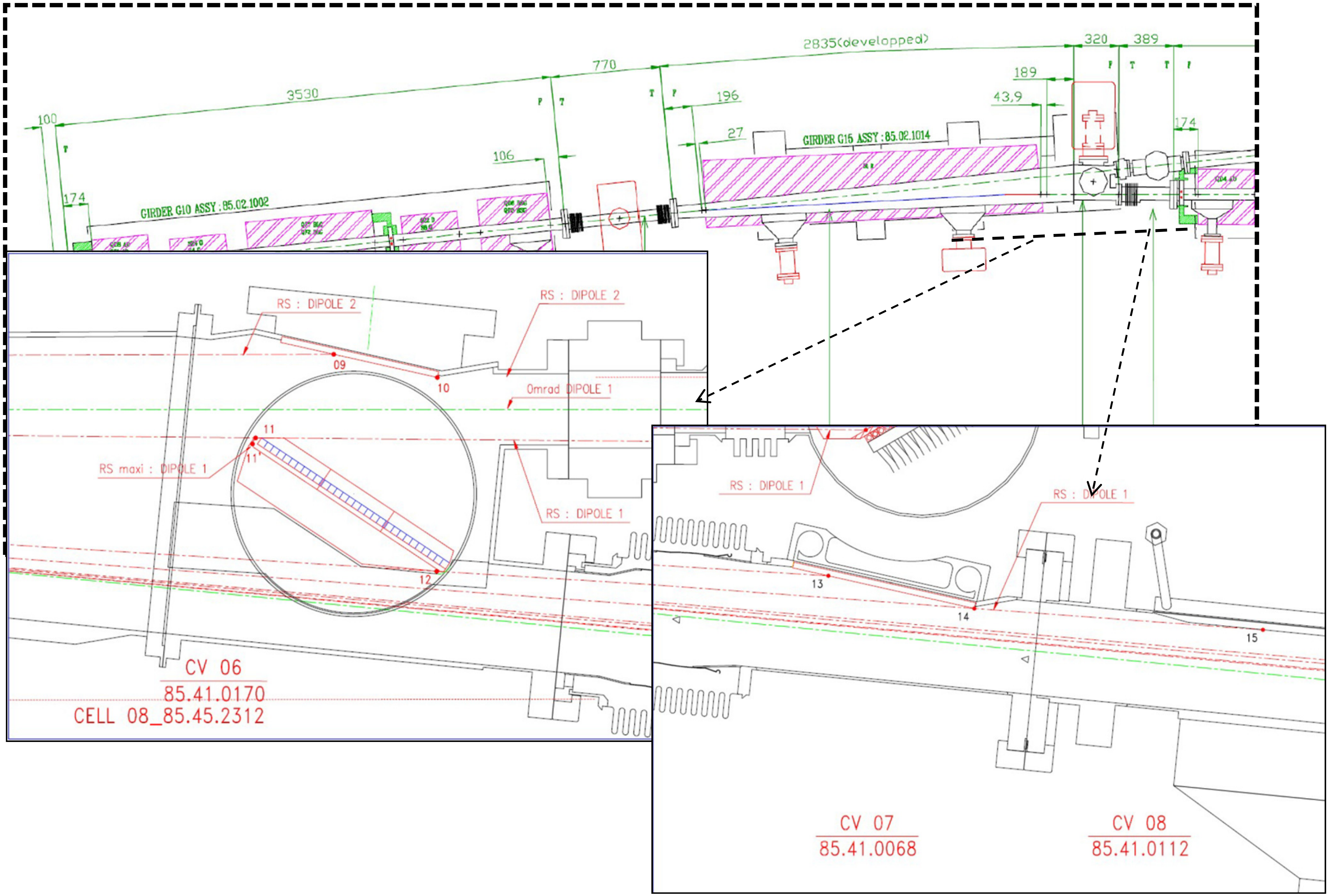

ESRF "Blue Book" CAD ray-tracing (in the plane of the orbit only):

Synchrotron Radiation Power Distribution on the Absorbers in the ESRF Storage Ring : *Standard part of a Cell*

common parts for all cells except cell 03-04-07-15

E=6 GeV, I=200 mA

64 bending magnets with soft end : B=0.857 T, B(softend)=0.40 T

Vertical emittance =4E-11 m.rad, Vertical dimension at source point 37 µm, Angular deviation =1.07 µrad

Pt n°	Src	Src n°	X *mm*	Y *mm*	α *°*	β *°*	σ *mm*	Pl *W/mm*	Pa *W/mm2*	Ptot *W*	CV n° / drawing n°
1	2H	2	10 614	37.00	0.199	0.199	0.912	**0.05**	**0.02**	**130**	CV 03 / 85.41.0073
2		2	12 728	37.00	0.166	0.166	1.090	**0.04**	**0.01**		
3		2	12 846	37.34	0.166	9.628	1.101	**2.03**	**0.73**		
4		2	12 848	37.00	0.165	9.627	1.101	**2.02**	**0.73**		
5		2	13 965	37.00	0.151	0.151	1.195	**0.03**	**0.01**		
6	2H	2	14 200	37.62	0.151	9.614	1.215	**1.83**	**0.60**	**18**	CV 04 / 85.41.0107
7		2	14 204	37.00	0.149	9.611	1.216	**1.83**	**0.60**		
8		2	14 620	37.00	0.145	0.145	1.251	**0.03**	**0.01**		
9	2H	2	17 750	44.90	0.145	12.770	1.517	**1.94**	**0.51**	**167**	CV 06 / fixed absorber 85.41.0170
10	2H	2	17 835	26.00	0.083	12.708	1.522	**1.93**	**0.50**		
11	1H	1	249	127.02	5.064	56.936	0.214	**52.90**	**98.51**	**8 160**	CV 06 / crotch absorber 85.41.0170
11'	1H	1	247	121.48	4.939	90.000	0.210	**64.51**	**122.71**		
12	1H	1	406	35.20	2.074	30.074	0.126	**55.65**	**176.88**		
6_a	2H	2	18 273	26.64	0.083	29.917	1.560	**4.26**	**1.09**	**1 759**	Beam Port
6_b	2H	2	18 227	0.00	0.000	30.000	1.553	**4.29**	**1.10**		
6_b'	1H	1	781	204.89	5.625	150.000	0.279	**24.11**	**34.52**		
6_c	1H	1	732	169.79	5.064	149.789	0.255	**26.57**	**41.57**		
13	1H	1	717	46.46	2.074	9.074	0.151	**14.34**	**37.88**	**1 833**	CV 07 / 85.41.0068
14		1	843	31.00	1.403	8.403	0.139	**14.54**	**41.79**		

CROTCH-2 AND CV13 GEOMETRY:

Total flux @200ma: 5.82E+18 ph/s (46mrad)

TOP-VIEW

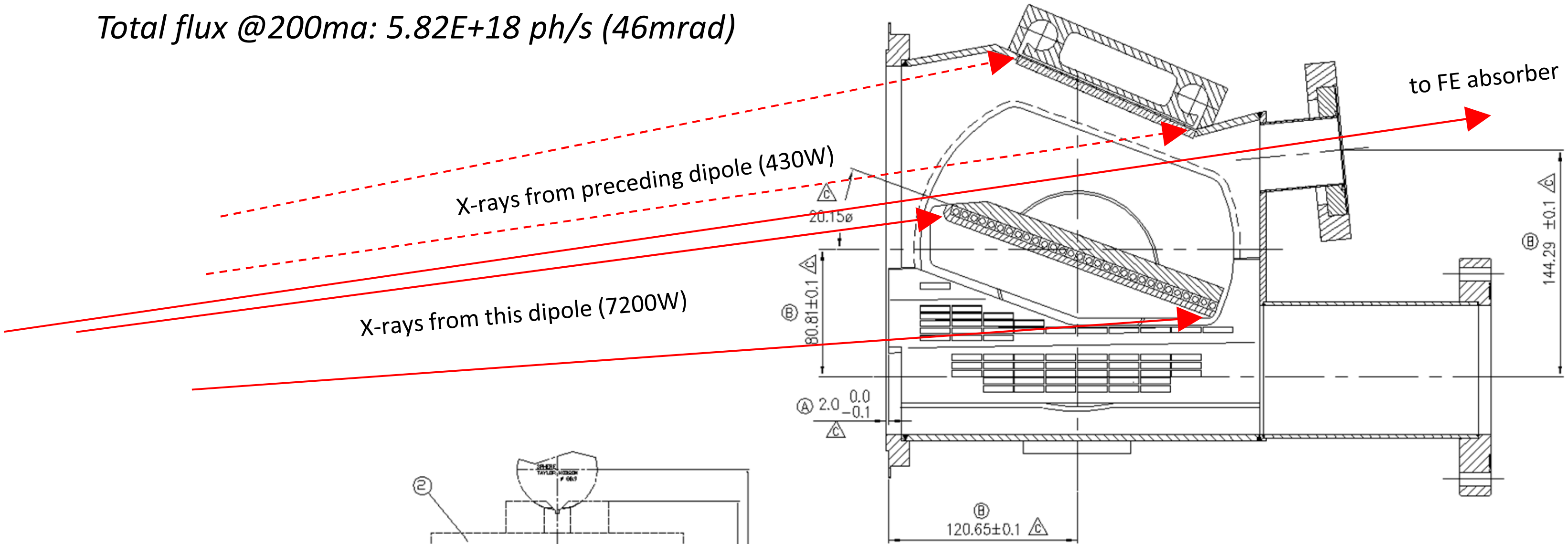

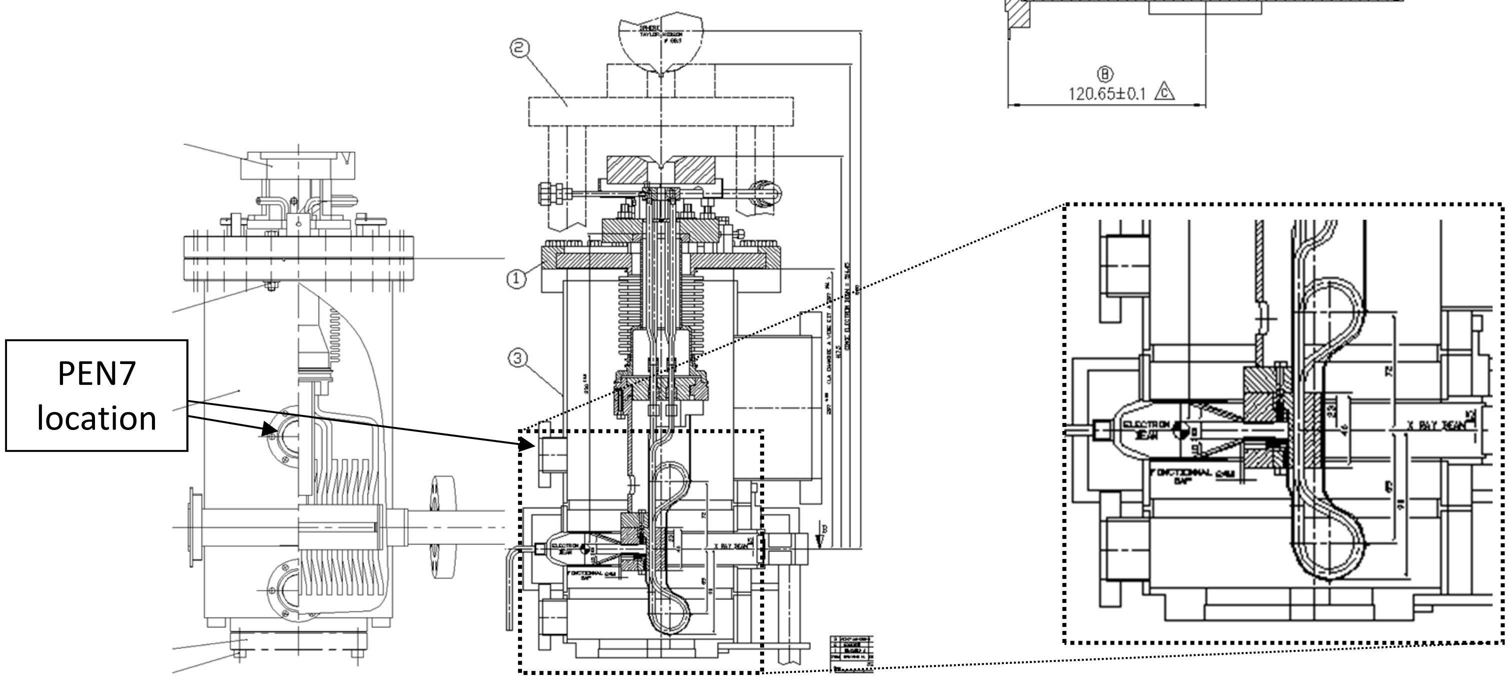

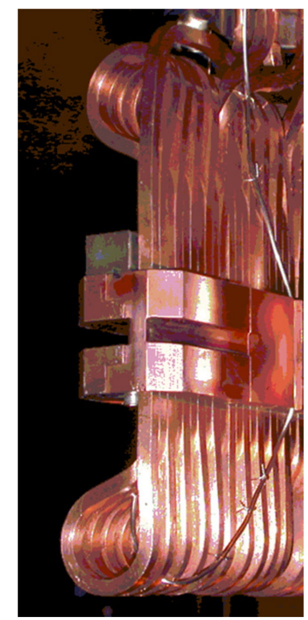

< -------------------------- SIDE-VIEW / CUT-OUTS -------------------------- >

DIPOLE-2 (CV12) GEOMETRY:

radius of curvature: 23.366 m

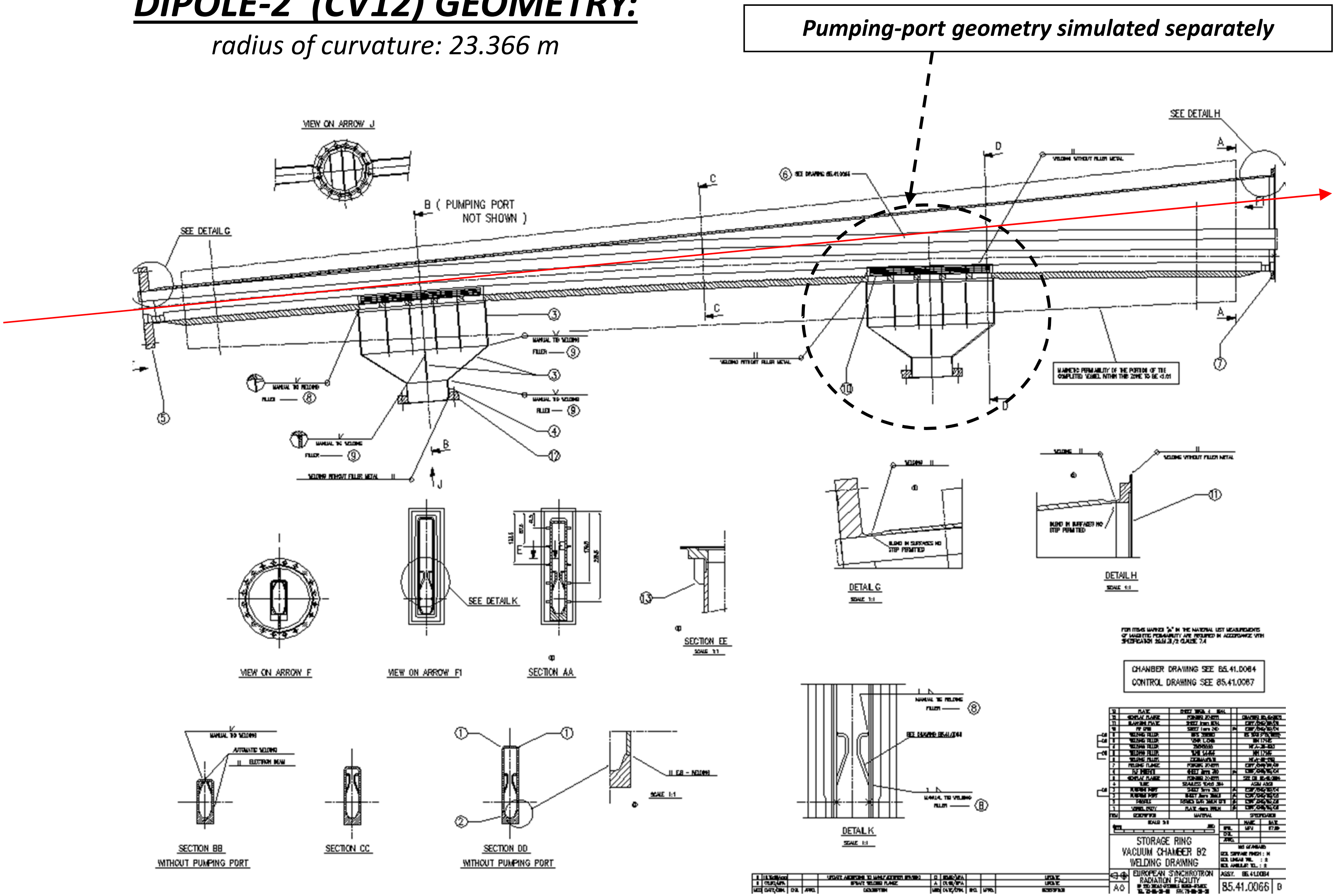

400 l/s SIP + GP500 NEG: simulated total pumping speeds of 500, 750, 1000 l/s

OLD DOS-based Molfow code (1989 → 2008)

pressure test facet:

320x20mm^2

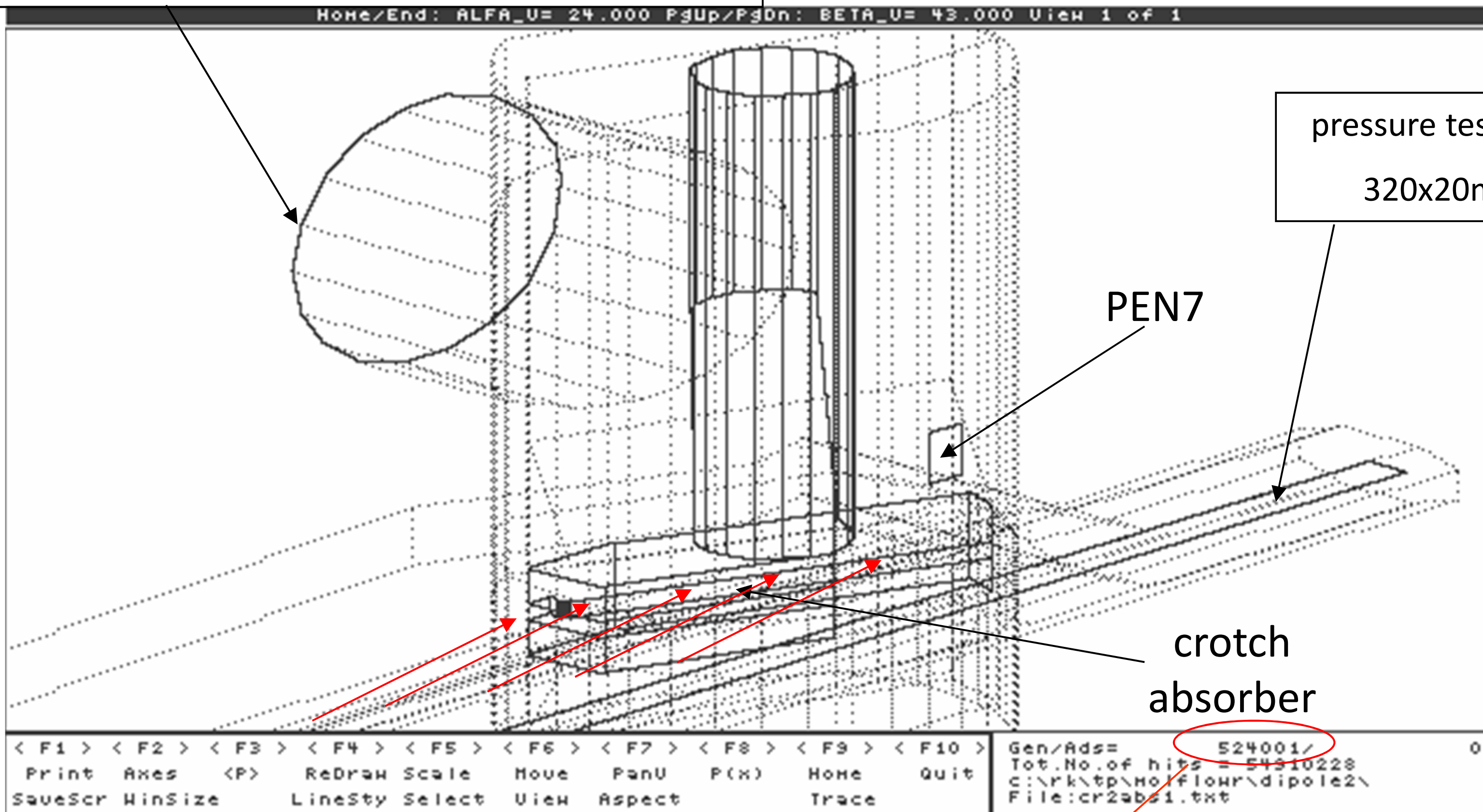

Closer view of the Molflow simulation model:

total number of points: 339; total number of facets: 131

computation time: ~15 hours

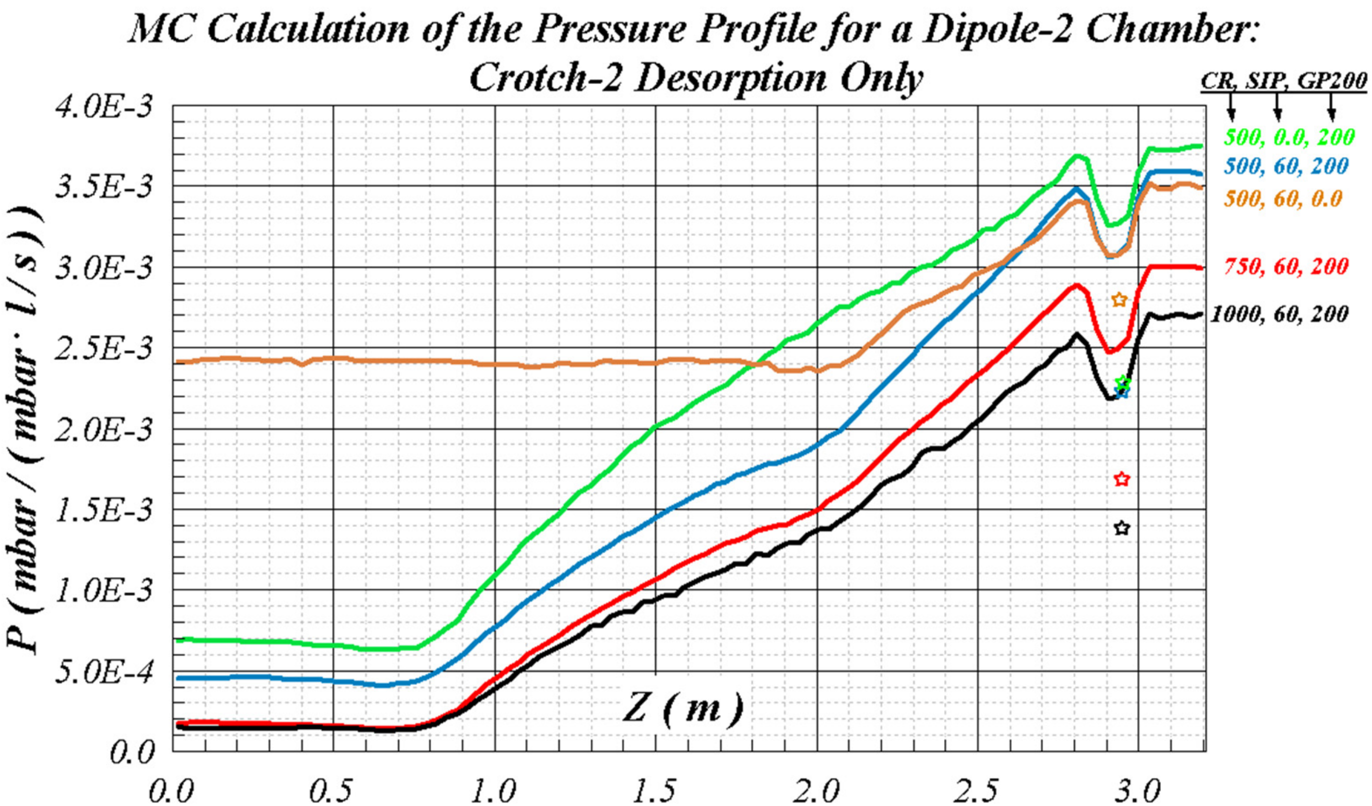

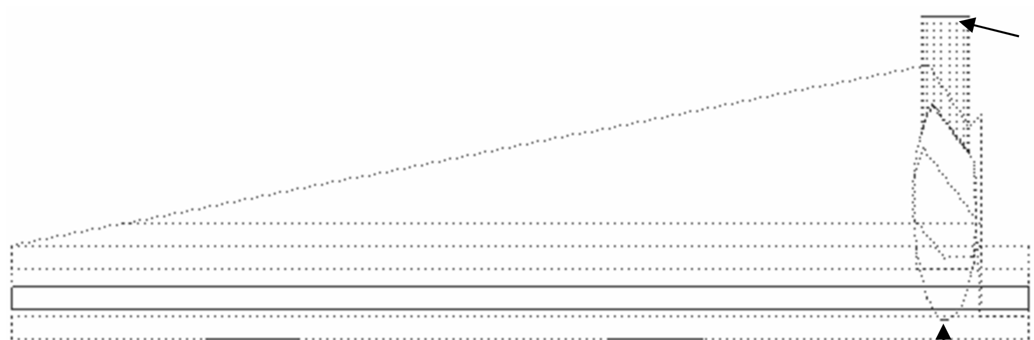

400 l/s
+
GP500

GP200
Pumping Port

60 l/s SIP
Pumping Port

PEN7
(star symbols)

ESRF DIPOLE PUMPING PORT GEOMETRY

MODELED AND SIMULATED WITH MOLFLOW:

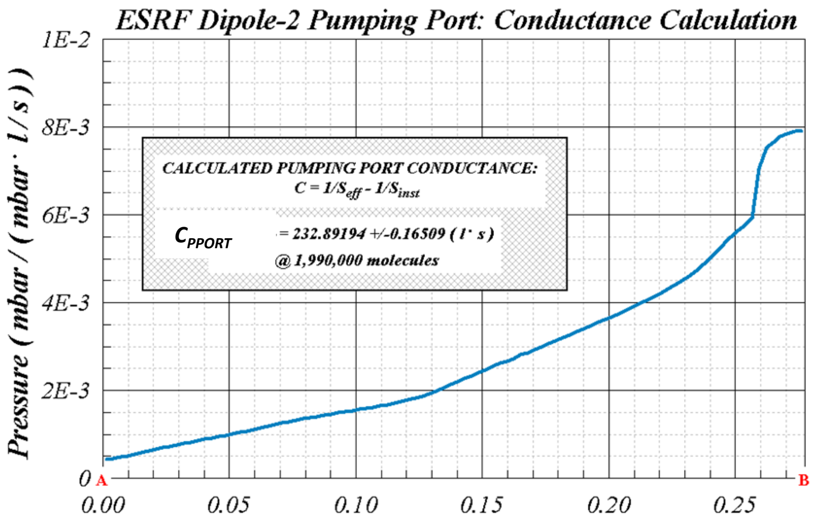

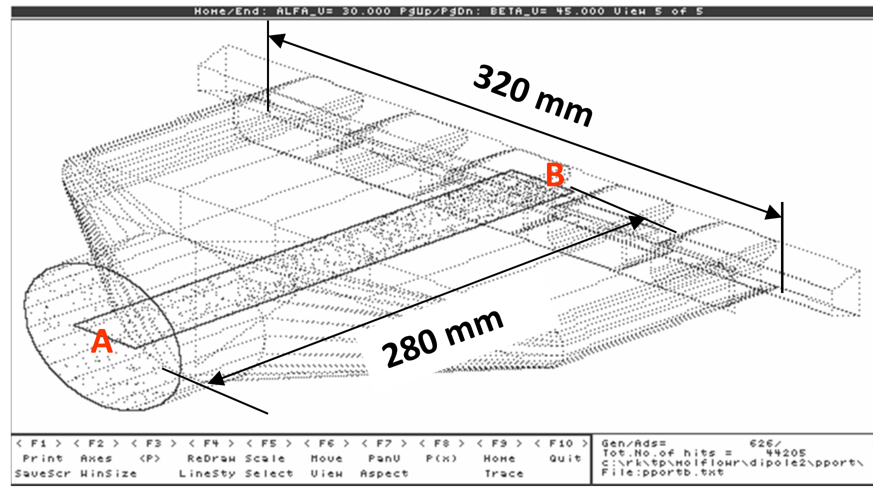

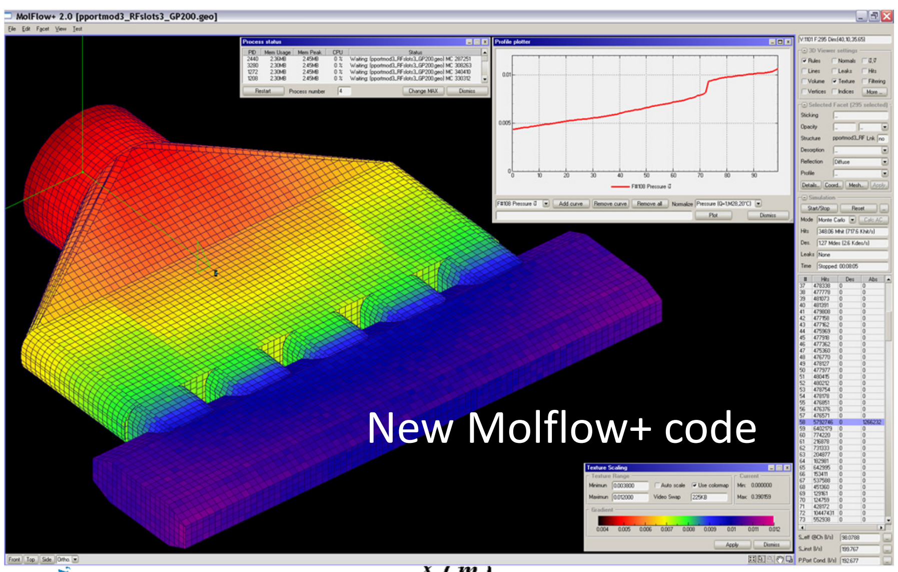

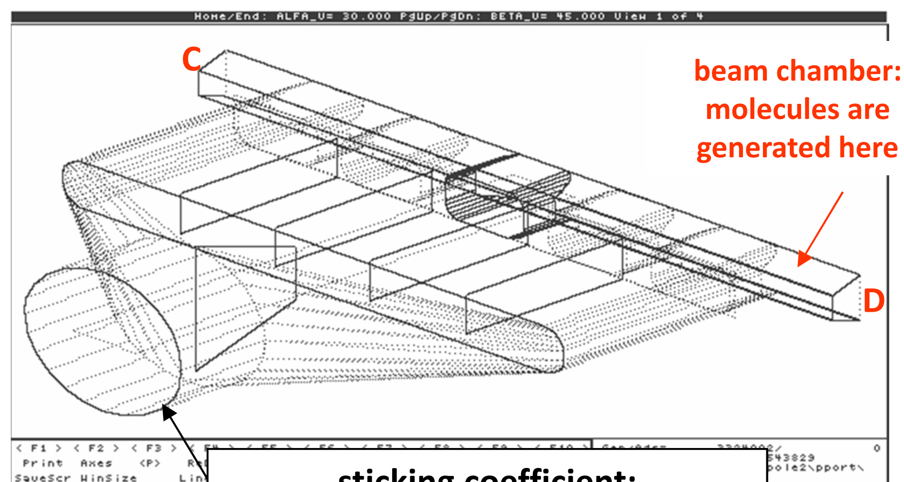

sticking coefficient:

s=1.0 → 913 l/s

s=0.0656 → 60 l/s

Molflow+ TPMC code: sample of modelling of one ESRF dipole/crotch 2 vacuum chamber and its pressure profile

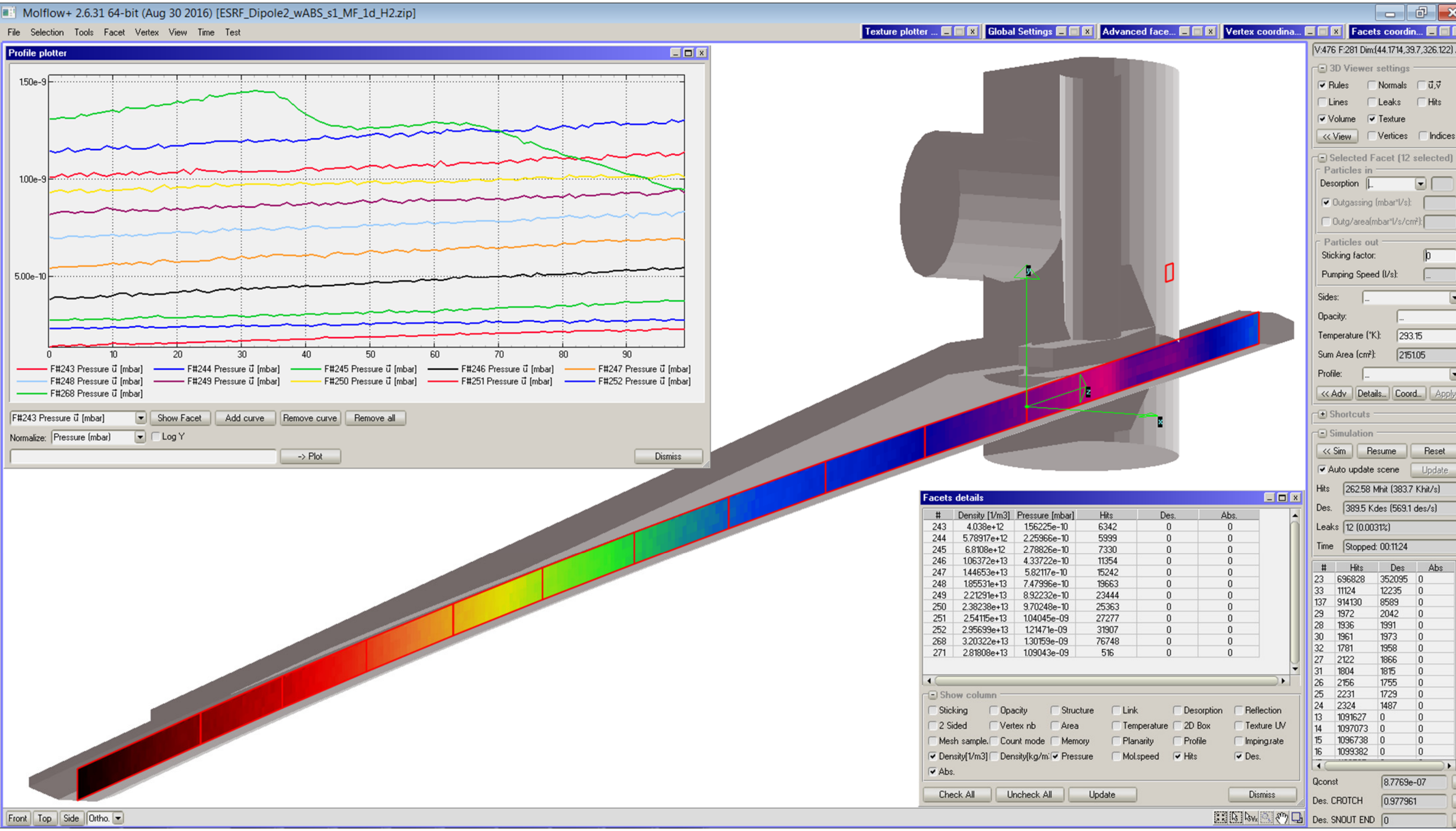

Modern version of Molflow code:

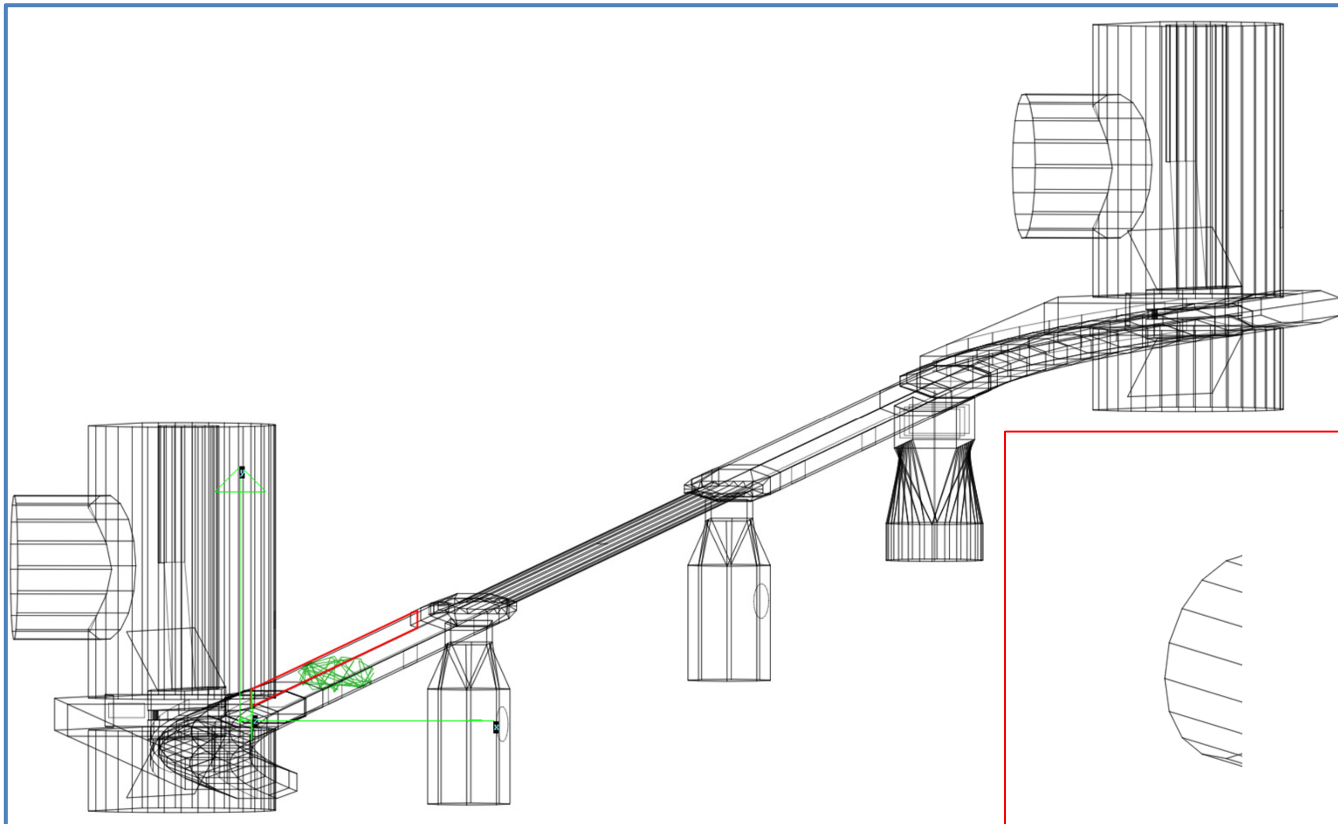

Modern version of SYNRAD+ code:

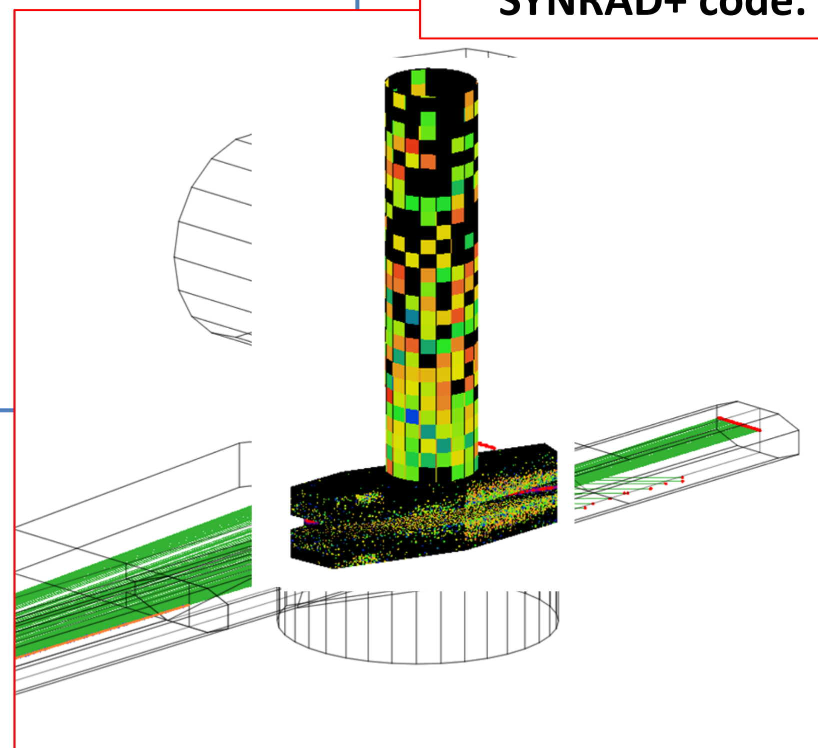

Details of a crotch absorber ray-tracing with SYNRAD+; Texture scale proportional to flux absorbed by corresponding facet

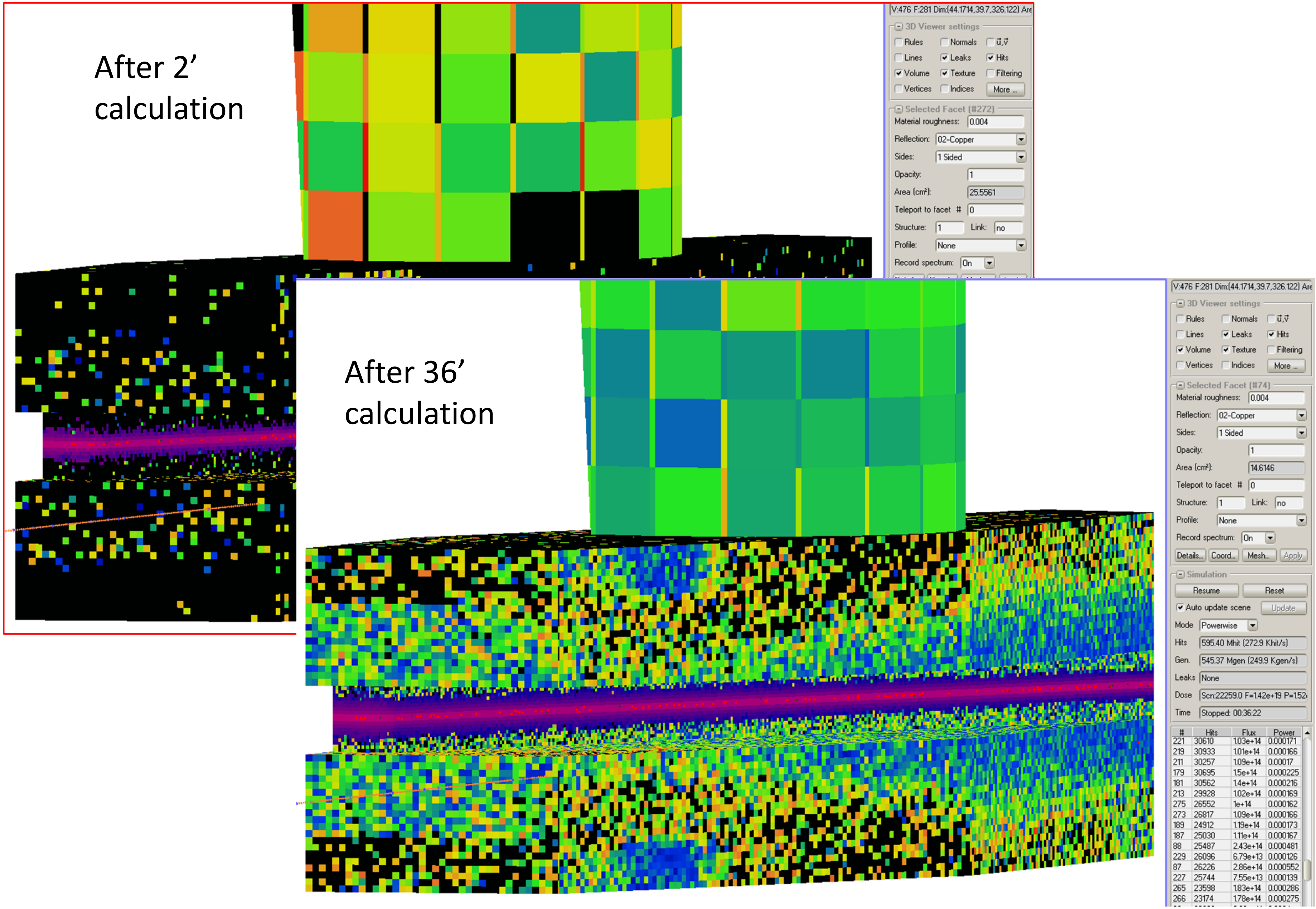

SR flux and power distribution and flux and power spectra with SYNRAD+

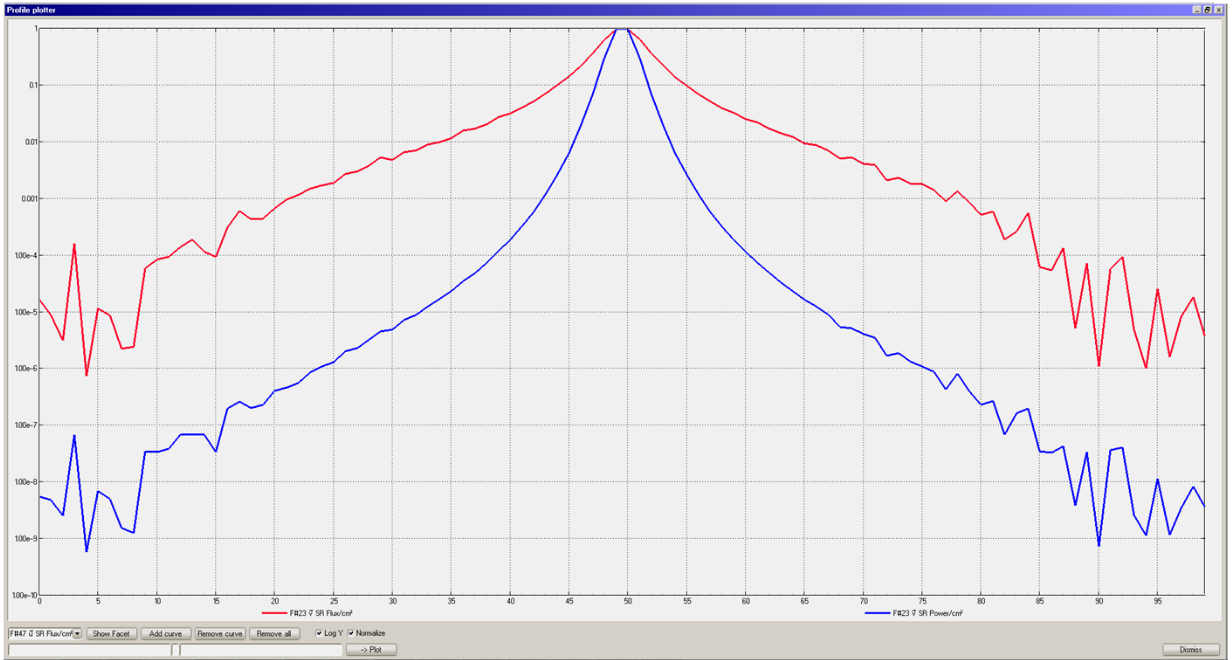

Left:

- SR flux and power distributions along the ~ 150 mm long flat absorber facet
- Note different width of “Gaussian” profile for F and P in the vertical direction (Red vs Blue curve)
- All curves normalized to 1

Right:

- SR flux and power spectra generated by SYNRAD+, normalized to 1;

SR-induced desorption and its consequences

MOPMA008 Proceedings of IPAC2015, Richmond, VA, USA

SIMULATION OF GAS SCATTERING LIFETIME USING POSITION- AND SPECIES-DEPENDENT PRESSURE AND APERTURE PROFILES *

M. Borland, J. Carter, H. Cease, and B. Stillwell, ANL, Argonne, IL 60439, USA

BREMSSTRAHLUNG SCATTERING LIFETIME

The differential bremsstrahlung cross-section for atomic number Z is [8, 9]

$$\frac{d\sigma}{dk} = 4\alpha r_e^2 \left\{ \left(\frac{4}{3k} - \frac{4}{3} + k \right) T_1(Z) + \frac{T_2(Z)}{9} \left(\frac{1}{k} - 1 \right) \right\}, \tag{9}$$

where k is the energy of the emitted photon as a fraction of the electron energy,

$$T_1(Z) = Z^2(L_{rad}(Z) - f(Z)) + ZL'_{rad}(Z), \tag{10}$$

and $T_2(Z) = (Z^2 + Z)$. The functions $L_{rad}(Z)$, $f(Z)$, and $L'_{rad}(Z)$ are described in [9]. The fractional change in energy of the electron is $u = -k$.

Gas-bremsstrahlung power:

electron stopping power
pressure in straight section
electron beam intensity
length of straight section

$$P = C \times \frac{dE}{dx}(E_e) \times p \times I \times L,$$

$$\frac{dE}{dx}(E_e) \propto E_e$$

$$p \propto E_e \times I$$

$$\boxed{P \propto E_e^{\,2} \times I^2 \times L}$$

ESRF: going from 200 mA → 300 mA: P × 2.25

Ref.: P. Berkvens et al., "Assessment of beamline shielding at the ESRF", 7th RadSynch Workshop, Saskatoon, CA, 2007

3. SR-induced desorption and

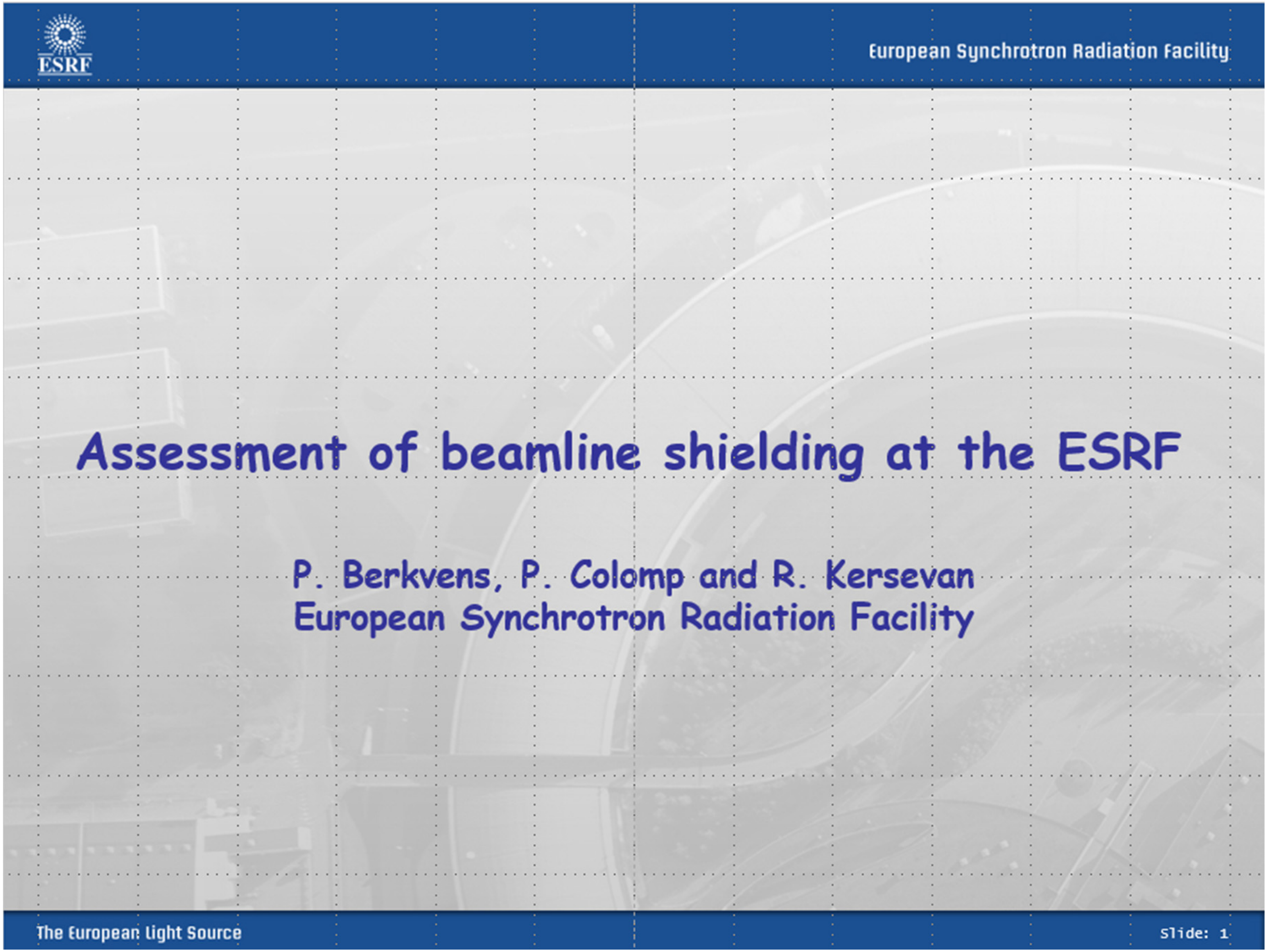

MOLFLOW: 3D Monte Carlo calculation of pressure distribution in storage ring vacuum chamber (developed by R. Kersevan)

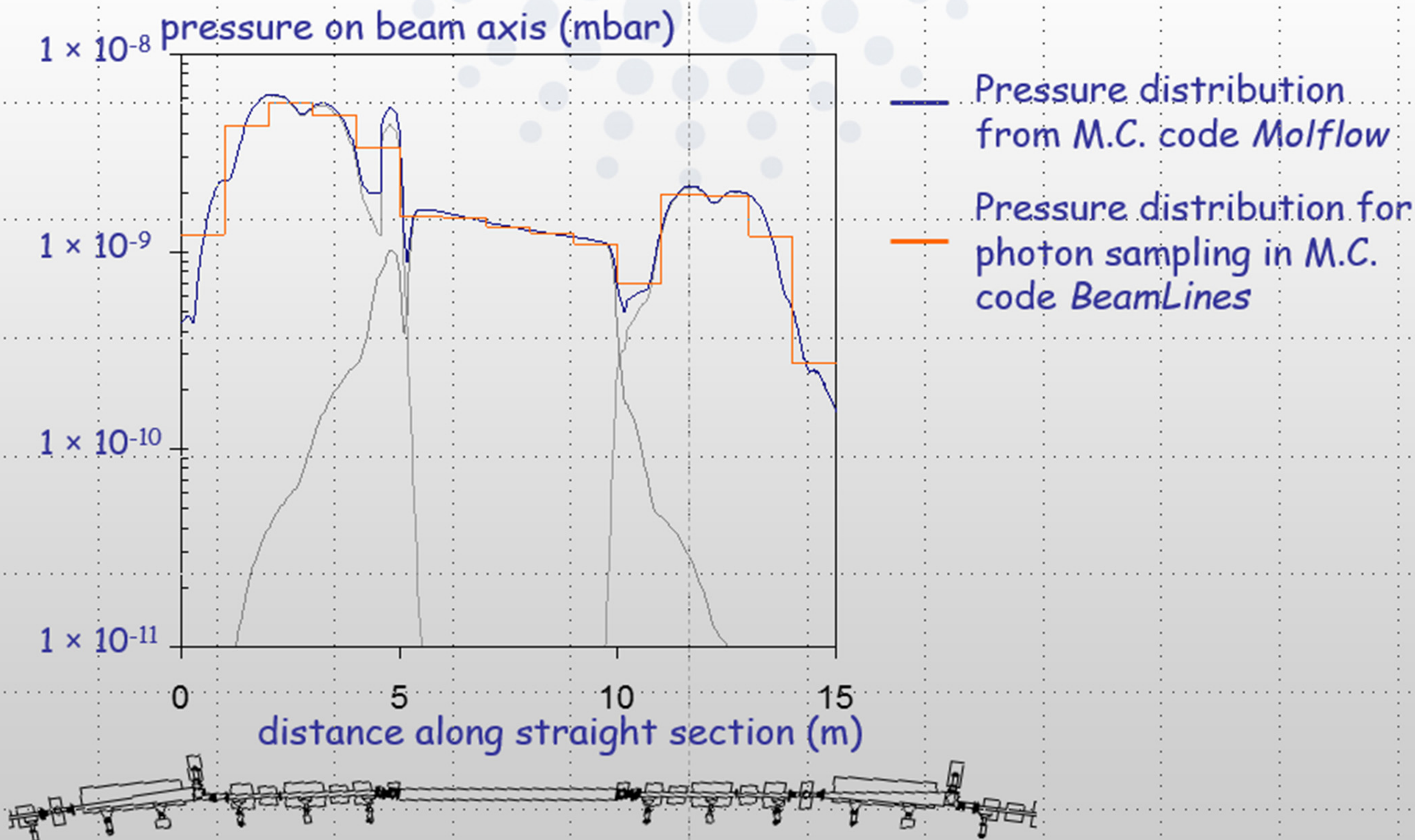

MOLFLOW: 3D Monte Carlo calculation of pressure distribution in storage ring vacuum chamber (developed by R. Kersevan)

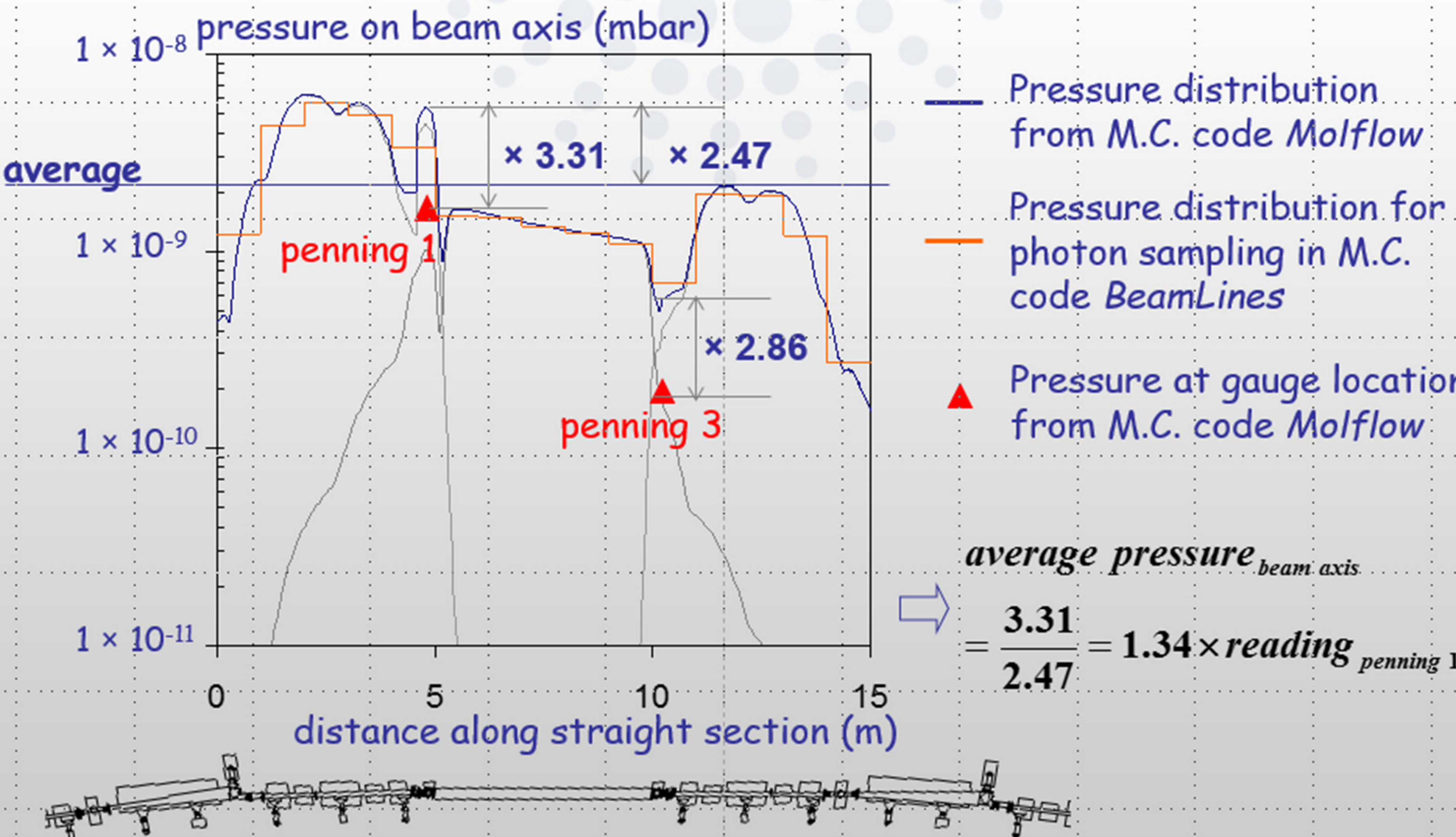

$$\Rightarrow \textit{average pressure}_{\textit{beam axis}} = \frac{3.31}{2.47} = 1.34 \times \textit{reading}_{\textit{penning 1}}$$

MOLFLOW: 3D Monte Carlo calculation of pressure distribution in storage ring vacuum chamber (developed by R. Kersevan)

average pressure$_{\text{beam axis}}$ = 1.34 × reading$_{\text{gauge}}$

for average pressure of 1×10^{-9} mbar in straight section :

- CV500: 6.37×10^{-10} mbar
- rest: 1.18×10^{-9} mbar

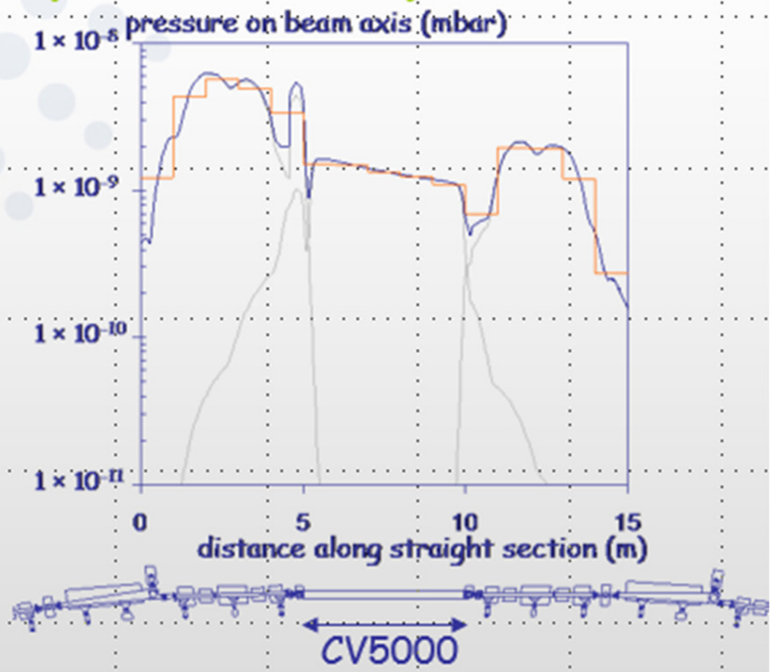

Residual gas composition in straight section (from RGA analysers)

molecule	relative pressure (%) inside CV5000	relative pressure (%) rest of straight section
H_2	85	80
CO	15	10
CO_2	-	5
CH_4	-	3
H_2O	-	2

Shielding calculations are done with Monte Carlo code *BeamLines* developed by P. Berkvens:

- Electromagnetic shower description based on EGS4.
- Bremsstrahlung differential fluence calculated from theoretical cross sections, using realistic pressure distributions and residual gas compositions in the storage ring straight section.
- Direct sampling of photons (instead of electrons).
- 3D description of front end and optical components.
- Photo neutron dose distributions using differential photon track lengths and assuming an isotropic angular distribution.

Examples:

- ID20 Magnetic scattering beamline;
- ID12 Circular polarisation beamline.

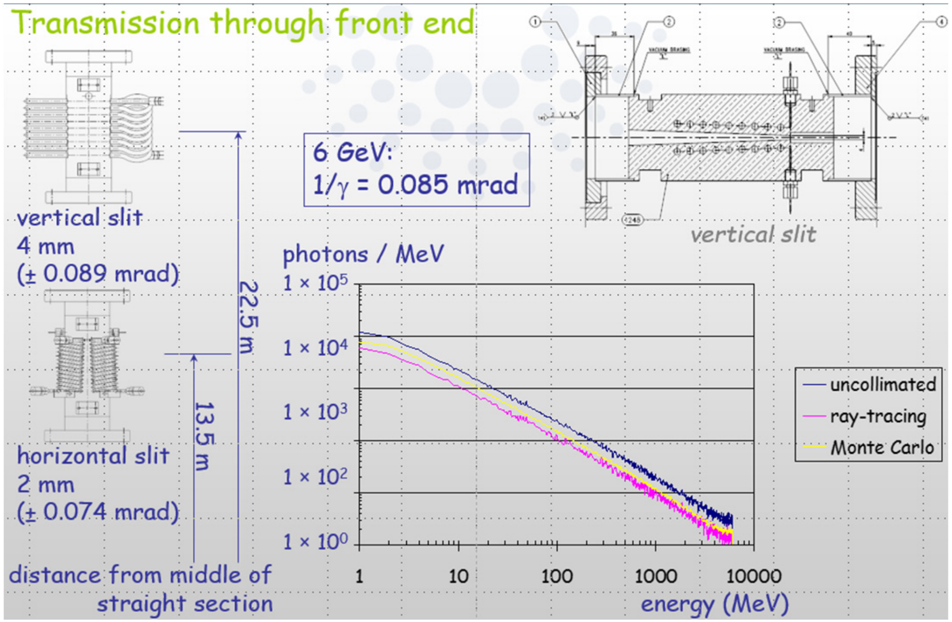

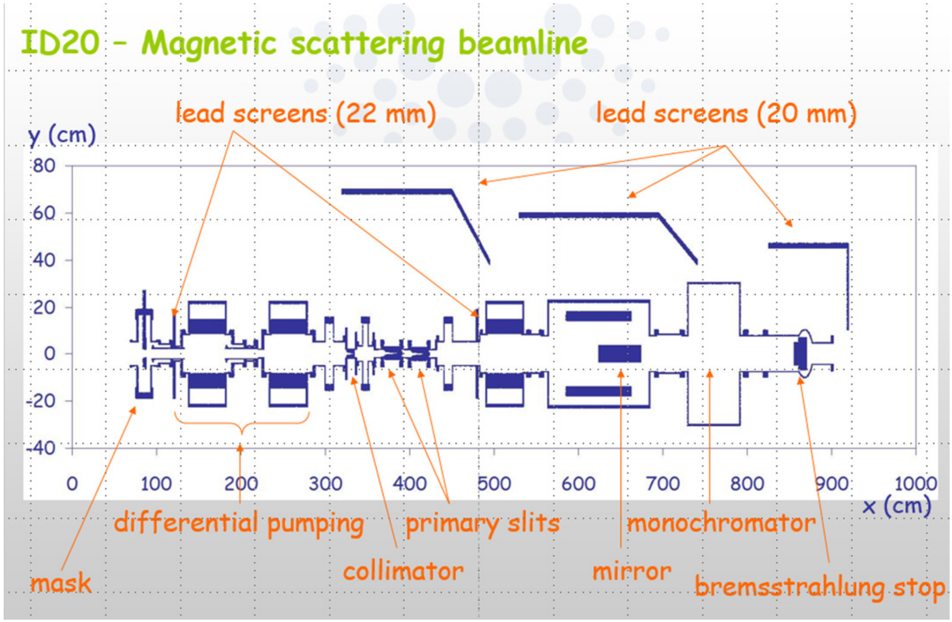

Summarizing: a double MC scheme is used;

- First a detailed 3D model of the storage ring's vacuum system is made:
  - SR ray tracing (SYNRAD+) generates the photon flux
  - TPMC simulation (Molflow+) converts the flux on all surfaces to local desorption, and then calculates the pressure profile along the e- beam path
- A second detailed model of the shielding of the Front-Ends (absorbers, collimators, etc…) and of the experimental beamline hutches is made:
  - Another independent MC simulation (based on EGS4-derived custom code) is run taking into account as source terms the beam-gas scattering in the storage ring and the subsequent scattering of the high-energy gamma rays along the FE and the BL components

Another example: Analysis and optimization of the crotch absorber of MAX-IV

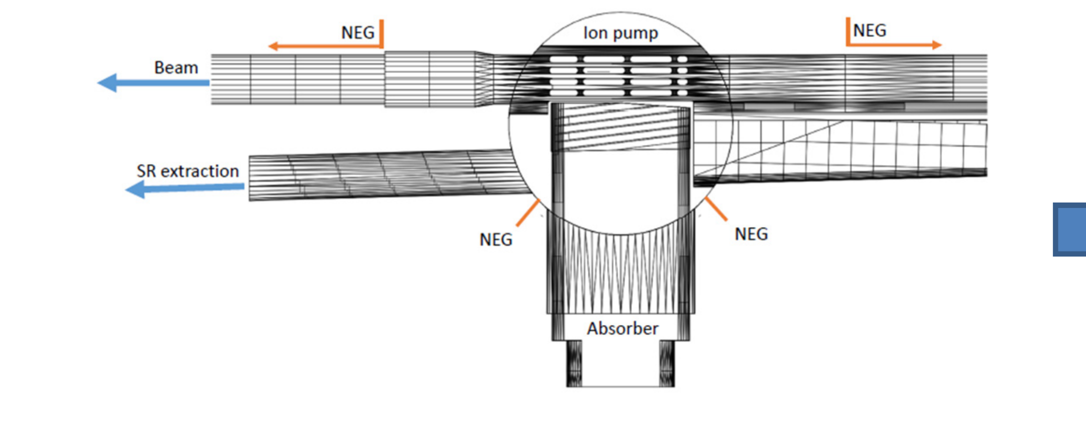

Figure 4.7: Top view of the vacuum chamber with the MAX IV crotch absorber

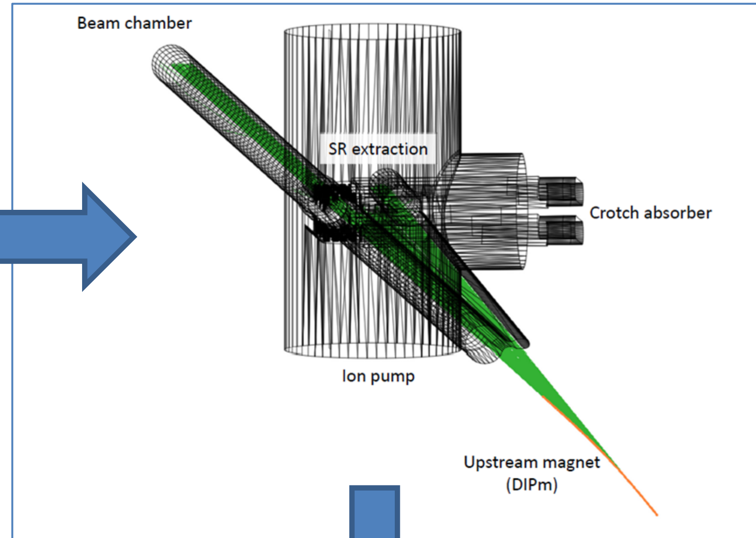

Figure 4.9: The dipole magnet and SR radiation schematics in Synrad+

From CAD model to SYNRAD+ simulation

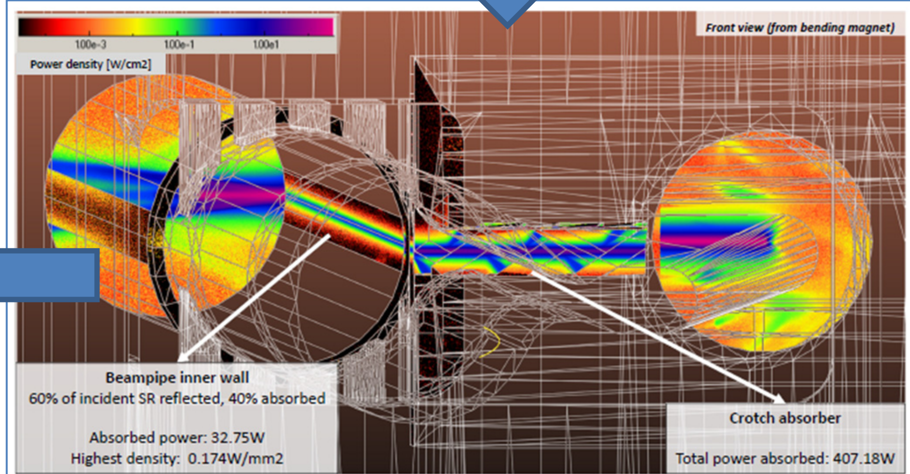

Figure 4.10: Power distribution on the walls

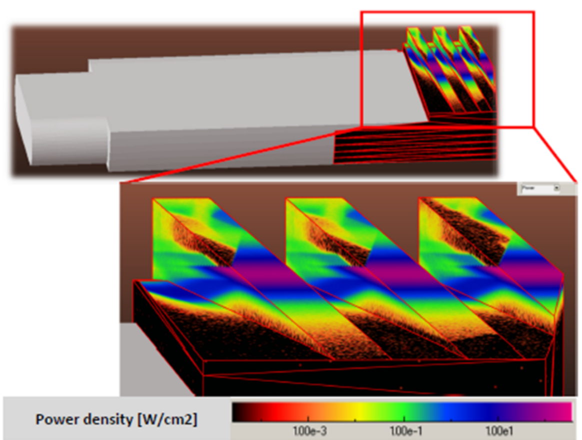

Figure 4.11: Power density on the lower jaw of the absorber

Ref.: "Monte Carlo simulations of Ultra High Vacuum and Synchrotron Radiation for particle accelerators", M. Ady, CERN, doctoral dissertation at EPFL, Lausanne, CH, May 2016; also as an IPAC-15 paper;

From SYNRAD+ simulation to Molflow+: → Pressure profile for CH_4

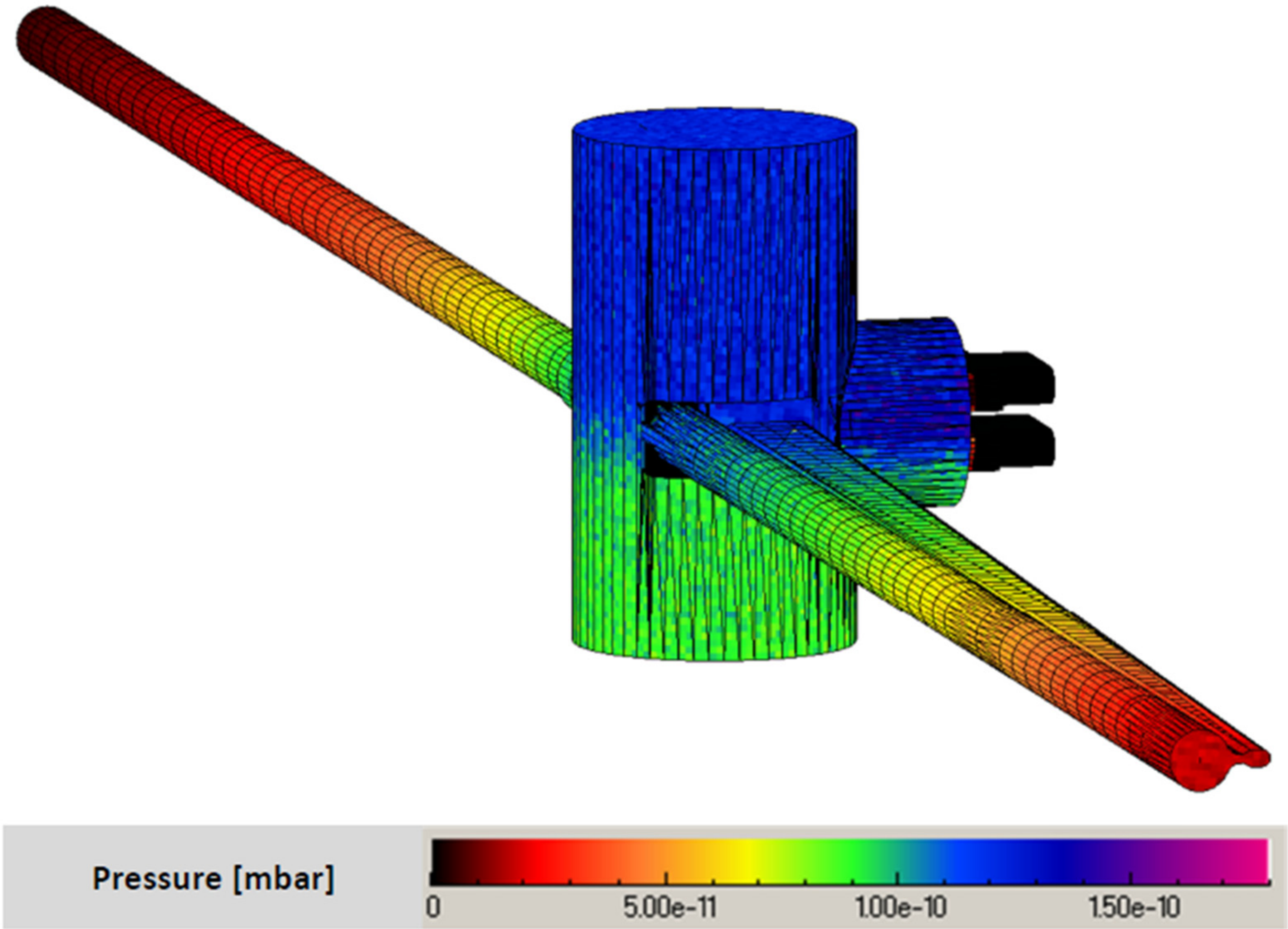

Figure 4.12: CH_4 simulation at 100Ah dose

Molflow+ : simulation of NEG-coating saturation

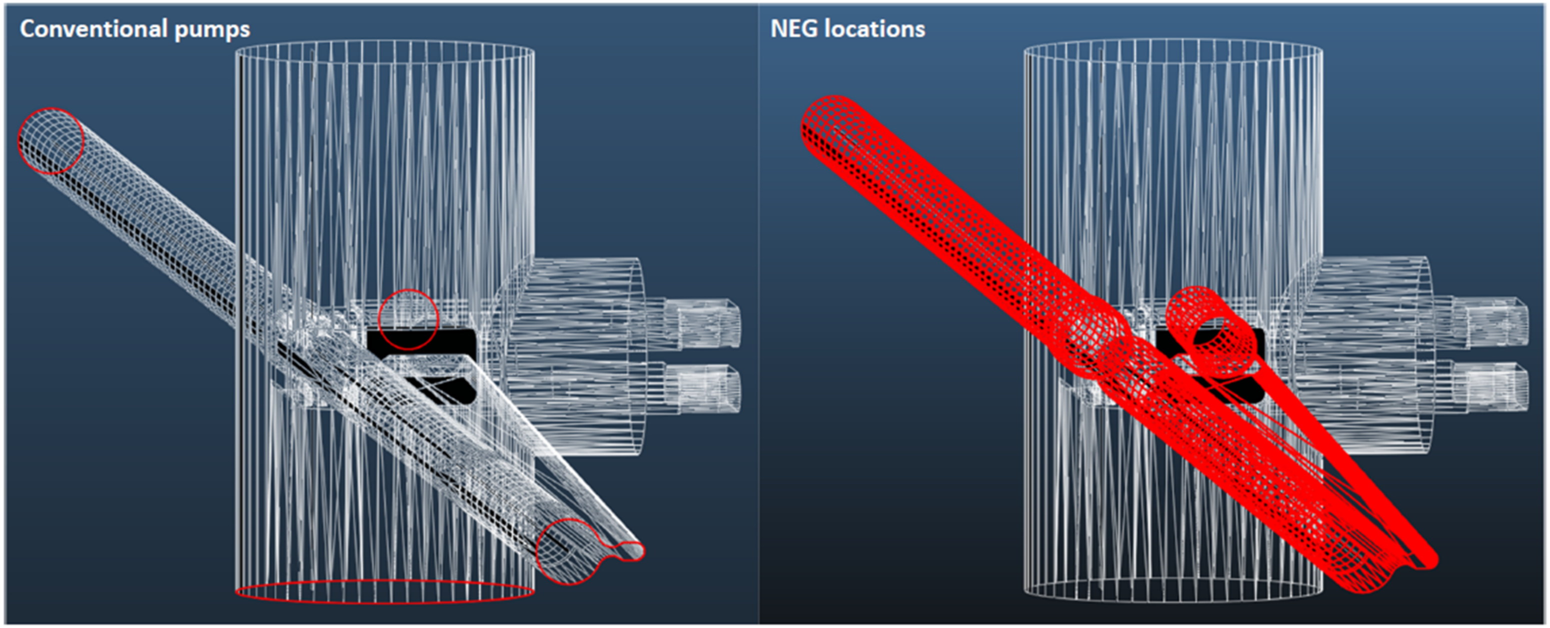

Figure 4.14: Pump locations defined for CO and CO2 for the Molflow simulations.
Left: End of modeled regions (sticking 0.1) and ion pump
Right: NEG locations (The central vertical cylinder is also NEG-coated, not shown for visibility)

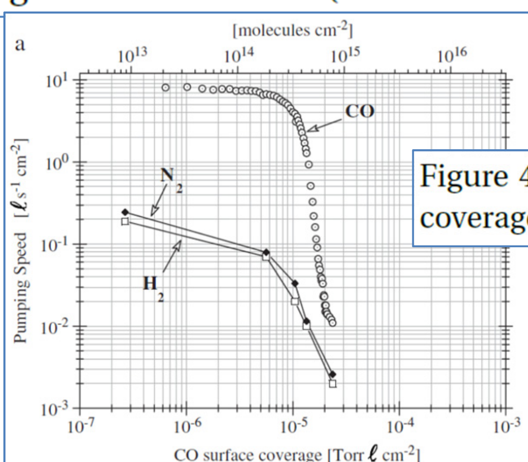

Figure 4.13: Figure 1.a from [79]: NEG pumping speed of CO as a function of its surface coverage

Molflow+ : simulation of NEG-coating saturation

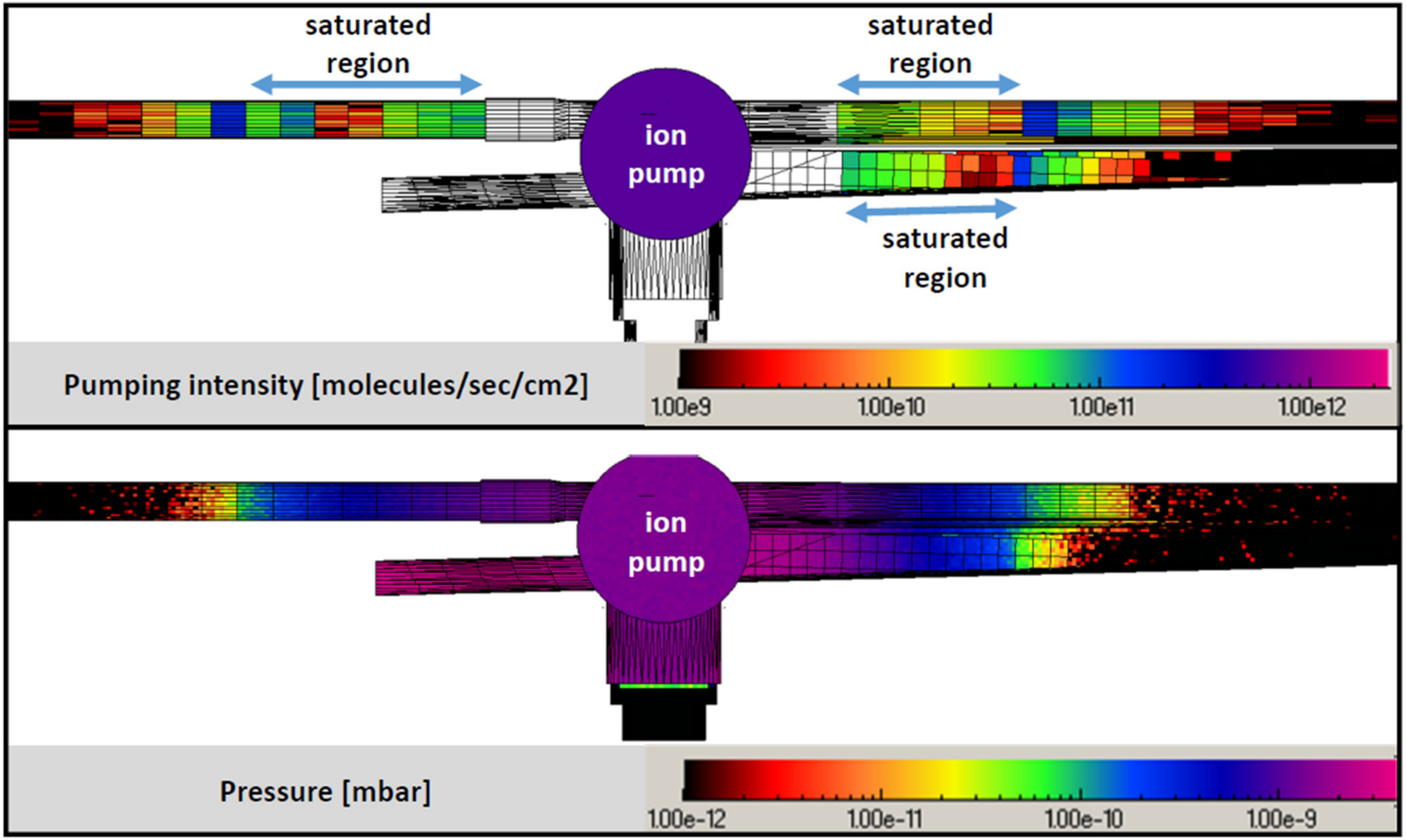

Figure 4.15: NEG saturation and its effect on pumping speed and pressure profile

Molfow+ : simulation of NEG-coating saturation, pressure profile for several gas species

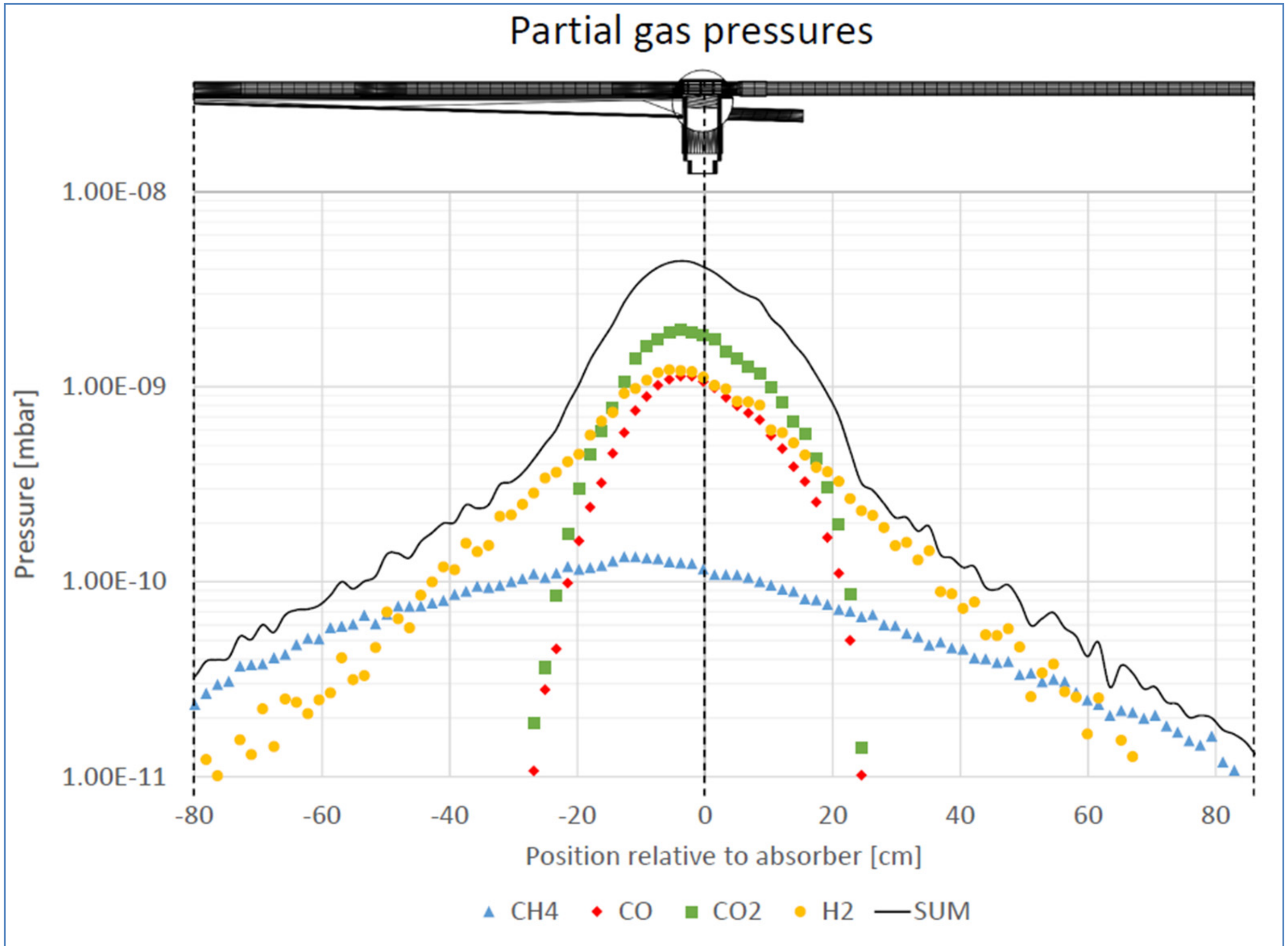

Figure 4.16: Partial gas pressures around the absorber

SYNRAD+ : simulation of SR power and flux on crotch absorbers of the APS ring

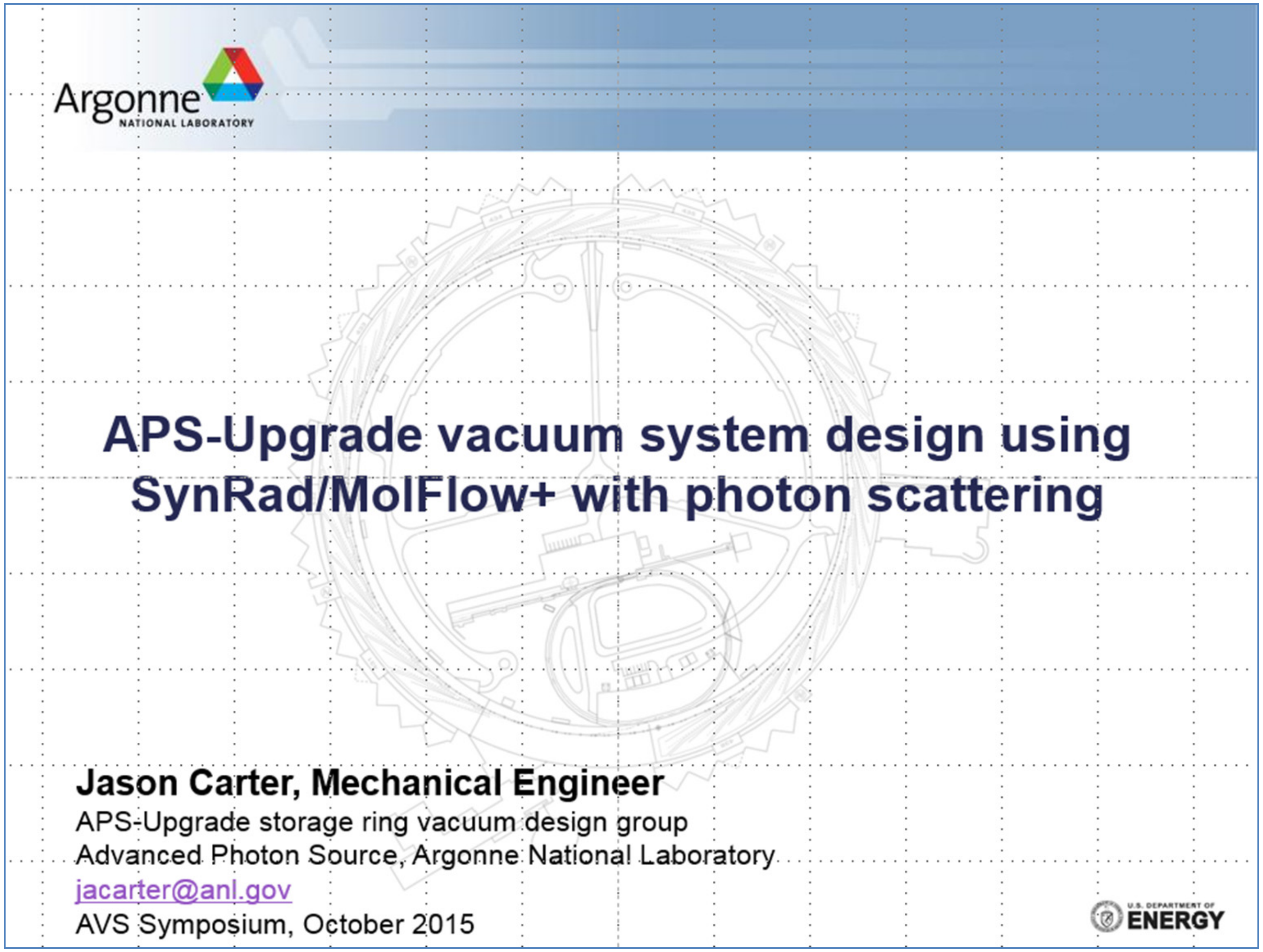

Source: J. Carter, APS Upgrade team, ANL, Argonne, AVS Conference, 2015

SYNRAD+ : simulation of SR power and flux on crotch absorbers of the APS ring

How SynRad works

- Demonstrate SynRad applications with APS photon absorber example

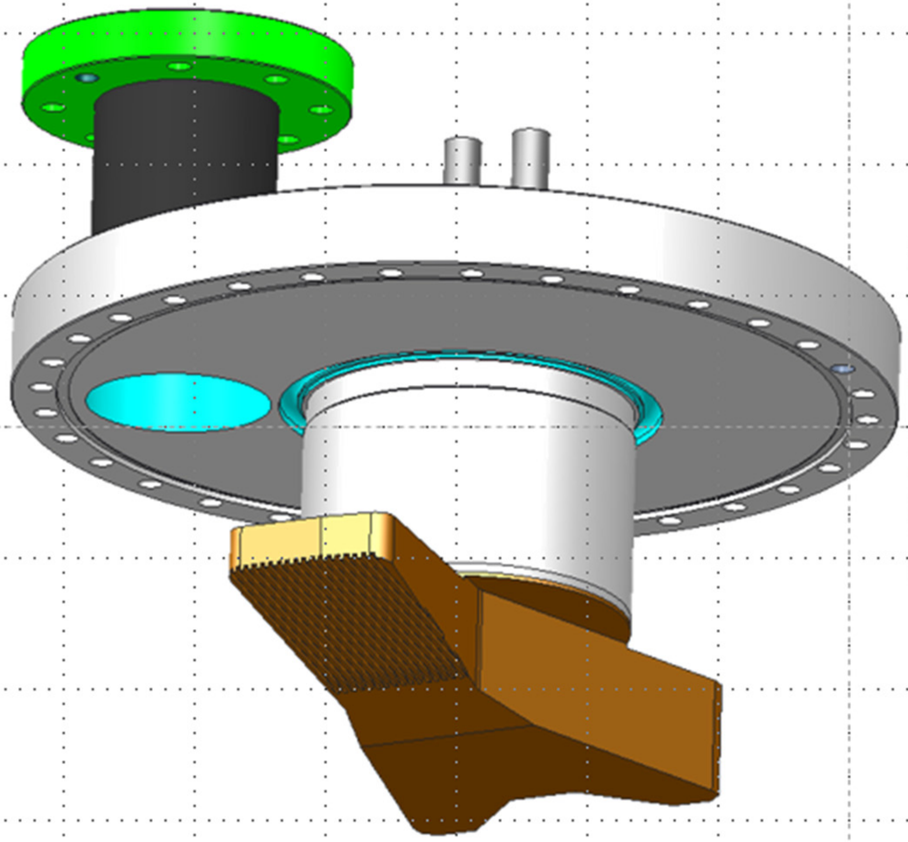

3D CAD model of absorber assembly

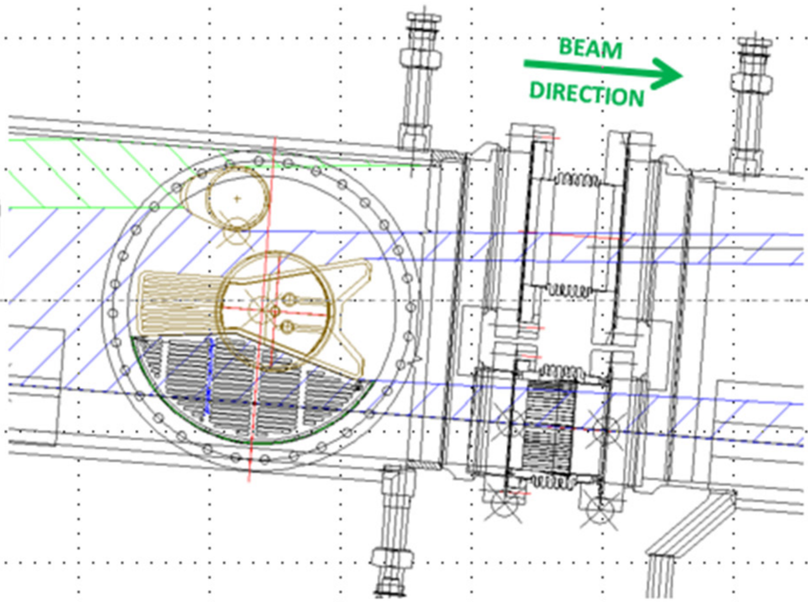

Top view of 2D CAD synchrotron ray trace

SYNRAD+ : simulation of SR power and flux on crotch absorbers of the APS ring

How SynRad works

- 3D CAD model built representing interior volume of vacuum system and all surfaces under vacuum

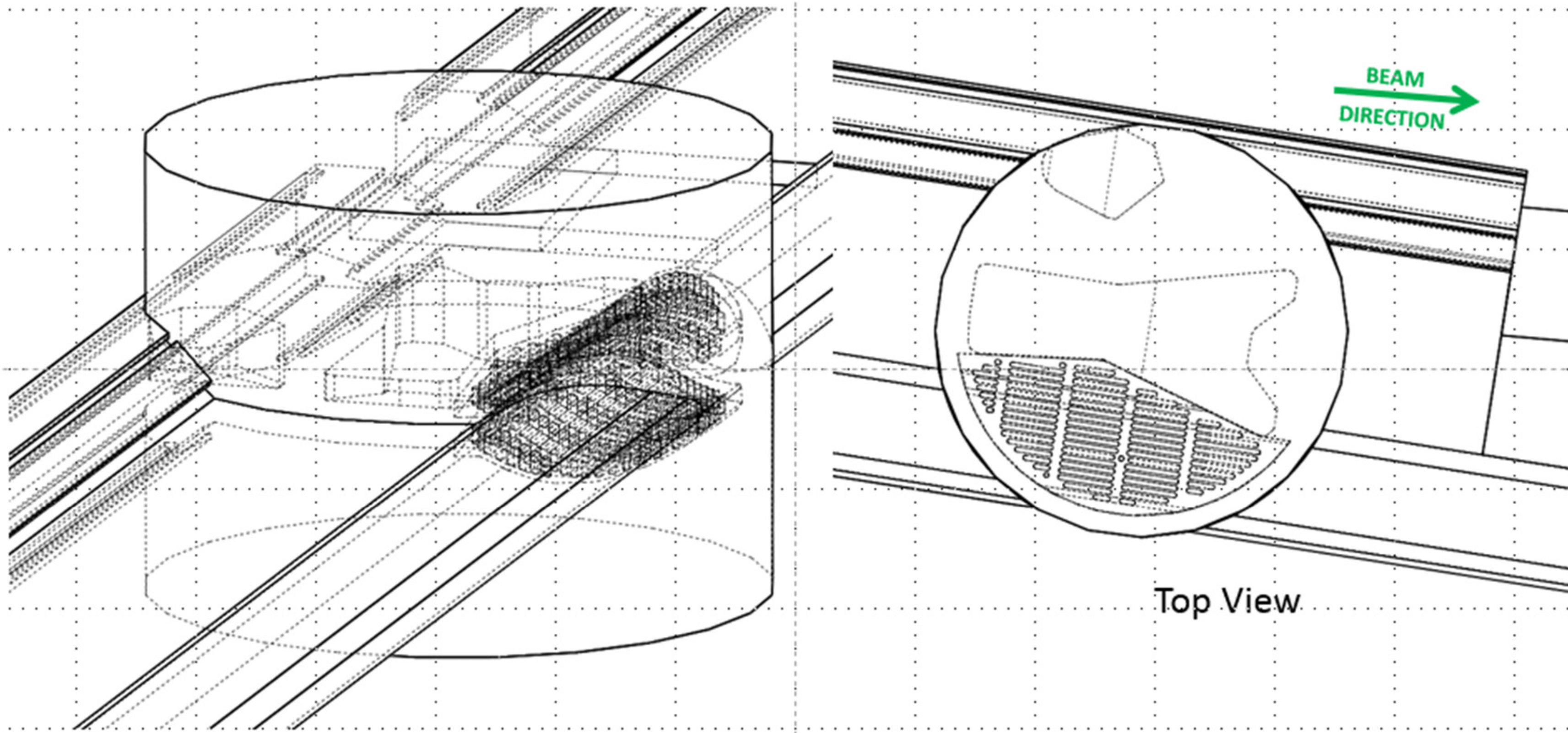

3D CAD with hidden lines shows
two absorbers and an RF screen within a pumping port

SYNRAD+ : simulation of SR power and flux on crotch absorbers of the APS ring

How SynRad works

- Model exported as STL file type, imported into SynRad as planar surface 'facets'
  - Material definitions applied to surfaces to induce photon scattering

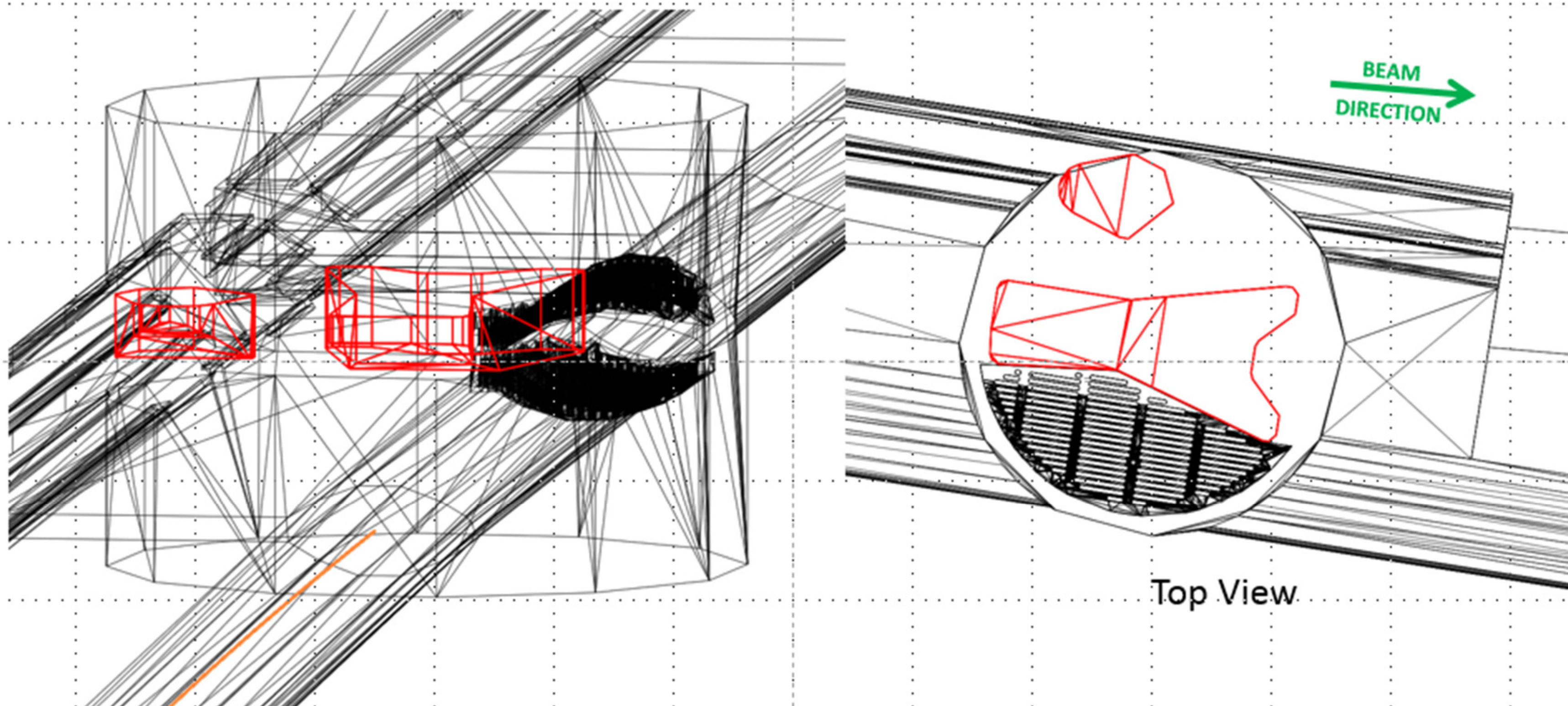

Absorber bodies highlighted in **red**

SYNRAD+ : simulation of SR power and flux on crotch absorbers of the APS ring

How SynRad works

- Magnetic elements generate synchrotron rays within 3D space

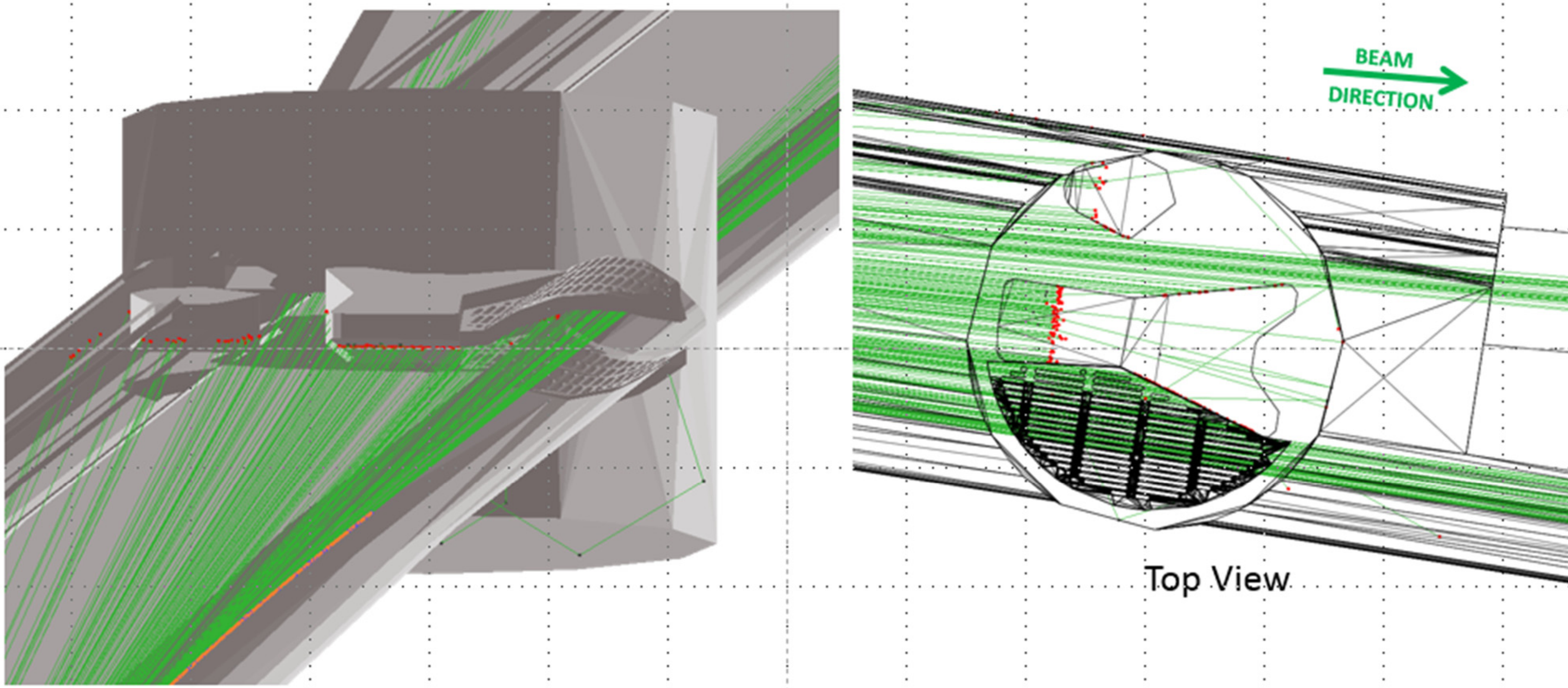

Magnetic elements in orange, program generated synchrotron fan in green, surface hit points in red

SYNRAD+ : simulation of SR power and flux on crotch absorbers of the APS ring

How SynRad works

- Flux gradient collected on meshed surfaces
  - Finer mesh for direct incidence surfaces, coarser mesh on surfaces receiving scattered photons

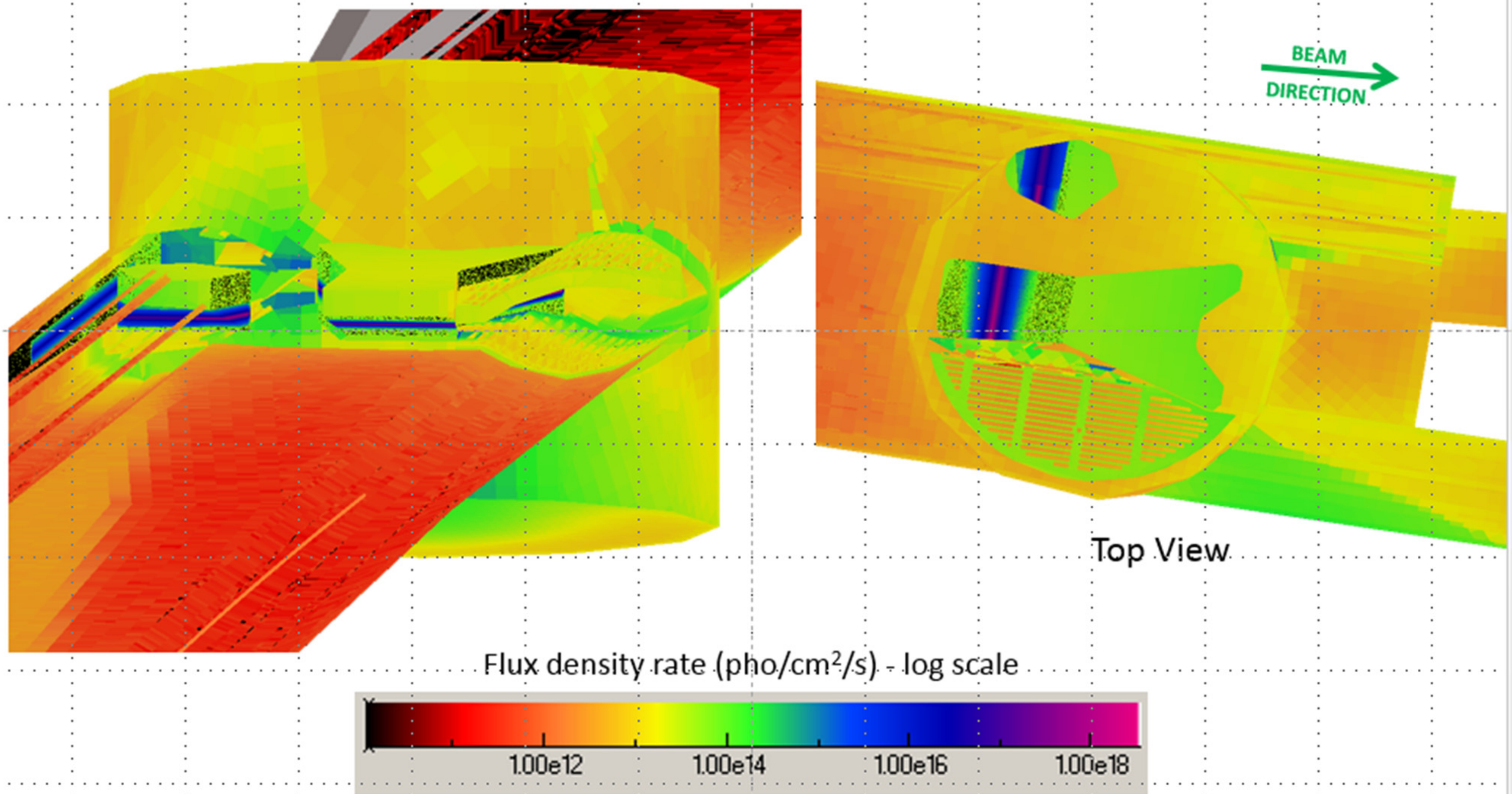

SYNRAD+ : simulation of SR power and flux on crotch absorbers of the APS ring

SynRad model of APS-U sector

- Bending magnet elements generate photon flux in model
- Symmetric boundary condition passes downstream photons back to upstream
- Heat load ray trace verified to high accuracy
- Mesh applied to all vacuum surfaces
- Material reflection tables referenced to determine surface scattering

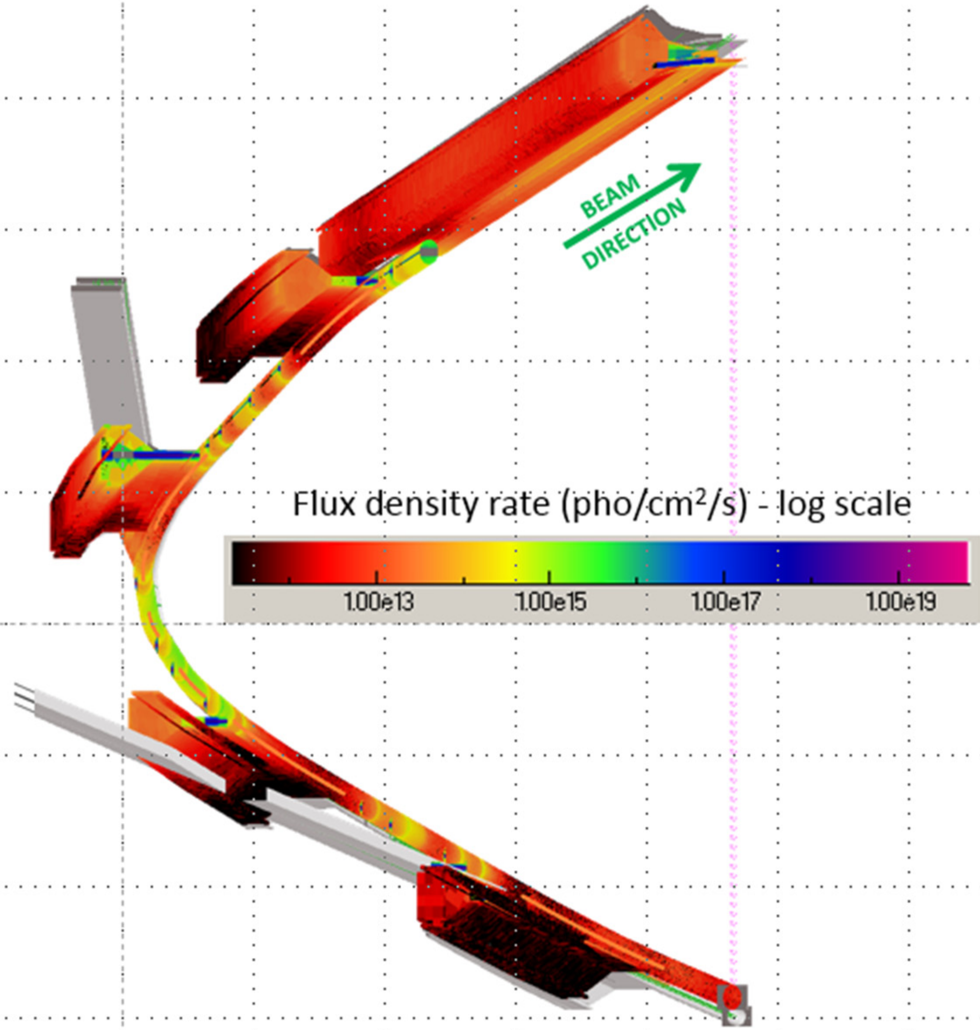

SynRad simulation of synchrotron radiation flux distributions with photon scattering

SYNRAD+ : simulation of SR power and flux on crotch absorbers of the APS ring

Pressures for each UHV gases

- Total pressure equals the sum of individual gases
- No distributed pumping assumed for CH_4 leading to unique profile
- Individual gas pressures used to estimate beam lifetime

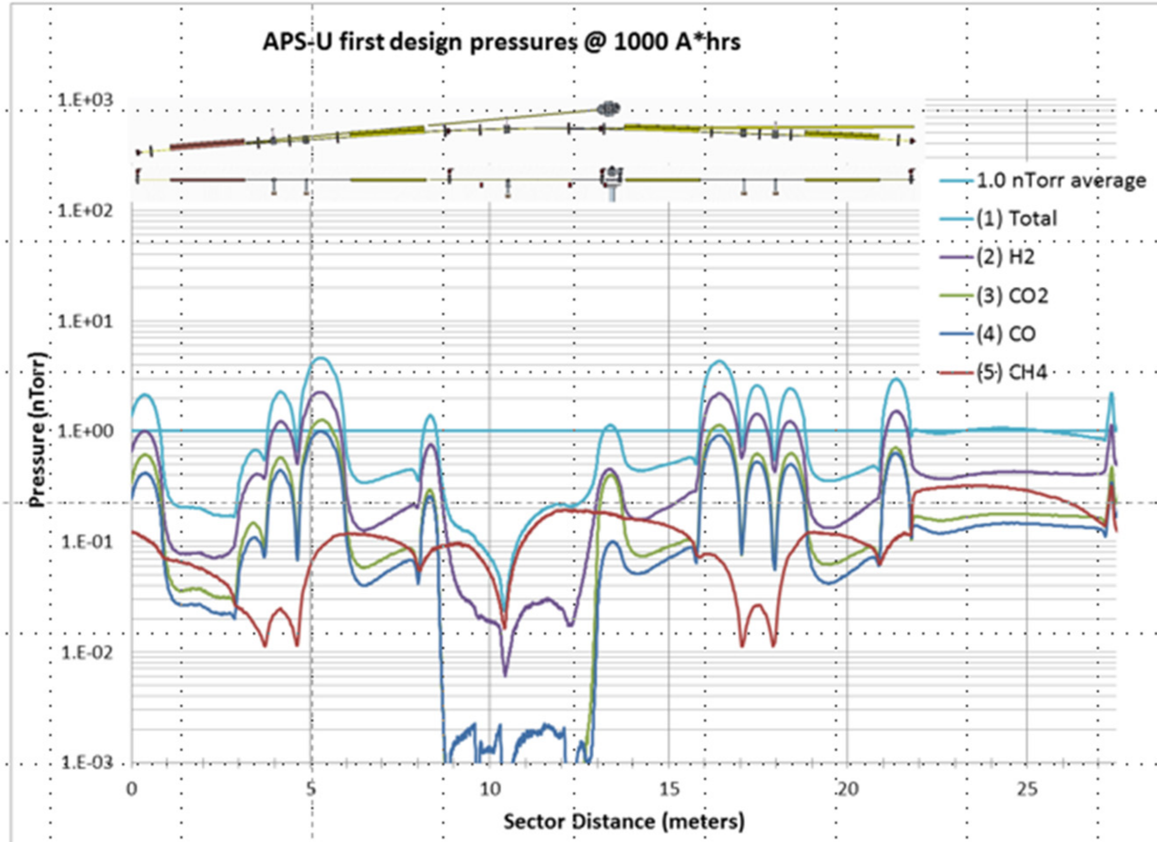

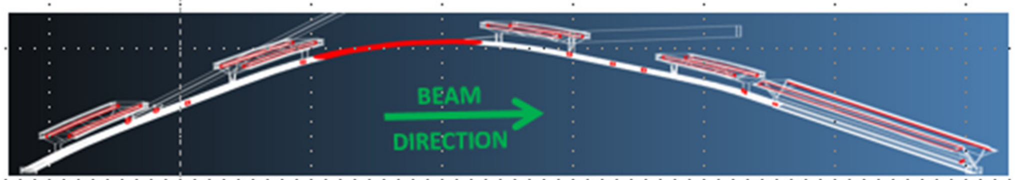

Summary and conclusions

- Some basic concepts of vacuum technology and gas dynamics have been recalled
- We have then briefly seen how important it is to be able to calculate the pressure/gas density along the path of the e- beam stored in a synchrotron radiation light source
- Various methods used in literature and by the vacuum community for calculating relevant quantities have been highlighted
- The advantages of modern, fast computers and their application to Montecarlo simulation codes have been also highlighted with several examples
- The importance of a two-stage approach to the calculation of pressure profiles has been also discussed at length, with examples
- The relevance of this two-stage approach with respect to accelerator issues other than vacuum has been demonstrated with the example of the reduction of bremsstrahlung radiation fluence on the experimental beamline hutches
- Bibliographical references have been given, although a complete and detailed list would need many pages… there are literally hundreds of papers to be read in order to have a clear picture about these issues
- It is hoped that this 2-hour tutorial will push at least some of the participants to look at the literature and get involved in this exciting field of research, which is particularly important for the design of many future accelerators (not only SR light sources, see the 100-km FCC rings design at CERN, for instance)
- Do not forget to mark down and/or to advertise to your colleagues the CERN Accelerator School on Vacuum Technology of June 2017!... http://cas.web.cern.ch/cas/Lund2017/Lund-advert.html

... and many thanks for your patience and attention! ☺

CERN